

## CHARACTERIZATION OF COAL LIQUEFACTION RESIDS BY FIELD IONIZATION MASS SPECTROMETRY: CORRELATING SPECTRAL FEATURES WITH PROCESSING PARAMETERS

Ripudaman Malhotra, Donald F. McMillen, and David L. Huestis  
Chemical Kinetics Department, SRI International, Menlo Park, CA 94025-3493.

**Keywords:** FIMS, Resid analysis, Resid processing

### INTRODUCTION

Under a contract with the U.S. Department of Energy, Consolidation Coal Company (Consol) has provided a range of well-documented samples obtained from process development units to various analytical researchers, who then apply their chosen methodology to determine the value of the method to process understanding and development (1). One objective of Consol's program is to provide a bridge between direct coal liquefaction process development and analytical chemistry. At SRI International, we have analyzed 15 resid samples, taken from three sampling points in five close-coupled two-stage liquefaction runs at the Wilsonville facility by field ionization mass spectrometry (FIMS) to help answer several questions relating to the chemistry of liquefaction, specifically as it relates to resid conversion, and how to improve the overall process.

The technique of field ionization (FI) consists of passing the vapors of a material through a region of intense electric field to polarize and ultimately ionize the molecules. The ions are then mass analyzed using standard mass spectrometric techniques. For most organic compounds, this procedure causes minimal fragmentation and produces only the molecular ions (2). The resulting spectra are thus true representations of the molecular weight profiles of the volatilized materials. FIMS has been used for a variety of applications relevant to coal liquefaction. However, its ability to answer the very difficult questions pertaining to the chemistry of resid reactivity has not been demonstrated. The objective of the task on FIMS analysis was to evaluate the utility of FIMS for addressing the issue of resid reactivity by analyzing a reasonably large set of related samples.

### EXPERIMENTAL PROCEDURES

The samples were the vacuum resid portions of the oils samples collected at the end of the first stage, the second stage and following the ROSE-SR deashing unit. They are referred to as the interstage oil (V1235), product oil (V1067), and recycle oil (V131B) respectively. These samples are from five different two-stage liquefaction runs: Lignite (Run 255), Wyo-dak (Run 251-II), Illinois No. 6 (run 250) in the thermal-catalytic mode, and Illinois No. 6 (Run 257) and Pittsburgh (Run 259) in the catalytic-catalytic mode.

The analyses were conducted using SRI's FIMS instrument, which consists of a foil-type field ionizer interfaced with a 60-degree magnetic-sector mass analyzer and a PDP 11/23 computer for instrument control, data acquisition, and report production. The spectrometer has a resolving power ( $M/\Delta M$ ) of 1300, although it is capable of scanning up to 3000 Da. Typically, approximately 20  $\mu\text{g}$  of the sample is taken in a melting point capillary and introduced into the spectrometer with a heatable direct insertion probe. The sample is heated at a fixed rate from ambient (or  $\sim 67^\circ\text{C}$  for samples with sufficiently high vapor pressure) to about  $700^\circ\text{C}$ . The pressure in the ion source chamber is generally in the  $10^{-6}$  Torr range, although the pressure in the capillary sample holder is considerably higher. We estimate the sample pressure to be around  $10^{-4}$  Torr. Under these conditions, materials with atmospheric equivalent boiling points (AEBP) up to about  $1400^\circ\text{F}$  are expected to vaporize completely, and those with AEBPs in between  $1400^\circ$  and  $1600^\circ\text{F}$  to vaporize at least partially. What often limits the vaporization of these high boiling materials are the coupling reactions with other species present in the sample. Hence the quoted limits should be regarded as a rough guide. (Similarly, other pyrolytic reactions can occur that produce volatile species not present at such in the original mixture.) The spectra of the evolving volatiles are continuously recorded, and at the end of a run, they are added to produce a "sum" spectrum of the total volatiles.

## RESULTS AND DISCUSSION

### General Spectral Features

Figure 1 shows the spectrum of the recycle oil from cat-cat run with the Pittsburgh coal (Run 259), and is typical of the entire set. All of the spectra consist of a broad distribution of molecular weights ranging from about 200 to 1000 Da. There is an additional group of peaks in the 50 to 120 Da range corresponding to small fragment ions. The total intensity of this low-mass group is typically extremely low compared to that of the main profile, reflecting the minimal ion fragmentation that is typical of most liquefaction product streams during FIMS analysis. Immediately apparent from these spectra are two profiles: a more intense profile for the even masses and the other (dark profile) corresponding to the odd masses. Peaks at odd masses generally arise due to  $^{13}\text{C}$ , N, or fragmentation. Because FIMS does not cause much fragmentation and these spectra have been corrected for natural abundance of  $^{13}\text{C}$ , the odd-mass profile arises mainly from compounds containing nitrogen.

At first glance, the FI mass spectra of all the resids look very similar. The similarity is reassuring because several processing requirements tend to provide resids of similar molecular weight range and polarity. Apart from being similar, the spectra also show that the resids are very complex mixtures. The bulk of the material in these samples falls in the 200-1200 molecular weight range and considering coal-origin and heteroatom content of the products, the "average" molecule at, say,  $m/z$  600 would contain one oxygen, one-half nitrogen, and one-quarter sulfur. Therefore, most of the resid molecules are polyfunctional, and not classifiable, even in principle, according to simple chemical type or class. (3) For these reasons, we focused primarily on the overall profiles. We note here that there are a few peaks in the 240 to 340 Da range in each of the spectra that do stand out in all the spectra, and we examined them in some detail. However, before discussing this group of peaks, we first describe our attempt at a semi-quantitative characterization of the overall profiles.

In many instances, the spectra appear to be composed of two partially overlapping clusters of peaks: one such cluster, which we will call Component A, is centered around 350 Da and the other cluster, which we will call Component B, is centered around 600 Da. Relative to Component B, Component A appears to span a relatively narrower MW range. In other work, we had observed the somewhat bi-modal distribution of molecular weights in coal liquefaction resids. However, those observations were with isolated samples, and we were not sure if they were indicative of a general trend. Examination of fifteen closely related samples in this project confirmed the general nature of this distribution, and we felt encouraged to examine this distribution and see if the relative amounts of the two components can be correlated with some process-related parameters.

Several steps are involved in deconvoluting the spectra into Components A and B. First, we have to assign a general functional form to each of the component envelopes; second we perform a least-squares fit on a few selected samples to derive the parameters for the general formula describing the two components; and third we fit the spectra using these expressions while varying only the relative amplitude factors. We chose to express the rising part of each envelope as a power function of the molecular weight ( $m^\alpha$ ) and the decline as an exponential ( $e^{-\beta m}$ ). The parameters  $\alpha$  and  $\beta$  were to be different for each of the two components, but the overall functional form was constrained to be the same. The following expression gives the intensity ( $I_m$ ) at any mass:

$$I_m = Q_A m^{\alpha_A} e^{-\beta_A m} + Q_B m^{\alpha_B} e^{-\beta_B m}$$

Here  $Q_A$  and  $Q_B$  are the weighting factors for the two curves. The parameters  $\alpha_A$ ,  $\beta_A$ ,  $\alpha_B$ , and  $\beta_B$  were determined by a regression analysis. Rather than fit all of the spectra by regression, we decided that a more meaningful test would be to select for regression five of the most divergent looking spectra. Once the parameters  $\alpha$  and  $\beta$  were determined, they were fixed and the remaining spectra were fitted by varying only the  $Q$ 's. Figure 2 shows an example of the deconvolution. The dots are the data for the even masses in the FIMS of the recycle oil from the run with the Pittsburgh coal (Run 259). This spectrum was not among the ones used in the least-squares fit to obtain the parameters defining A and B. The continuous line through the data is the fit obtained by varying the amounts of A and B. The contributions of A and B components to the total fit are shown by the two dashed lines. The fit in this case is reasonably good over most of the mass range, except at high masses where the fit gives a lower intensity than the data. The break in the curve around 450 Da is well mimicked by the fit. Those spectra without a distinct break in the curve were not fit quite so well.

To obtain the relative *weight* fractions of the two components, A and B, we integrate the product of mass with the fitted expressions over the mass range. Thus:

$$\%A = \frac{100 \times \int Q_A m^{\alpha_A} e^{-\beta_A m} \cdot m \, dm}{\int Q_A m^{\alpha_A} e^{-\beta_A m} \cdot m \, dm + \int Q_B m^{\alpha_B} e^{-\beta_B m} \cdot m \, dm}$$

The data in Table I show the wt% A in the various samples.

### Correlation of Lumped Component Levels with Process Parameters and Yields

Having in hand the deconvolution results summarized in Table I, an attempt can be made to see how the levels of Components A and B correlate with process conditions and product character and yields as previously summarized.<sup>(4)</sup> The Illinois No. 6 catalytic-catalytic product oil (Run 257) has a very pronounced low-mass intensity (200-400 Da) as is also reflected in the large A content (32%). This low-mass grouping is somewhat less prominent in the "younger" interstage oil (22%). Evidently, under the catalytic-catalytic conditions, high yields of material that is low molecular weight are produced from the coal or "fresh" resid in the first-stage reactor, and most noticeably, in the second-stage reactor.

In significant contrast to the prominent low-mass intensity in the Run 257 product oil, the recycle oil (which nominally differs from the product oil only in that a portion of the stream has been split off, sent through a vacuum flash separator, and had the ash and insoluble organic matter removed in the ROSE-SR unit) has substantially less of the 200 to 400 Da intensity (13%). Whereas one expects some of the high molecular weight organic material visible with FIMS to be rejected along with the ash, and therefore for the *higher* end of the molecular weight profile to be trimmed in the recycle oil (as compared with the product oil), it is the *lower* end of the profile that has shrunk. This observation suggests significant retrogression between V1067 and V131B; in other words, that significant coupling occurs when the high temperatures are maintained during the "physical" separation process or subsequently in the holding tanks, but catalyst and H<sub>2</sub> pressure are largely absent.

In the case of the Pittsburgh coal, which was also processed in the catalytic-catalytic mode (Run 259), as we move from the interstage oil to the product oil, we see that Component B dominates over Component A. In this case, the fresh resid seems to be much less readily converted (in the second-stage reactor) into A; the net change in fact is for the B to become *more* important as a result of reaction in the second stage. The differences between the Pittsburgh product oil and the recycle oil seem to reflect mainly removal of high molecular weight material, B. This is as would be expected, but is in contrast to the Illinois catalytic-catalytic case, where the effect of putting a side stream through the ROSE-SR unit (and the holding tanks) was curiously to *increase* the amount of B.

The next appropriate comparison is between the Illinois catalytic-catalytic run (Run 257), and the Illinois thermal-catalytic run (Run 250). In Run 250, the level of Component A in the interstage oil is only about half that in Run 257, and passage through the Stage 2 reactor *decreases* Component A still further (rather than increasing it as in Run 257). We conclude (since Stage 2 is catalytic in both cases) that the product of the thermal first stage is less reactive. Apparently the "fresh" resid is more refractory because of the absence of catalyst and/or the slightly higher temperatures used during operation of a thermal first stage.

Moving to the two lower rank coals in this series, also processed in a therm-cat configuration, we see that for both the Wyodak coal and the lignite, second-stage reaction causes a decrease in the percentage of Component A — a change that is qualitatively similar to that seen for the Illinois therm-cat run (Run 250). With respect to changes between the product oil and the recycle stream, there is a slight increase in Component A for both the Wyodak and the lignite, whereas for the Illinois No. 6 coal (Run 250), Component A had decreased. Since we associated the decrease in Component A between the product and recycle streams for the Illinois No. 6 runs with a proclivity for retrogression, we would conclude from the slight *increase* in A that the Wyodak and lignite resids are actually less prone to retrograde reaction than the Illinois No. 6 resids. The observed increase in A supports the conclusion that PCAH species, which are expected to be less abundant in the lower rank coals and their products, are the primary candidates for retrogressive reactions in these highly processed resids. The observed increase in Component A is thus most likely due to a greater rejection of Component B as was observed with the Pittsburgh coal.

To summarize, the attempt to make a straightforward association between the amounts of Components A and B in each resid was surprisingly successful, however some loose ends remain. For instance, a decrease in

Component A as a resid moves through the processing stream can reflect not only regression to the heavier component, B, but also upgrading to distillate. For simplicity, we have simply chosen to try first to rationalize the data in terms of the possibility that is more troublesome in process terms, namely retrogression of Component A to B.

### Examination of Prominent Individual Peaks

While a large part of each of the FI-mass spectral profiles is basically quite smooth, with few prominent masses, it is noteworthy that at the low mass end (240 to 350 Da), there is substantial "structure" in the spectra. Moreover, the same peaks appear as prominent in spectra of all the fifteen resids. The six major series apparent in the spectra of these resids begin at  $m/z$  242, 276, 282, 300, 308, and 316. In Figure 1 we have labeled some of these prominent peaks.

Curiously enough, the six major peaks apparent in these resid spectra are either the same as, or closely related to, those recently identified by Sullivan, Boduszynski, and Fetzer (5) as showing substantial increases during hydrotreating of petroleum vacuum gas oil fractions. Based on the evidence presented by Sullivan et al. (5), and the very striking correspondence between the major peaks seen here and some of those identified by them, we consider it to be very likely that most of the prominent peaks noted here are causally related to the difficulty of catalytic/thermal breakdown to smaller species (distillate) and to the buildup of more refractory resid and IOM. At present, it is difficult to make a more quantitative statement regarding the importance of these peaks. However, a few of the trends that emerge from an initial examination are listed below.

- Consistent with the fact that the Pittsburgh resid is the most difficult to upgrade, the intensities for  $m/z$  276, benzo[ghi]perylene, observed for the Pittsburgh coal (Run 259) are generally higher than those for any other sample. However, this relationship appears not to always hold. In the interstage and recycle oils for Run 259, the levels are 2 to 2.5 times higher than the respective samples for Run 257, the catalytic/catalytic Illinois No. 6 run, but for the product oil the levels are essentially equal.
- The cat/cat run with Illinois No. 6 coal (Run 257), produces more of  $m/z$  276 by about a factor of two than the therm/cat run (Run 250), even though the resid produced in 250 was considered to have been more difficult to upgrade. If the large PCAH are produced in significant part by the cracking activity of the alumina-supported catalysts, we might rationalize that without the first stage catalyst, less benzo[ghi]perylene is formed. But if we accept this explanation, we are then forced to say that the difficulty in upgrading the Illinois therm/cat fresh resid is not due to benzoperlylenes, coronenes, etc., but is due instead to the fact that less cracking occurred in the first stage. While this latter rationalization may be correct, it is apparent that the situation is complex and not susceptible to analysis by simple inspection.
- If instead of comparing the absolute levels, we compare the ratios of peaks at  $m/z$  276 and 300, we find that in going from the recycle stream to the interstage oil the relative amount of benzo[ghi]perylene increases in the more difficult-to-process Runs 250 and 259, while it decreases in Run 257.
- Changes in the ratios of hydroaromatic/aromatic pairs as the resid moves through the system provide an additional point for comparison. We find that the hard-to-convert Runs 250 and 259 show distinct decreases in the ratio of hexahydrobenzo[ghi]perylene to benzo[ghi]perylene. On the other hand, the "good" run 257 actually shows an increase in this hydroaromatic/aromatic ratio as a result of addition of coal to the recycle oil and reaction in the first stage reactor. The appearance of high levels of benzoperlylene in Run 259 is presumably related to the fact that the level of cyclic- $\beta$ -hydrogen (i.e., hydroaromatic hydrogen, as determined by NMR) in the recycle oil was the lowest of these three runs.

These trends do not extend to the entire set of runs. In other words we were not able to construct a consistent set of correlations between the most prominent homologous series and the processing behavior in all five runs. However we believe it is very likely that the difficulty in significant part is that the run-to-run comparisons attempted are anything but all-other-things-being-equal comparisons. A more careful examination of these data is warranted. One correction that ought to be included in this analysis is for the background intensity of all other components that might be present at these specific masses. The background could be adequately represented by the "fit" to the profile described in the previous section. The correction is small for peaks at 242 Da, but probably substantial for those at 300 Da. An alternative strategy would be to perform a

factor analysis on this set of peaks and identify the major trends. We suggest that these tasks be undertaken in a future effort.

## SUMMARY

During this research effort we found that FIMS of many of the liquefaction resid samples exhibited a bimodal molecular weight distribution. The relative amounts of the low and high molecular weight components differ significantly from sample to sample, and simple mathematical deconvolution into Components A and B has revealed a correlation between the variations in A and B on the one hand and coal type, process conditions, and process performance on the other. While the correspondence is not perfect, the deconvolution leads to conclusions reasonably in concert with what is already recognized in coal liquefaction. It is satisfying to see so many observations about reactivity reiterated, not on the basis of yields, but on the basis of differences in molecular weight distribution of streams that are already constrained by process conditions and product fractionation to be as similar as possible. The mass spectra consistently showed a same set of few prominent peaks in the low mass end. Interestingly, these masses were identical with those previously associated by Sullivan et al. with increased difficulties in hydrotreating vacuum gas oils. This similarity prompted us to seek correlations between processing variables the intensity of these peaks. Our partial success in finding such correlations warrants a more extensive examination of the variations in these prominent masses, which when coupled with the deconvolution into lumped low and high molecular weight components, is likely to provide substantial independent information for cross-correlation with other resid properties and processing parameters.

**Acknowledgement.** This work was performed as a subcontract under Consolidation Coal Company's prime contract with the U.S. Department of Energy, Contract No. DE-AC22-89PC89883. Helpful discussions with Drs. R. A. Winschel, F. P. Burke, and S. D. Brandes are gratefully acknowledged.

## REFERENCES

1. Brandes, S. D.; Winschel, R. A.; Burke, F. P. "The Application of Advanced Analytical Techniques to Direct Coal Liquefaction," *Am. Chem. Soc., Div. Fuel Chem. Preprints*, 1991, 36(3), 1172.
2. St. John, G. A.; Buttrill, S. E., Jr.; Anbar, M., in *Organic Chemistry in Coal*, J. Larsen, Ed.; ACS Symposium Series 71, Washington, D. C., 1978, p. 223.
3. Boduszynski, M. M.; "Characterization of Heavy Crude Components," *Am. Chem. Soc., Div. Fuel Chem. Preprints*, 1985, 30(3), 365.
4. Burke, F. P.; Winschel, F. P.; Robbins, G. A., "Coal Liquefaction Process Solvent Characterization and Evaluation," Final Report, U.S. DOE Contract No. DE-AC22-84PC70018, 1989.
5. Sullivan, R. F.; Boduszynski, M. M.; Fetzer, J. C. *Energy Fuels* 1989, 3, 603.

Table 1

### PERCENTAGE OF LOW-MOLECULAR WEIGHT COMPONENT A IN RESIDS TAKEN FROM DIFFERENT RUNS AND SAMPLING POINTS

Wt% A in the Sample Determined from Even-Mass Profile

Sample point	255	251-II	250	257	259
	Lignite Therm-Cat	Wyodak Therm-Cat	Illinois Therm-Cat	Illinois Cat-Cat	Pittsburgh Cat-Cat
Interstage oil	21.5	11.4	13.9	22.4	13.7
Product oil	18.2	9.0	10.4	32.0	9.2
Recycle oil	21.6	10.0	8.6	13.1	18.5

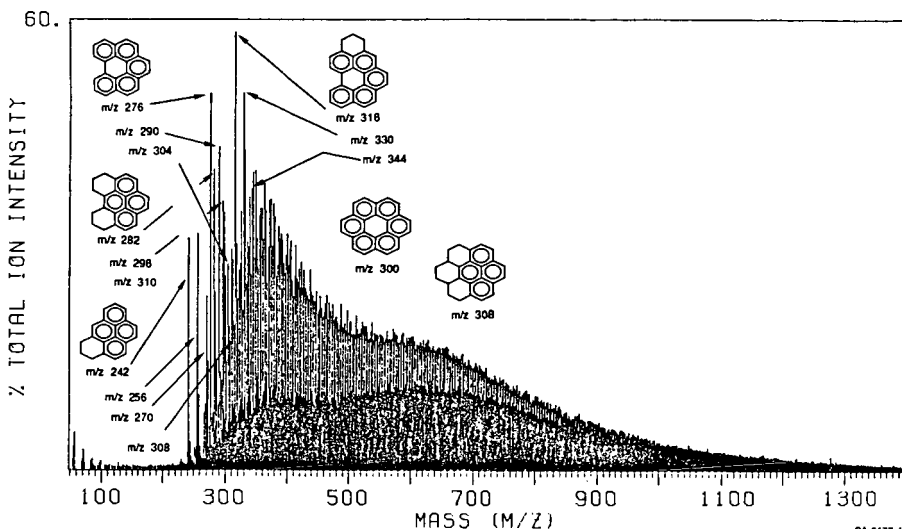


Figure 1. FIMS of the Pittsburgh (Run 259) recycle oil showing the prominent PCAH structures in the 200-350 Da range. CA-2177.4

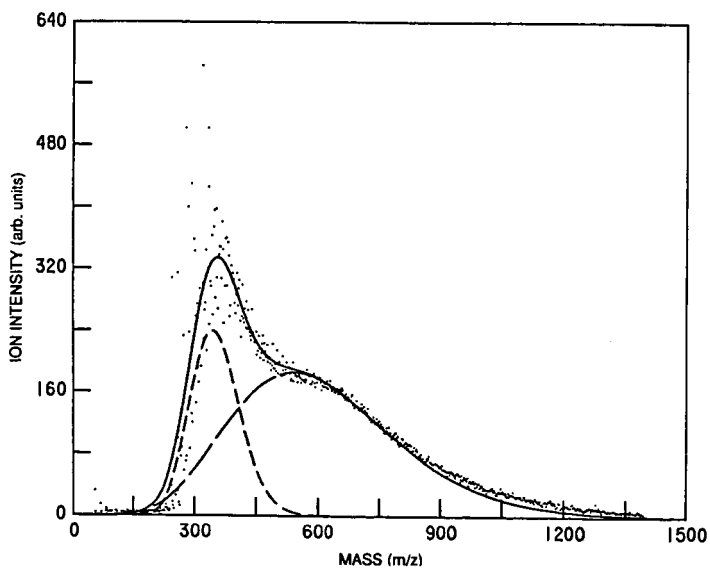


Figure 2. Deconvolution of the FIMS of Pittsburgh (Run 259) recycle oil into Components A and B.

## THE EFFECT OF CROSS-LINKING ON THE THERMAL DECOMPOSITION OF DIPHENYLALKANES

Phillip F. Britt and A. C. Buchanan, III  
Chemistry Division  
Oak Ridge National Laboratory  
P. O. Box 2008  
Oak Ridge, Tennessee 37831-6197

Keywords: Pyrolysis mechanisms, model compounds, retrogressive reactions

### ABSTRACT

In the early stages of the thermal depolymerization of coal, its cross-linked macromolecular structure may restrict the diffusion of reactive intermediates and alter the reaction pathways. In an effort to model the effects of restricted mass transport on the thermally induced free radical decomposition of polymethylene units bridging aromatic clusters in coal, a series of diphenylalkanes [Ph(CH<sub>2</sub>)<sub>n</sub>Ph] have been cross-linked to an inert silica surface by the condensation of the corresponding phenol, HOC<sub>6</sub>H<sub>4</sub>(CH<sub>2</sub>)<sub>n</sub>C<sub>6</sub>H<sub>4</sub>OH. Results from the thermolysis of the diattached substrates at 350-400 °C will be presented and compared to the thermolysis of fluid phase and mono-attached diphenylalkanes [≈Ph(CH<sub>2</sub>)<sub>n</sub>Ph] to highlight the impact that restricted diffusion has on the reaction mechanisms.

### INTRODUCTION

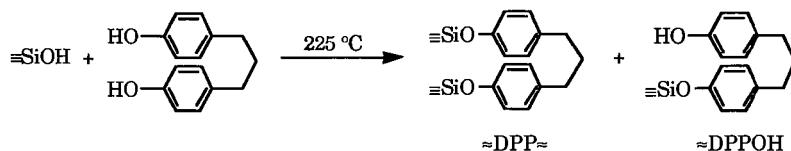
The study of the fundamental reaction mechanisms associated with the thermal decomposition of coal is hindered by its heterogeneous, cross-linked, macromolecular structure. One solution to this problem has been to investigate the thermal decomposition of model compounds representing structural features present in coal, but extrapolation of the results back to coal is difficult and sometimes unreliable.<sup>1</sup> In order to provide a more relevant model for exploring the reaction mechanisms associated with coal pyrolysis, some of the complexities imparted by the macromolecular network structure of coal must be taken into account.

Our research has focused on modeling the effects of restricted mass transport on thermal free radical reaction pathways.<sup>2-6</sup> Thermolysis studies at 350-400 °C of  $\alpha$ ,  $\omega$ -diphenylalkanes covalently attached to an inert silica support has provided evidence that restricted radical and substrate diffusion can alter the free radical reaction pathways as compared to their liquid or gas phase behavior. In the thermolysis of surface-immobilized 1,2-diphenylethane, unimolecular rearrangement and cyclization were favored over bimolecular coupling reactions.<sup>2</sup> Thermolysis of surface-immobilized 1,3-diphenylpropane (≈DPP)<sup>3</sup> and 1,4-diphenylbutane (≈DPB)<sup>4</sup> showed that a free radical chain reaction can efficiently occur under the effects of restricted diffusion, and an unexpected regioselectivity in the hydrogen abstraction process was observed. These studies have also shown that cross-linking reactions can occur under conditions of restricted diffusion. For example, in the thermolysis of ≈DPP and ≈DPB, surface-attached benzyl radical adds to a surface-attached styrene

to form a cross-linked DPP ( $\approx\text{Ph}(\text{CH}_2)_3\text{Ph}\approx$  or  $\approx\text{DPP}\approx$ ) after hydrogen abstraction. Although the reactions responsible for cross-linking have been investigated,<sup>7</sup> the effects of cross-linking on the thermal decomposition reaction pathways has not been investigated. Therefore, in this paper, we will explore the effects of cross-linking on the thermolysis of 1,3-diphenylpropane and 1,4-diphenylbutane as model compounds for coal.

## EXPERIMENTAL

1,3-di(*p*-hydroxyphenyl)propane and 1,4-di(*p*-hydroxyphenyl)butane were prepared by the procedure of Richardson<sup>8</sup> and purified by repeated crystallizations from benzene/hexanes until the purity was >99.9% by GC. The surface-attached materials were prepared by the condensation (225 °C for 1-4 h) of the diphenol with the surface hydroxyls of a high purity fumed silica (Cab-O-Sil, M-5, Cabot Corp.) and sublimation



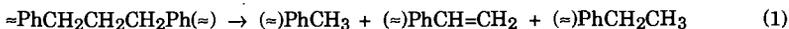
of the excess phenol under vacuum ( $5 \times 10^{-3}$  Torr) at 275 °C, as previously described.<sup>2-4</sup> Complete diattachment could not be obtained even at the lowest surface coverages, and the surface contains a mixture of mono- and diattached material. Surface coverages were determined by liberation of the surface-attached phenol by base hydrolysis, silylation to the corresponding trimethylsilyl ethers, and analysis by GC. Three batches of  $\approx\text{DPP}\approx/\approx\text{DPPOH}$  were prepared with surface coverages of 0.465, 0.181, and 0.105 mmol of organic per gram of derivatized silica with purities of 99.9, 99.5, and 99.6%, respectively, and one batch of  $\approx\text{DPB}\approx$  was prepared with surface coverage of 0.113 mmol/g and purity of 99.6%. The fraction of mono-attached substrate was determined from the quantity of  $\text{HOPhCH}_3$ , a product from the thermolysis of  $\approx\text{DPPOH}$  and  $\approx\text{DPBOH}$ , which distills into the cold trap.

Thermolyses were conducted in sealed, evacuated ( $<5 \times 10^{-6}$  Torr) T-shaped tubes as previously described.<sup>2-4</sup> Volatile products were collected in a cold trap and analyzed as phenols and their trimethylsilyl ethers, while surface-bound products were removed from the surface by base hydrolysis and silylated to the trimethylsilyl ethers. The samples were analyzed by GC and GC-MS with the use of internal standards.

## RESULTS AND DISCUSSION

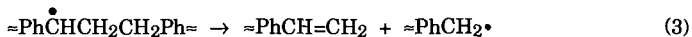
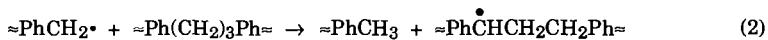
**Thermolysis of  $\approx\text{DPP}\approx$ .** In order to determine the effect of cross-linking on the thermolysis of 1,3-diphenylpropane, a series of surface-attached DPPs were synthesized in which the fraction of diattachment was varied. As shown in Table 1, the extent of diattachment increased with decreasing surface coverage, but complete diattachment could not be achieved. This is most likely a consequence of the

geometric constraints of the short aliphatic chain (see  $\approx$ DPB $\approx$  below). Thermolysis of the high coverage  $\approx$ DPP $\approx$  at 375 °C at low conversion produces approximately equal amounts of surface-immobilized toluene and styrene as the major products and a small amount of surface-immobilized ethylbenzene (ca.1%), eq 1. The parentheses



indicate that both a surface-immobilized species and a gas-phase species are present since the starting DPP is not completely cross-linked to the surface. At higher conversions, isomers of  $\text{C}_{22}\text{H}_{22}\text{O}_3$  and  $\text{C}_{23}\text{H}_{24}\text{O}_3$  (after work-up) are formed as secondary products.

The products from the thermolysis of  $\approx$ DPP $\approx$  can be rationalized by a free radical chain reaction analogous to the one determined for  $\approx$ DPP $^3$  and DPP. $^9$  Assuming that all of the DPP is diattached to the surface, the chain propagation steps are shown in equations 2 and 3. The mono-attached DPP ( $\approx$ DPPOH) decomposes analogously, but

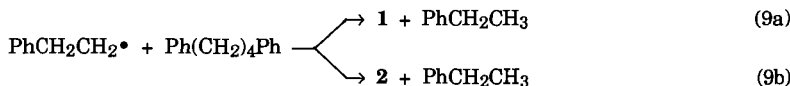
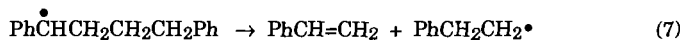
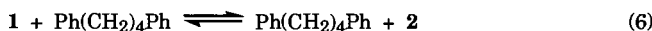
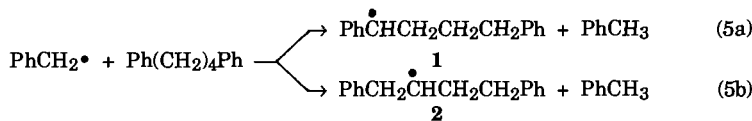


produces a mobile gas-phase (vide infra) benzyl radical ( $p$ -HOPhCH $_2\cdot$ ). The surface-immobilized ethylbenzene could result from the initiation reaction or hydrogenation of styrene. Alkenes such as stilbene and styrene are known to be reduced to the alkane in the presence of hydrogen donors such as tetralin as well as DPP itself. $^9\text{a}$  The secondary products  $\text{C}_{23}\text{H}_{24}\text{O}_3$  and  $\text{C}_{22}\text{H}_{22}\text{O}_3$  are formed from reaction of the diattached 1,3-diphenyl-1-propyl radical with surface-attached styrene or benzyl radical. $^{10}$  Although radical addition to styrene has been observed in the thermolysis of  $\approx$ DPP and DPP, radical coupling involving a 1,3-diphenyl-1-propyl radical is a unique chain terminating reaction that has not previously been observed.

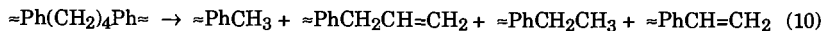
The rate of decomposition of  $\approx$ DPP $\approx$  should be sensitive to the extent of cross-linking since the geometric constraints placed on the chain carrying benzyl radical and the neighboring DPP molecules would influence the hydrogen abstraction reaction. Comparing the rate of conversion of a high coverage  $\approx$ DPP $\approx$  and  $\approx$ DPP (see Table 1), it is found that the small degree of cross-linking (24%) has only a modest effect on the rate. The free phenolic functionality of the mono-attached DPP is not expected to inhibit the rate of decomposition since it has been shown that in the thermolysis of DPP in the liquid phase at 350 and 400 °C, phenol and alkylated phenols have no effect on the rate of decomposition or product distribution. $^{11}$  Surprisingly, at lower coverages, the rate of decomposition of  $\approx$ DPP $\approx$  is only slightly slower than that of  $\approx$ DPP. This could indicate that (1) hydrogen abstraction reactions are not more hindered by diattachment at these surface coverages, (2) gas phase HOPhCH $_2\cdot$ , from the decomposition of the mono-attached DPP, is an effective chain carrying radical, or (3) the rate of initiation is accelerated by strain introduced into the aliphatic chain by cross-linking. The effects of cross-linking on the rate of decomposition is under further investigation.

No new products are observed from the thermolysis of  $\approx$ DPP $\approx$  as the fraction of cross-linking increases. However, retrogressive reactions dramatically increase as a consequence of cross-linking. A comparison of the mole % secondary products from the thermolysis  $\approx$ DPP $\approx$  and  $\approx$ DPB $\approx$  at similar coverages and conversions reveals that as cross-linking increases, retrogressive reactions increase over 100-fold at the lowest surface coverage as shown in Table 2. Additionally, the mole % of  $\approx$ PhCH<sub>2</sub>CH<sub>3</sub> increases with decreasing surface coverage and is approximately independent of conversion. If the ethylbenzene is formed from the reduction of styrene, the yields would likely be conversion dependent.<sup>3</sup>

**Thermolysis of  $\approx$ DPB $\approx$ .** The thermolysis of a diattached 1,4-diphenylbutane ( $\approx$ DPB $\approx$ ) was used to study the effects of cross-linking on the selectivity of hydrogen abstraction. In thermolysis of 1,4-diphenylbutane (DPB), four products are formed (eq 4) by a free radical chain mechanism in which the chain propagation steps are shown in equations 5-9.



A  $\approx$ DPB $\approx$  was prepared with a surface coverage of 0.113 mmol/g with 94% of the material cross-linked. The fraction of diattachment is larger than that found for  $\approx$ DPP $\approx$  (82%) and must be a result of the longer aliphatic chain. Thermolysis of  $\approx$ DPB $\approx$  at 400 °C produced the four products shown in eq 10. A mechanism similar



to that proposed for the thermolysis of DPB can be invoked for the cross-linked DPB. The selectivity of formation of 1 to 2 as determined by the PhCH<sub>2</sub>CH<sub>3</sub>/PhCH<sub>3</sub> ratio is dramatically altered compared to selectivity found for  $\approx$ DPB (see Table 3), and favors

the thermodynamically less stable aliphatic radical 2. This perturbation of selectivity could result from the geometric constraints placed on the hydrogen abstraction reaction by restricted mass transport. Additionally, the rate of decomposition is significantly reduced as a consequence of cross-linking. The impact of cross-linking on the selectivity will be studied further.

## CONCLUSION

This paper presents the preliminary results from the study of the effects of cross-links on the thermolysis of coal model compounds. Our previous studies have shown that restricting mass transport can alter reaction pathways. Results from this study indicate that cross-linking can dramatically increase retrograde reactions, alter the selectivity of hydrogen abstraction reactions and reduce the rate of decomposition. Additional studies are in progress to probe the impact of restricted mass transport on retrograde reactions.

## ACKNOWLEDGEMENTS

Research was sponsored by the Division of Chemical Sciences, Office Of Basic Energy Sciences, U. S. Department of Energy under contract DE-AC05-84OR21400 with Martin Marietta Energy Systems, Inc.

## REFERENCES

1. Larsen, J. *Prepr. Pap.-Am. Chem. Soc., Div. Fuel Chem.* **1990**, *35*, 376.
2. Buchanan, III, A. C.; Dunstan, T. D. J.; Douglas, E. C.; Poutsma, M. L. *J. Am. Chem. Soc.* **1986**, *108*, 7703.
3. Buchanan, III, A. C.; Biggs, C. A. *J. Org. Chem.* **1989**, *54*, 517.
4. Britt, P. F.; Buchanan, III, A. C. *J. Org. Chem.* **1991**, *56*, 6132.
5. Britt, P. F.; Buchanan, III, A. C.; Hitsman, V. M. *Prepr. Pap.-Am. Chem. Soc., Div. Fuel Chem.* **1990**, *36(2)*, 529.
6. Buchanan, III, A. C.; Britt, P. F.; Biggs, C. A. *Energy Fuels* **1990**, *4*, 415.
7. (a) Suuberg, E. M.; Lee, D.; Larsen, J. W. *Fuel* **1985**, *64*, 1668. (b) Suuberg, E. M.; Unger, P. E.; Larsen, J. W. *Energy Fuels* **1987**, *1*, 305. (c) Solomon, P. R.; Hambeln, D. G.; Carangelo, R. M.; Serio, M. A.; Deshpande, G. V. *Energy Fuels* **1988**, *2*, 405. (d) Solomon, P. R.; Serio, M. A.; Deshpande, G. V.; Kroo, E. *Energy Fuels* **1990**, *4*, 42.
8. Richardson, E. W.; Reid, E. E. *J. Am. Chem. Soc.* **1940**, *62*, 413.
9. (a) Poutsma, M. L.; Dyer, C. W. *J. Org. Chem.* **1982**, *47*, 4903. (b) Gilbert, K. E.; Gajewski, J. J. *J. Org. Chem.* **1982**, *47*, 4899.
10. C<sub>22</sub>H<sub>22</sub>O<sub>3</sub> could also be formed from reaction of =PhCH=CHCH<sub>2</sub>Ph= with =PhCH<sub>2</sub>• but =PhCH=CHCH<sub>2</sub>Ph= was not detected as a product.
11. (a) Gilbert, K. E. *J. Org. Chem.* **1984**, *49*, 6. (b) Stock, L. M.; King, H.-H. *Fuel* **1982**, *61*, 1172.

Table 1. Rate of Conversion of  $\approx$ DPP $\approx$  and  $\approx$ DPP as a Function of Surface Coverage.

Compound	Coverage (mmol/g)	% Diattachment	Rate <sup>a</sup> (% h <sup>-1</sup> )
$\approx$ DPP $\approx$	0.465	24	3.5
	0.181	60	0.56
	0.105	82	0.096
$\approx$ DPP	0.57	-	7.0
	0.14	-	0.40
	0.10	-	0.26

<sup>a</sup>Determined from the slopes of the linear regression of conversion vs time

Table 2. Yield of Secondary Products as a Function of Surface Coverage.

Coverage (mmol/g)	Secondary Products: $\approx$ DPP $\approx$ / $\approx$ DPP <sup>a</sup>	$\approx$ PhCH <sub>2</sub> CH <sub>3</sub> <sup>c</sup> (mole %)
0.465	2.8	1.2
0.181	22	5.3
0.105	>120 <sup>b</sup>	8.5

<sup>a</sup>Ratio of the mole % secondary products from thermolysis of  $\approx$ DPP $\approx$  and  $\approx$ DPP compared at similar coverages and conversion.

<sup>b</sup>Secondary products for 0.10 mmol/g  $\approx$ DPP below detection limit of 0.05 mole %. <sup>c</sup>Independent of conversion.

Table 3. Selectivity and Rate of Decomposition of  $\approx$ DPB $\approx$  and  $\approx$ DPB.

Compound	Coverage (mmol/g)	1/2 Selectivity <sup>a</sup>	Rate (% h <sup>-1</sup> ) <sup>b</sup>
$\approx$ DPB $\approx$	0.113	0.60	1.1%
$\approx$ DPB	0.117	2.0	9.5%

<sup>a</sup>PhCH<sub>2</sub>CH<sub>3</sub>/PhCH<sub>3</sub> product ratio. <sup>b</sup>Rate determined from the slope of a conversion vs time plot.

## DIDEUTERIUM INCORPORATION DURING THE COPROCESSING REACTION OF LLOYDMINSTER PETROLEUM RESID AND ILLINOIS NO. 6 COAL IN D<sub>2</sub>

Michael Ettinger and Leon M. Stock  
Department of Chemistry, University of Chicago, Chicago, IL 60637

John G. Gatsis, UOP Research Center, Des Plaines, Illinois 60017

Keywords: Coprocessing, NMR, Liquefaction

### INTRODUCTION

Coal petroleum resid coprocessing is fast becoming a cost effective means of coal liquefaction. The reaction mechanisms, however, are not well understood and are very important to the development and improvement of the technology. The coprocessing reaction is carried out at high temperatures and under a dihydrogen atmosphere that donates hydrogen to the fossil fuels to provide higher yields of liquids and to increase their hydrogen content. Accordingly, we have undertaken a study of the role of dihydrogen in the coprocessing reaction. The initial research in which Illinois No. 6 coal or Wyodak coal and Lloydminster resid or Hondo resid was mixed with a molybdenum based UOP proprietary catalyst was carried out under a 3000 psi dideuterium atmosphere at 420°C with a heat up time of 120 minutes and a residence time of 120 minutes<sup>1</sup>. Quantitative 1H and 2H NMR analyses yielded similar results for the four combinations of coals and resids. Specifically, the degree of deuteration, (D/H+D), of the coprocessed products approached 0.25, the value that was expected for complete equilibration of the isotopes among the available positions in the oil, resin, and asphaltene. These results established the unselective character of the severe coprocessing reaction. However, we sought information on the limiting processes. Accordingly, additional coprocessing reactions with Illinois No. 6 coal and Lloydminster resid have been carried out under less severe conditions to investigate how the dideuterium utilization in the reaction products is affected by changes in the temperature and pressure.

### EXPERIMENTAL

**Materials.** Illinois No. 6 coal was prepared by the Kentucky Center for Energy Research (KCER) and used as received (Anal. %C, 68.60; %H, 4.51; %N, 1.39; %S, 3.04; %O, 9.65; %H<sub>2</sub>O, 3.15; %Ash, 9.65). Lloydminster Resid (Anal. %C, 83.6; %H, 11.5; %S, 4.77; %N,) was obtained by UOP Research Center and used as received. The catalyst used was a molybdenum based UOP proprietary catalyst.

**Coprocessing Reaction Procedure.** Weighed amounts of Lloydminster and Illinois No. 6 coal in a two to one ratio (resid/MAF coal) and the catalyst (2%wt) are added to an 1800ml rocking autoclave. The autoclave is sealed and is pressurized first with hydrogen sulfide and then with dihydrogen or dideuterium to give a 10 vol% hydrogen sulfide and 90 vol% dideuterium such that the desired pressure is obtained at reaction temperature. The autoclave is heated to the desired temperature for a residence time of 0.0, 0.5, or 2 hours. At the reaction conditions, dideuterium is added automatically so that the desired reaction pressure (1770 or 3000psi at temperature) is maintained. After the desired time-at-temperature, the autoclave is cooled to room temperature, and is then depressurized with the gas passing through a foam trap, caustic scrubbers, metering system, and then a sample is collected for analysis. To remove additional gas from the remaining reaction mixture, the material in the autoclave is stripped with dinitrogen. This gas also is passed through the foam trap, caustic scrubber, metering system, and analyzed. Any slurry product recovered in the foam trap is recovered with toluene and added to the toluene rinse solution. The slurry product from the autoclave is decanted. The material that remains in the autoclave is removed by rinsing the vessel with toluene until the autoclave is clean. The combined slurry

product is solvent separated into four fractions (oil, resin, asphaltene, and insoluble) according to a previously reported procedure<sup>1</sup>.

Analysis. Deuterium spectra were obtained on a Varian XL 400 MHz spectrometer. Two hundred fifty six scans were acquired by using a 90° pulse and a .5 second delay between pulses. Benzaldehyde- $\alpha$ -d-1 was used as a quantitative internal standard. Proton spectra were obtained similarly on the same instrument by using a 90° pulse and a 20 second delay between pulses. Elemental analyses for carbon and hydrogen for each solvent separated product were obtained from Huffman Laboratories by using an instrument that detected both hydrogen and deuterium<sup>2</sup>.

## RESULTS

The autoclave reactions were carried out with Illinois No. 6 coal, Lloydminster resid and a molybdenum based UOP proprietary catalyst. Temperature was varied from 390 to 420°C and pressure was varied from 1770 to 3000 psi of dideuterium. The actual reaction time is a sum of the heat up time, approximately two hours, and the residence time, 0.0, 0.5, or 2 hours. The coprocessed products were solvent separated into four fractions; oil (isopentane soluble), resin (heptane soluble-isopentane insoluble), asphaltene (toluene soluble-heptane insoluble), and insolubles (toluene insoluble). The yields of each fraction, the coal conversion, and the asphaltene conversion for each reaction are provided in Table I.

The solvent separated products were quantitatively analyzed by proton and deuterium NMR methods and elemental analysis. The NMR spectra were partitioned into regions: aromatic resonances (12.0 - 6.0 ppm), total aliphatic resonances (5.0 - (-2.0) ppm), alpha aliphatic resonances (5.0 - 2.0 ppm), beta aliphatic resonances (2.0 - 1.0 ppm), and gamma aliphatic resonances (1.0 - (-2) ppm). Hydrogen content, deuterium content, and % deuteration at each position in the oil, resin, and asphaltene fractions were determined as shown in Table II, and (H+D)/C ratio is shown in Figure 1.

The data in Tables I and II clearly show the effects of temperature and pressure on the yields and conversions in the coprocessing reaction. Temperature proves to be the dominant driving force for conversion. An increase in dideuterium pressure from 1770 to 3000 psi at 390°C has essentially no effect on either coal or asphaltene conversion, or on the yields of any of the solvent separated products. However, except for the aromatic positions, an increase in pressure does increase the deuteration at all positions, and the (H+D)/C ratio increased in the oil, resin, and asphaltene fractions. Aromatic deuteration increased from 17.2 to 19.1%, mainly in the resin and asphaltene fractions. The increase in aliphatic deuteration from 9.1 to 12.1% was dominated by incorporation at the alpha position.

An increase in reaction temperature from 390 to 405°C and then to 420°C had a dramatic effect on the coal and asphaltene conversions. The coal conversion increased from 42.6 to 75.0% at 405°C, and then to 92.1% at 420°C. The coal conversion reached its maximum of about 92% at 420°C with no residence time. The same result was realized both when the residence time was 0.5 hours and 2.0 hours. The asphaltene conversion steadily increased from 13.0 to 29.6% at 405°C, and then to 40.1% at 420°C. The oil and asphaltene yields increased slightly, but most importantly the insoluble yield decreased significantly from 19.3% at 390°C to 2.7% at 420°C enabling the high coal conversions. In addition, the increase in temperature from 390 to 405°C, and from 405 to 420°C provided almost linear increases in deuteration at all positions. Approximately 9-10% increases are seen in the deuteration of all the aliphatic positions in the oil, resin, and asphaltene fractions with the exception of the alpha position in the resin and asphaltene fractions. The lack of a comparable increase in alpha % deuteration is almost certainly the result of the already high level

of deuterium incorporation in the alpha position at 390°C. Increases in the aromatic region averaged about 7.5%.

Both coal conversion and alpha D exchange reach their maximum at 420°C with no residence time. As the residence time was increased, coal conversion remained constant and % alpha deuteration declined in all three fractions while the asphaltene conversion exhibited its largest increase. As the residence time and, consequently, the asphaltene conversion were increasing, the % aliphatic and % overall deuteration remained essentially constant in the asphaltene fraction while the % aromatic deuteration and the % alpha deuteration decreased. The increase in % deuteration in the beta and gamma positions compensated for the decreases in the other positions to keep the overall % aliphatic deuteration of the asphaltene fraction constant indicating the approach to equilibrium of H and D in the asphaltenes. The alpha position was still slightly favored.

However, as the residence time at 420°C is increased, the % deuteration at the other positions (aromatic, beta, and gamma) in all three fractions increases, and lead to an increase in the overall aliphatic and total deuteration in the oil and resin fractions. In addition, (H+D)/C significantly decreases in the resin and asphaltene, and to some extent in the oil.

## CONCLUSIONS

Increasing pressure and temperature both lead to increased deuterium uptake from the dideuterium atmosphere. Temperature is, however, the driving force behind the conversion chemistry. Deuterium uptake, asphaltene conversion, and coal conversion all increase as temperature is raised from 390 to 420°C. Once 420°C is reached, coal conversion chemistry and % alpha deuteration have reached their maximum levels. As residence time at 420°C is increased, the chemistry responsible for increased asphaltene conversion and the upgrading of these asphaltenes to resins and then to oils takes place. The initially high levels of deuterium atoms in the alpha positions decrease as reactions at the less reactive beta and gamma positions occur. The deuteration at all sites in the asphaltene fraction essentially remains constant at about 27% as residence time at 420°C is increased, but the (H+D)/C ratio decreases as the asphaltene conversion and upgrading of asphaltenes to resins and oils takes place. Concurrently, (H+D)/C is also decreasing in the oil and resin. However, the overall deuterium uptake is still increasing from 18.6 to 26.7% in the oil, and from 23.9 to 30.9% in the resin.

## REFERENCES

1. Ettinger, M.; Stock, L. M.; Gatsis, J. G.; Prepr. Pap. - Am. Chem. Soc., Div. Fuel Chem. 1991, 36(2), 635.
2. Total %wt H+D was calculated by correcting the elemental analysis %wt H using quantitative deuterium values provided by NMR analysis. The calculation can be found in the dissertation of Michael D. Ettinger, University of Chicago Libraries.

Table I. Reaction Conditions, Yields (wt%MAF), and Conversions (wt%MAF)

Conditions	Oil	Resin	Asphaltene	Insolubles	Recovered Products	Coal Conversion	Asphaltene Conversion
0.0 hr at 390, 1770psi	53.4	3.8	17.1	18.9	93.2	43.3	15.1
0.0 hr at 390, 3000psi	54.1	3.3	17.7	19.3	94.4	42.6	13.0
0.0 hr at 405, 3000psi	59.7	1.1	21.2	8.3	90.3	75.0	29.6
0.0 hr at 420, 3000psi	55.4	3.6	22.8	2.7	84.5	92.1	40.1
0.5 hr at 420, 3000psi	60.8	1.7	19.3	2.7	84.4	91.9	47.3
2.0 hr at 420, 3000psi	62.3	3.9	8.5	2.4	77.1	92.8	74.2

Figure I. (H + D) / C

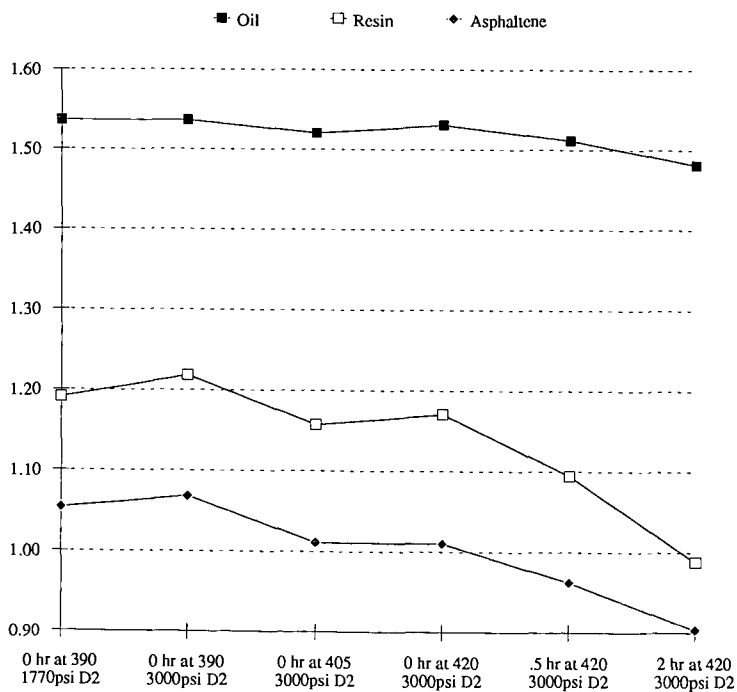


Table II. % Deuteration in Solvent Separated Products

Conditions	Oil	Resin	Asphaltene	Total
<u>% TOTAL D 12.0 - 6.0 &amp; 5.0 (-2) PPM</u>				
0.0 hr at 390, 1770psi	6.59	10.33	14.76	10.03
0.0 hr at 390, 3000psi	8.60	13.97	17.95	12.89
0.0 hr at 405, 3000psi	13.05	17.75	24.43	17.62
0.0 hr at 420, 3000psi	18.57	23.88	27.89	22.78
0.5 hr at 420, 3000psi	20.33	25.07	26.67	23.55
2.0 hr at 420, 3000psi	26.70	30.88	27.59	28.17
<u>% AROMATIC D 12.0 - 6.0 PPM</u>				
0.0 hr at 390, 1770psi	13.28	16.30	20.38	17.23
0.0 hr at 390, 3000psi	13.25	19.10	22.69	19.14
0.0 hr at 405, 3000psi	16.97	22.05	27.42	23.00
0.0 hr at 420, 3000psi	22.50	26.22	29.47	26.70
0.5 hr at 420, 3000psi	22.00	25.47	26.58	25.18
2.0 hr at 420, 3000psi	25.30	31.25	26.66	28.12
<u>% ALIPHATIC D 5.0 - (-2.0) PPM</u>				
0.0 hr at 390, 1770psi	6.09	9.42	13.58	9.06
0.0 hr at 390, 3000psi	8.26	13.25	16.99	12.08
0.0 hr at 405, 3000psi	12.72	17.04	23.70	16.82
0.0 hr at 420, 3000psi	18.23	23.40	27.46	22.11
0.5 hr at 420, 3000psi	20.17	24.98	26.70	23.23
2.0 hr at 420, 3000psi	26.85	30.75	27.97	28.18
<u>% ALPHA D 5.0 - 2.0 PPM</u>				
0.0 hr at 390, 1770psi	19.38	21.30	25.27	22.09
0.0 hr at 390, 3000psi	25.14	29.41	30.36	28.46
0.0 hr at 405, 3000psi	29.63	31.65	34.42	32.02
0.0 hr at 420, 3000psi	36.29	35.44	36.52	36.06
0.5 hr at 420, 3000psi	35.61	34.35	33.64	34.45
2.0 hr at 420, 3000psi	34.27	35.01	31.69	33.68
<u>% BETA D 2.0 - 1.0 PPM</u>				
0.0 hr at 390, 1770psi	3.82	5.14	8.25	5.19
0.0 hr at 390, 3000psi	5.43	7.54	10.25	7.15
0.0 hr at 405, 3000psi	9.65	11.30	16.96	11.62
0.0 hr at 420, 3000psi	15.85	17.48	21.20	17.41
0.5 hr at 420, 3000psi	18.72	20.31	21.39	19.70
2.0 hr at 420, 3000psi	27.35	28.61	24.74	27.13
<u>% GAMMA D 1.0 - (-2.0) PPM</u>				
0.0 hr at 390, 1770psi	2.48	5.25	8.47	4.87
0.0 hr at 390, 3000psi	3.26	7.54	11.32	6.54
0.0 hr at 405, 3000psi	6.86	11.57	18.36	11.11
0.0 hr at 420, 3000psi	9.86	16.26	21.72	14.16
0.5 hr at 420, 3000psi	11.56	17.98	22.72	15.54
2.0 hr at 420, 3000psi	18.70	24.19	25.35	21.25

## ON-LINE GC/MS ANALYSIS OF HIGH PRESSURE CONVERSION REACTIONS OF MODEL COMPOUNDS FOR COAL-DERIVED LIQUIDS

Huaying Huai, Chung H. Tsai\*, Joseph Shabtai\* and Henk L.C. Meuzelaar  
Center for Micro Analysis and Reaction Chemistry, \*Fuels Engineering Department,  
University of Utah, Salt lake City, Utah 84112

**Keywords:** (on-line GC/MS, high pressure reaction, model compounds)

### INTRODUCTION

Direct coal liquefaction involves complex and insufficiently defined chemical reactions. In order to improve direct coal liquefaction processes, it is necessary to improve our understanding of key chemical reactions. Unfortunately, due to the high pressure and high temperature requirements of most coal liquefaction processes, real-time on-line reaction monitoring by advanced spectroscopic and/or chromatographic techniques has generally been impossible until now. Thus, relatively little is known about the precise reaction pathways as well as the intermediate reaction products involved. This is particularly true for conversion reactions carried out in batch reactors such as autoclaves. Due to the relatively long residence times primary reaction products formed in batch type autoclaves are quite susceptible to secondary, or even tertiary reactions. Consequently, real-time on-line monitoring experiments are needed to elucidate reaction pathways in autoclaves.

Although several on-line systems have been developed for coal conversion at near-ambient pressure or high vacuum conditions [1-4], there are no reports of on-line chromatography/spectroscopy based systems built for monitoring high pressure conversion reactions. Therefore, the development of a direct GC/MS interface for near-real time analysis of high pressure reaction products, while minimally disturbing the reaction process, has been undertaken in our laboratory.

It is well established that coal contains fused aromatic and hydroaromatic ring clusters, composed of an average of two to four condensed ring units, connected by various alkylene, ether, sulfide and direct (Ar)C-C(Ar) bridges [5]. Liquefaction reactions are primarily thought to involve these connecting bridges, especially ether linkages and alkylene linkages [6]. In recent years, a number of workers [7-17] have subjected coal-model compounds to various coal conversion conditions in order to confirm that certain coal structures are reactive during coal conversion and to infer the conversion mechanisms of real coals from mechanisms determined for such compounds.

The present paper reports the design and testing of a newly developed on-line GC/MS monitoring system for high pressure reactions and its application to the investigation of hydrogenation and hydrodeoxygenation (HDO) of model compounds, such as diphenyl methane and dibenzyl ether, under both catalytic and thermal conditions.

### EXPERIMENTAL

**Instrumental Design:** Figure 1 shows that the on-line system consists of: (1) a 50 ml flow-through micro-autoclave reactor (Autoclave Engineers Inc.), with a continuous stream of mixture feed flowing through a preheater, entering the reactor from the bottom, and continuously sweeping solubilized products into a collecting reservoir; (2) a pressure reduction line (15  $\mu$ m i.d. fused silica capillary) which reduces the pressure from about 1650 psig to ambient at a mass flow of approximately 1 mg/min for toluene while minimizing dead space at the high pressure end and minimally disturbing the reaction process; (3) a novel automated vapor sampling (AVS) inlet developed at the University of Utah, Center for Micro Analysis and Reaction Chemistry (U.S. Patent No. 4,970,905) for diluting

and pulsed sampling of ambient vapor sample streams; and (4) a GC/MS system with a 1 m long, 150  $\mu\text{m}$  i.d. fused silica capillary "transfer line" GC column directly coupled to a Finnigan Mat Ion Trap Mass Spectrometer (ITMS) with tandem MS capabilities and electron ionization (EI) as well as chemical ionization (CI) options.

**Materials:** Diphenylmethane, dibenzyl ether, decalin and biphenyl, were obtained from Aldrich Chemical Co. as G.R. grade without further purification. A commercial catalyst,  $3\text{Co}8\text{Mo}/\gamma\text{-Al}_2\text{O}_3$ , was sulfided before use for the reaction. A protonic acid catalyst,  $\text{FeCl}_3/\text{SiO}_2\text{-Al}_2\text{O}_3$ , was prepared by means of a special impregnation technique in this laboratory.

**Experimental procedure:** About 300 ml of a mixture containing 10%(wt) feed, 86% solvent (decalin) and 4% internal standard (biphenyl) were used for each experiment. Under catalytic reaction conditions, about 1 g of the catalyst was placed in a self-containing basket with 52 wire mesh. The liquid flow was about 30 ml/hr after the first reactor fill with feed mixture. The reactor was pressurized at 1600 psi with a continuous  $\text{H}_2$  supply. After analysis start-up, normally 10 samples were taken at 2 min/sample at ambient temperature for checking system stabilization. Then the GC/MS was started at the same time as the reactor started heating. The reactor temperature was recorded for each sample. After the reactor reached the reaction temperature, the reaction time was recorded. Detailed parameters for each reaction are listed in Table 1. Both reactor temperature and reaction time effects will be discussed.

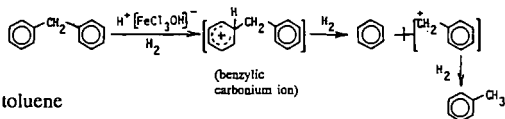
## RESULTS AND DISCUSSION

**On-line system function:** Aside from occasional plugging of the 15  $\mu\text{m}$  i.d. capillary pressure reduction line and the protective 2.0 and 0.5  $\mu\text{m}$  frits the system exceeded design specifications with regard to GC/MS performance, especially isothermal GC results (note the separation of decalin isomer peaks in Figure 2) and dynamic range (solvent peaks representing > 80 % of the reactor contents were as readily measurable as small product peaks representing less than 100 ppm thus establishing an effective dynamic range >  $10^4$ ). As also demonstrated in previous work, the combination of automated pulsed vapor sampling and short column capillary "transfer" line GC enabled repetitive recording of complete isothermal GC runs at 1-4 minute intervals. Moreover, the transfer time of nonretained sample components between reactor and detector was found to be less than 1 minute. In short, the system shown in Figure 1 is capable of detecting minute changes in sample composition in a time which is short compared to typical reaction times in autoclave reactors.

**Diphenylmethane:** Figure 2 shows the reactor temperature effect on diphenylmethane decomposition under thermal and acid-catalyzed reaction conditions. As seen, the first products can be detected at about 330°C for the catalytic reaction, but not for the corresponding thermal reaction (even at about 350°C). Kinetic profiles of the effect of reaction time on the decomposition of diphenylmethane at thermal and catalytic reaction conditions at 350°C are illustrated in Figure 3. As expected, the concentrations of the products and the feed are increasing and decreasing, respectively, as a function of reaction time for both thermal and catalytic reactions. At 350°C, conversion yield at the equilibrium stage (flow reactor!) is about 50% of the feed for the acid-catalyzed reaction, whereas the thermal reaction produces detectable products by GC/MS, but achieves a very low conversion yield, which is consistent with previous results [15,17]. Figure 4 shows typical single ion chromatograms with the corresponding mass spectra of the decomposition product of diphenylmethane (benzene, toluene, and xylene) under catalytic reaction conditions. Figure 5 demonstrates the concentration of benzene, toluene and xylenes as a function of reaction time under catalytically controlled conditions. Obviously, benzene is the dominant product, whereas the concentration of toluene is increasing with reaction time, and xylene concentrations attain only about 1% of the benzene concentration. The results infer that  $\alpha$ -bond cleavages are preferable under the

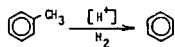
acid-catalyzed conditions which agrees with other results [11]. That the active form of the metal chloride is aqua complex [18],  $H^+[MCl_4OH]^-$ , has been considered. Thus, the mechanism of diphenylmethane decomposition under the acid-catalyzed condition is proposed as follows:

Main Reaction (hydrodealkylating cleavage of the  $\alpha$ -bond)

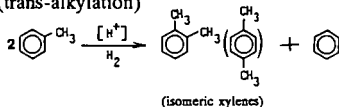


Secondary Reactions of toluene

(a) hydrodealkylation



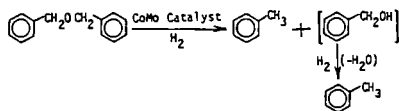
(b) disproportionation (trans-alkylation)



The rate-limiting step in the overall process is protonation of diphenylmethane to form an intermediate carbonium ion, which undergoes  $\sigma$ -cleavage to yield benzene and toluene. The small extent of secondary reactions of toluene can not be avoided under the acid-catalyzed reaction condition.

In the thermal reaction, toluene is the most important product and the ratio of toluene to benzene shows no clear trend with reaction time. A free radical mechanism is suggested. Due to very low conversion yields, the reaction pathway of diphenylmethane under the thermal conditions is not discussed.

**Dibenzyl Ether:** Figure 6 illustrates dibenzyl ether decomposition under both thermal and catalytic reaction conditions. This reaction proceeds at much lower temperatures than the diphenyl methane decomposition reaction, due to the bond energy differences listed in table 2. Figure 7 shows the kinetic profiles of the decomposition of dibenzyl ether under both thermally and catalytically controlled reaction conditions. The conversion of dibenzyl ether under catalytic reaction conditions is approximately 96%, as opposed to 30% under thermal reaction conditions. The GC/MS results reveal six products, namely: benzene, toluene, benzaldehyde, dibenzyl, 4-methyl diphenyl methane and 2-methyl diphenyl methane, from the thermally controlled reaction, while only one product, toluene, is observed from the catalytically controlled reaction. This implies that the reaction pathways under both conditions are different. The thermal decomposition of dibenzyl ether has been well defined following the free radical mechanism [8-10]. The reaction pathway of the HDO reaction of dibenzyl ether in the presence of a sulfided  $3\text{Co}8\text{Mo}/\gamma\text{-Al}_2\text{O}_3$  catalyst is as follows:



The benzyl alcohol intermediate has been observed as the only intermediate at temperatures between 140-260°C in the presence of the same type of catalyst (3Co8Mo) at 1000-1500 psig  $\text{H}_2$  [19]. Due

to the more severe conditions under which our experiment was performed (300 C), the intermediate benzyl alcohol was not detected.

## CONCLUSIONS

A newly developed, on-line GC/MS monitoring system for high pressure reactions performed reliably. This represents a significant over conventional off line methods and should facilitate elucidation of the mechanisms and kinetics of coal liquefaction.

The results obtained suggest that the protonic acid catalyst,  $\text{FeCl}_3/\text{SiO}_2\text{-Al}_2\text{O}_3$ , acting as an aqua complex,  $\text{H}^+[\text{FeCl}_3\text{OH}]$ , causes cleavage of the  $\alpha$ -bond in diphenylmethane to produce approximately 50% each of benzene and toluene, whereas very low product yields ( $< 1\%$ ) are observed in the absence of a catalyst.

The decomposition of dibenzyl ether under catalytic conditions is almost complete (96%). The only product, toluene detected, under such conditions reveals that an HDO reaction occurred. The thermal reaction mainly breaks C-O bonds by a free radical mechanism.

## ACKNOWLEDGEMENT

The authors are grateful to N. Aronld, W.H. McClennen, J. Dworzanski for technical discussions and to G. Charkol for experimental assistance. This work was supported by the Consortium for Fossil Fuel Liquefaction Science (U.S. Department of Energy).

## LITERATURE REFERENCES

1. Yun Y.; Meuzelaar, H.L.C.; Chakravarty, T.; Metcalf, G. "Computer-Enhanced Pyrolysis Mass Spectrometry: A New Window on Coal Structure and Reactivity" in: *Advances in Coal Spectroscopy*, 1992 (in press).
2. Chakravarty, T.; Windig, W.; Taghizadeh, K.; Meuzelaar, H.L.C. *Energy & Fuels*, 1988, 2, 191-196.
3. Dworzanski, J.P.; Buchanan, R.M.; Chapman, J.N.; Meuzelaar, H.L.C. *ACS Preprints, Div. Fuel Chem.*, 1991, 36(2), 725-732.
4. Carangelo, R.M.; Solomon, P.R.; Gerson, D.J. *Fuel*, 1987, 66, 960.
5. Shabtai, J.; Zhang, Y. *Proc. Int. Conf. Coal Sci.*, 1989, Vol. II, 807-810.
6. Shabtai, J.; Saito, I. *U.S. Patent 4,728,418* (1988).
7. Poutsma, M.L. *Fuel*, 1980, 59, 335-338.
8. Kamiya, Y.; Yao, Y.; Oikawa, S. *ACS Preprints, Div. Fuel Chem.*, 1979, 24(2), 116-124.
9. Schlosberg, R.H.; Ashe, T.R.; Pancirov, R.J.; Donaldson, M. *Fuel*, 1981, 60, 155-157.
10. Schlosberg, R.H.; Davis, W.H.Jr.; Ashe, T. *Fuel*, 1981, 60, 201-204.
11. Taylor, N.D.; Bell, A.L. *Fuel*, 1980, 59, 499-506.
12. Ogo, Y.; Kuranuki, K. *Proc. Int. Conf. Coal Sci.*, 1989, Vol.II, 705-708.
13. Sharma, R.K.; Diehl, J.W.; Olson, E.S. *ACS Preprints, Div. Fuel Chem.*, 1990, 35(2), 414-422.
14. Futamura, S.; Koyanagi, S.; Kamiya, Y. *Fuel*, 1988, 67, 1436-1440.
15. Vernon, L.W. *Fuel*, 1980, 59, 102-106.
16. Husain, A.; Olah, G.A. *Proc. Int. Conf. Coal Sci.* 4, 1983, 191-194.
17. Wei, X.Y.; Ogata, E.; Futamura, S.; Kamiya, Y.; Niki, E. *ACS Preprints, Div. Fuel Chem.*, 1991, 36(2), 505-512.
18. Hayatsu, R.; Scott, R.G.; Moore, L.R.; Studier, M.H. *Nature*, 1975, 257, 378-
19. Shukla, Y., Ph.D. Dissertation, University of Utah, 1985.

TABLE 1  
EXPERIMENTAL CONDITIONS

Reactor Conditions:	
- Pressure	1600-1650 psig
- Feed Flow Rate	30 ml/hr
- Reaction Gas	Continuous flow H <sub>2</sub> 50 sccm
- Heating Speed	ambient--> 300°C in ~18 min
- Final Reaction Temperature	350°C for diphenylmethane, 340 and 300°C for dibenzyl ether under thermal and catalytic conditions, respectively
- Catalyst	~1 g sulfided 3Co8Mo/γ-Al <sub>2</sub> O <sub>3</sub>
Pressure Reduction Line Conditions:	
- Temperature	175°C
- Pressure	1600-1650 psig--> ambient
Sample Inlet Conditions:	
- Temperature	270°C
- Pressure	ambient
- Dilution He Flow Rate	100 ml/min
- Carrier Gas He Flow Rate	40 ml/min
- Sampling Valve Flow Rate	43 ml/min
- Bleed Flow Rate	10 ml/min
- Sampling Pulse	550 ms at 2 min intervals
Transfer Line Conditions:	
- Column	1 m x 150 μm i.d. coated with 0.12 μm CP-SIL 5CB
- Temperature	105°C
- Pressure	ambient -->10 <sup>-6</sup> torr
MS Conditions:	
- Pressure	10 <sup>-6</sup> torr
- Ion Trap Temperature	96°C
- Ionization	electron impact (with automatic gain control)
- Spectrum Scanning Speed	4 spectra/s
- Mass Range	m/z 50-100

TABLE 2  
PROPERTIES OF THE MODEL COMPOUNDS SOLVENT AND INTERNAL STANDARD

Name	Structure	Molecular Weight	Boiling Point (°C)	BDE (Kcal/mol)
diphenylmethane	ph-CH <sub>2</sub> -ph	168	264	350 <sup>a</sup> ,339 <sup>a</sup>
dibenzyl ether	phCH <sub>2</sub> -O-CH <sub>2</sub> ph	198	298	330 <sup>b</sup>
diphenyl	ph-ph	154	256	480 <sup>c</sup> ,485 <sup>a</sup>
decalin		138	187.1-196.4	--

- a - Ross, D.S. et al., in: *Coal Liquefaction Fundamentals*, (Whitehurst, D.D., ed.), 1980, ACS Symposium Series 139, p. 303.  
 b - Schlosberg, R.H., et al., *Fuel*, 1981, 60, 202.  
 c - Vernon, L.W., *Fuel*, 1980, 59, 103.

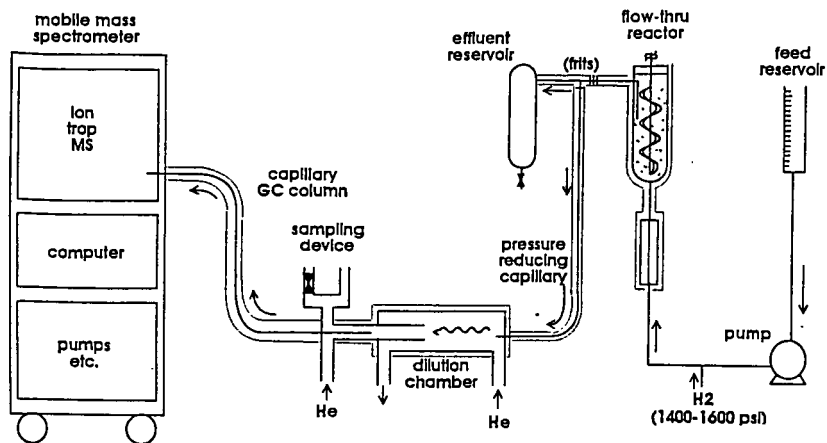


Figure 1. On-line GC/MS monitoring of high pressure reactor.

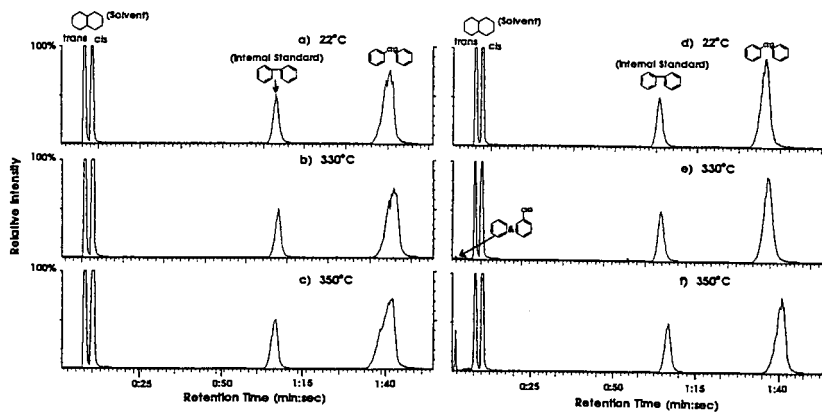


Figure 2. Total ion chromatograms of diphenylmethane at different reactor temperatures under thermal (a-c) and catalytic (d-f) conditions.

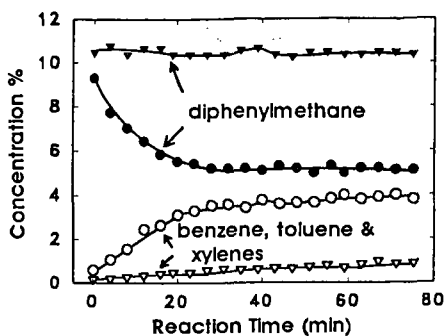


Figure 3. Kinetic profiles of the decomposition of diphenylmethane at 350 C under thermal and catalytic conditions.

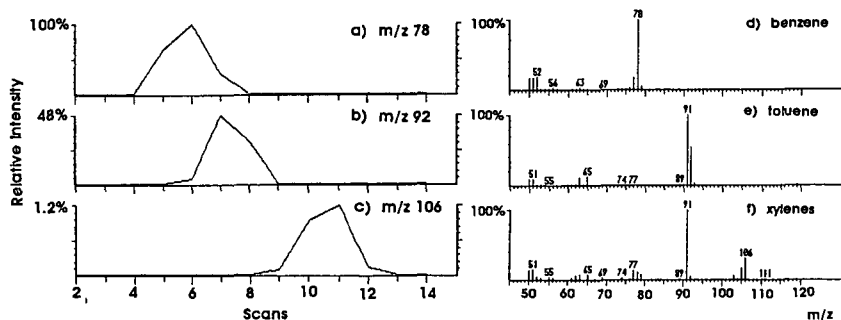


Figure 4. Typical single ion chromatograms (a-c) and corresponding mass spectra (d-f) of the products from the decomposition of diphenylmethane under catalytic conditions.

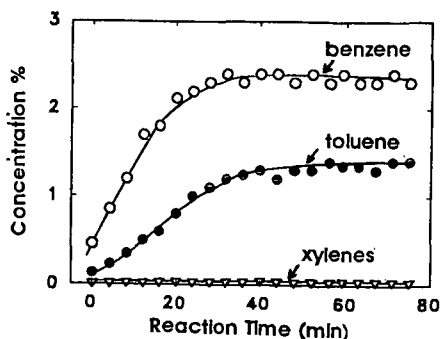


Figure 5. Relationship between reaction time at 350 C and the concentrations of the products from the decomposition of diphenylmethane under catalytic conditions.

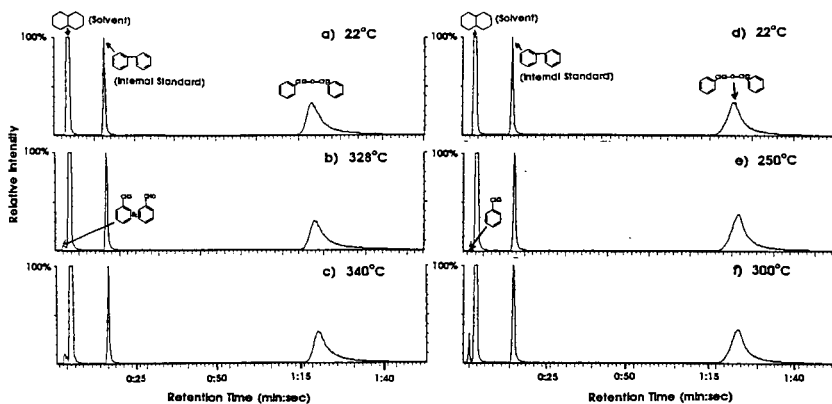


Figure 6. Total ion chromatogram of dibenzylether at different reactor temperatures under thermal (a-c) and catalytic (d-f) conditions.

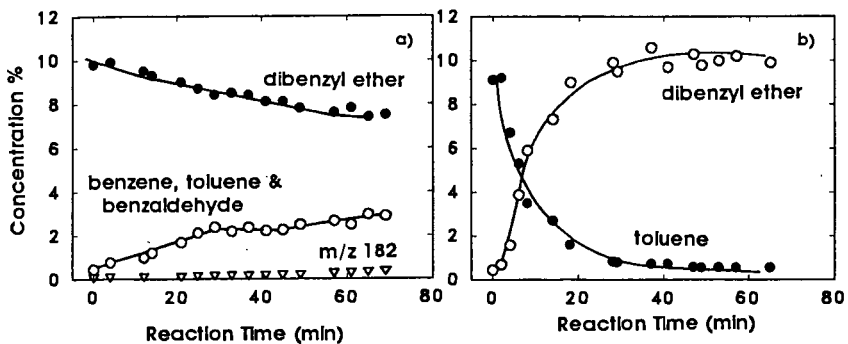


Figure 7. Kinetic profiles of the decomposition of dibenzylether under thermal (a) and catalytic (b) conditions.

**MASS SPECTROMETRIC ANALYSIS OF THE REACTION OF ISOTOPICALLY LABELLED ALCOHOLS ON GAMMA ALUMINA AND MODIFIED ALUMINA MATERIALS**

Vincent P. Nero and Elaine C. DeCanio  
Texaco Inc, Beacon, NY 12508

**INTRODUCTION**

A novel temperature programmed desorption (TPD) technique has been developed in which the direct insertion probe of a mass spectrometer is used as the reactor. This technique has been used to investigate the adsorption sites of alcohols on gamma alumina by monitoring the dehydration products and has been found to provide both greater sensitivity and a more precise experimental record for these reactions than conventional TPD techniques. Reactions involving O-18 labelled alcohol produce two isotopomeric ether products ( $R^{18}OR$  and  $R^{16}OR$ ), in addition to  $H_2^{18}O$ , and alkene. This shows that the alcohol is initially chemisorbed onto the  $Al_2O_3$  to form alkoxides via two routes, a) a dissociative adsorption on Lewis acid sites, and b) a nucleophilic attack by a surface oxide on an alcohol which is probably activated toward C-O cleavage.

Experiments involving either poisoning the alumina with 2,6-dimethylpyridine or modifying the alumina with fluorine treatments have been used to elucidate the mechanism of alkoxide formation and the dehydration reactions. Observed product distributions and temperature trends can be related to changes in the nature of the Lewis and Bronsted acid sites brought about by the inductive effect of fluorine and to site blocking by bulk  $AlF_3$  phases or dimethylpyridine.

**EXPERIMENT**

Both a Finnigan-MAT TSQ70, operating in a single quadrupole mode, and SSQ710 mass spectrometer were used. Both instruments were operated under electron impact conditions with a 70 eV ionizing potential and 200 ua ion current. The source temperature was 150°C. A mass range from 12 to 170 Daltons was scanned every 0.5 seconds.

Norton 6375C (20/40 mesh) gamma alumina with a surface area of 221.8  $m^2/g$  and a pore volume 1.4 cc/g was used for all experiments. The gamma alumina was calcined in flowing air (60 cc/min) at 500°C for 3 h and then stored in an air tight container. Approximately 0.2 g of the alumina was then transferred to a 5-ml beaker which was placed into a 25-ml sealed vessel containing about 0.5 ml of ethanol or ethanol- $^{18}O$  (99%) at room temperature and exposed to its vapor for at least 1 h. About 0.2 mg of the alumina with the absorbed alcohol was placed into a quartz insertion tube which loaded into the temperature programmed probe of the mass spectrometer. Immediately the probe was inserted into the mass spectrometer source, which is at a vacuum of  $1 \times 10^{-7}$  torr. The temperature of the sample was increased from 25°C to 300°C at a rate of 25°C per min. The probe tip was within 1 mm of the ionizing electrons which ensures that the desorbed species are immediately analyzed upon desorption from the alumina surface. This results in minimal diffusion losses and time delays and is therefore much more sensitive than conventional temperature programmed experiments.

For the experiment involving poisoning with 2,6-dimethylpyridine,

the calcined alumina was exposed to its vapor for 24 h. The poisoned alumina was then transferred to a clean vessel and exposed to the vapors of 0.5 ml ethanol- $^{18}\text{O}$ . For the experiments involving modified alumina with fluorine loading, the alumina was treated with ammonium fluoride at 2%, 5%, and 10% levels and then calcined before exposure to the alcohol.

#### RESULTS AND DISCUSSION

Reconstructed partial ion chromatograms of the reaction of ethanol (not enriched in  $^{18}\text{O}$ ) on calcined alumina are shown in Figure 1. At 25°C only desorption of physisorbed water and ethanol is observed as shown in the selected ion traces of  $m/z = 17, 18$  and  $m/z = 45, 46$ . The physisorbed water and ethanol is rapidly evolved in the vacuum of the mass spectrometer. As the temperature is increased to 100°C, diethyl ether begins to form and reaches a maximum at 200°C. This is shown in the selected ion trace  $m/z = 59, 74$ . At 210°C ethene starts to form, peaking at 260°C (selected ion trace  $m/z = 26, 28$ ). These products are the result of dehydration reactions involving ethoxide. The coproduction of water is seen in the  $m/z = 17, 18$  ion trace, which shows a broad peak with inflections corresponding to the formation of the ether and the ethene. The ether formation is a bimolecular reaction requiring the alkoxide groups to be on adjacent sites, while the alkene is presumably formed by the unimolecular elimination of water from isolated ethoxide species.<sup>1</sup>

The same experimental procedure was repeated substituting ethanol- $^{18}\text{O}$ . The ether formation splits into distinct regions as indicated in figure 2. The reaction produces two isotopomeric ether products as evidenced by the selected ion chromatograms for  $m/z = 59, 74$  and  $m/z = 61, 76$ , which correspond to  $\text{CH}_3\text{CH}_2^{18}\text{OCH}_2\text{CH}_3$  and  $\text{CH}_3\text{CH}_2^{16}\text{OCH}_2\text{CH}_3$ , respectively. The ether incorporating the  $^{18}\text{O}$  appears first and peaks at 179°C. The  $^{16}\text{O}$  ether does not reach its maximum intensity until 220°C. A summary of the peak temperatures and peak areas appear in Table I. The relative amounts of these isotopomers did not change even after the  $\text{Al}_2\text{O}_3$ -ethanol- $^{18}\text{O}$  was allowed to stand for several months. This indicates that the alkoxides leading to the ether products are irreversibly formed.

The two isotopomeric ethers originate from two different alkoxide species, one incorporating an  $^{18}\text{O}$  and the other,  $^{16}\text{O}$ . The presence of these two alkoxides suggest that alkoxide is formed via two routes. The first involves a direct reaction at a Lewis site resulting in deprotonation of the complexed alcohol and formation of  $^{18}\text{O}$ -alkoxide as shown in the upper scheme in figure 2. The second involves a reaction with a nucleophilic surface base site resulting in  $^{18}\text{OH}$  displacement and the formation of  $^{16}\text{O}$ -alkoxide, as shown in the lower scheme in figure 2. This latter pathway probably involves a secondary interaction of the alcohol hydroxyl with an adjacent acid site, since hydroxide itself is a relatively poor leaving group.

The 2,6-dimethylpyridine poisoning experiment provides further evidence for the formation of distinct alkoxide sites. This base is expected to adsorb onto either Bronsted acid sites or Lewis acid sites.<sup>2</sup> The adsorption of 2,6-dimethylpyridine prior to ethanol- $^{18}\text{O}$  adsorption has a significant effect on the ratio of ether- $^{18}\text{O}$  and ether- $^{16}\text{O}$  as shown in Table I. The untreated alumina yields ethers approximately 3:1 in favor of the  $^{18}\text{O}$  isotopomer. This ether ratio

changes to 0.6:1 for the base treated alumina. This clearly establishes that both ethers are formed from different alkoxide species and that the ether-<sup>18</sup>O is formed from an alkoxide associated with Lewis acid sites. It also shows that the relative amount of the ether-<sup>18</sup>O to the ethene actually is increased by effect of the 2,6-dimethylpyridine poisoning. This result also indicate that the ether-<sup>18</sup>O did not form at a Bronsted acid site (via protonolysis of alcohol hydroxide), since the latter would be strongly inhibited by the pretreatment with 2,6-dimethylpyridine; this would have led to a decrease in the ratio of ether-<sup>18</sup>O to ethene, rather than the observed increase.

Modification of alumina by fluorine treatment is known to increase the Bronsted acid character of the surface.<sup>3</sup> At 2% fluorine loadings the observed ether and ethene distributions show no significant changes, although the peak temperatures of various reactions

increased substantially, probably due to the the inductive effect of the fluorine. (Table I) At the 5% fluorine level the peak temperatures have increased to the point of favoring elimination as the major reaction pathway. The yield of the ether-<sup>18</sup>O is greatly reduced since the fluorine is now occupying sites previously occupied by the <sup>18</sup>O ethoxide. At the 10% fluorine level even the ether-<sup>18</sup>O is reduced. This can be attributed to site blocking due to the formation of bulk AlF<sub>3</sub> on the alumina surface.

1. Knozinger, H., Kockloefl, K. and Meyer, W., J. Catal., 28, 69 (1973)

2. Matulewicz, E. R. A., Kerhof, F. P. J. M., Moulign, J. A. and Reitsma, H. J., J. Coll. Interface Sci., 77, 110 (1980).

3. Ghosh, A. K, and Kydd, R. A., Catal. Rev. [Sci. Eng., 27 [4], 539-589 [1985]

TABLE I  
PEAK TEMPERATURES AND PRODUCT DISTRIBUTIONS  
FOR ETHANOL-<sup>18</sup>O ON ALUMINA AND MODIFIED ALUMINA

ALUMINA	PRODUCT	PEAK TEMP	Ethene to Et <sup>18</sup> OEt	Ethene to Et <sup>16</sup> OEt	Et <sup>18</sup> OEt to Et <sup>16</sup> OEt
UNTREATED	Et <sup>18</sup> OEt	179	22	69	3.2
	Et <sup>16</sup> OEt	220			
	Ethene	261			
2,6-DIMETHYL PYRIDINE	Et <sup>18</sup> OEt	220	36	23	.62
	Et <sup>16</sup> OEt	275			
	Ethene	286			
2% FLUORINE	Et <sup>18</sup> OEt	240	20	58	3.0
	Et <sup>16</sup> OEt	266			
	Ethene	295			
5% FLUORINE	Et <sup>18</sup> OEt	256	260	86	.32
	Et <sup>16</sup> OEt	269			
	Ethene	285			
10% FLUORINE	Et <sup>18</sup> OEt	260	120	290	2.4
	Et <sup>16</sup> OEt	280			
	Ethene	287			

FIGURE 1

ETHANOL

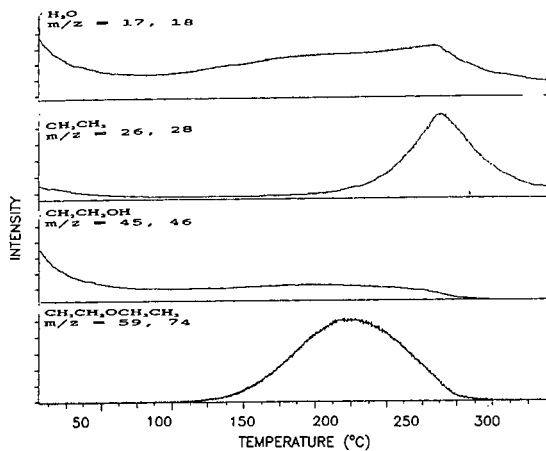
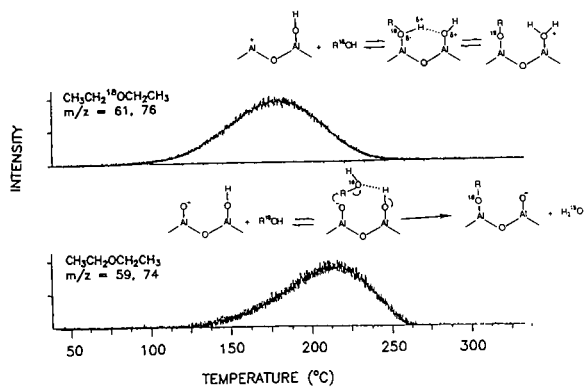


FIGURE 2

ETHANOL- $^{18}\text{O}$



# HYDROGENOLYSIS MECHANISMS FOR POLYCYCLIC ALKYLARENES

C. Michael Smith and Phillip E. Savage\*  
University of Michigan, Department of Chemical Engineering  
Ann Arbor, MI 48109-2136

**KEYWORDS:** Alkylpyrenes, Hydrogenolysis, Pyrolysis

## INTRODUCTION

Recent neat pyrolyses of polycyclic alkylaromatics have demonstrated the relatively facile cleavage of strong aryl-alkyl bonds.<sup>1-7</sup> Because these compounds mimic the analogous moieties in coal and oil, their reaction pathways and mechanisms provide insight to reactions occurring in co-processing, coal liquefaction and gasification, and heavy oil upgrading and coking. The hydrogenolysis mechanisms responsible for aryl-alkyl C-C bond cleavage in alkylarenes have not been fully elucidated, but the literature does provide some possibilities.<sup>6-8</sup>

We desired to understand this hydrogenolysis more completely and to employ this understanding to develop a general mechanistic model for alkylarene pyrolysis that was consistent with experimental observations. A general mechanistic reaction model can be developed by conducting experiments with different alkylarenes, taking advantage of results in the literature, and employing the principles embodied in thermochemical kinetics and molecular orbital (M.O.) theory. We have previously reported experimental data (e.g., product molar yields, selectivities, rate constants) for a large number of n-alkylarenes, and we proposed a general pyrolysis network.<sup>3</sup> We also conducted experimental studies using probe molecules to explore different mechanistic scenarios for the hydrogenolysis.<sup>1,2</sup> This paper reports our initial activities aimed at developing a general mechanistic model. We have relied on our experimental results and the literature to provide probable elementary reaction steps, and we used thermochemical kinetics and M.O. theory to estimate their reaction rate constants. Our initial mechanistic models explore the pyrolysis of 1-methyl- and 1-ethylpyrene. Our logic for studying these compounds is twofold. First, the mechanisms responsible for the cleavage of the aryl-alkyl bond in methyl- and ethylpyrene must also be operative during the pyrolysis of alkylarenes with longer chains. Second, the pyrolysis of these compounds leads to a smaller number of products than does the pyrolysis of long-chain alkylarenes. Thus, there is a smaller pool of species from which the hydrogenolysis agents can be chosen, and this reduces the complexity of the mechanistic models. Additionally, for methylpyrene neither  $\alpha$ -alkylpyrene radicals nor aliphatic radicals can participate in the radical hydrogen transfer reactions that others have suggested as potential hydrogenolysis steps<sup>6,8</sup> for long-chain alkylpyrenes. Thus, it is apparent that the simplicity of these pyrolysis systems makes them convenient initial tools for probing different mechanistic scenarios and developing more complex mechanistic models for long-chain alkylarenes.

## EXPERIMENTAL

1-Methylpyrene and 1-ethylpyrene pyrolyses were conducted neat at 400, 425, and 450°C in constant-volume, 316 stainless steel, micro-batch reactors. The reactors were typically loaded with about 10 mg of alkylpyrene and 10 mg of o-terphenyl as an internal standard. After being loaded, the reactors were purged and sealed in a nitrogen-filled glove box and then placed in an isothermal, fluidized sand bath. Upon reaching the desired holding time, the reactors were removed from the fluidized bath, and the reaction was quenched. The products were recovered by repeated extraction with benzene. The reaction products were identified by gas chromatography-mass spectrometry, and their molar yields (i.e., moles of product formed/moles of reactant loaded in reactor) were quantified by capillary column gas chromatography. Details about the experimental protocol have been given previously.<sup>1-4</sup>

## EXPERIMENTAL RESULTS

**1-Methylpyrene:** The pyrolysis of methylpyrene led to pyrene and dimethylpyrene as the major products, and Table I lists the molar yields of these products at different reaction conditions. The minor products included a second dimethylpyrene isomer, ethylpyrene, and four trimethylpyrene isomers. Of these minor products, only the dimethylpyrene isomer was present in yields sufficiently high to quantify. Its molar yield increased steadily at all three

temperatures, and its maximum yield was 1.8% at 150 minutes at 450°C. The recovery of pyrene moieties in the quantified products ranged from nearly 100% to a low of 72% for the reaction at 450°C and 300 minutes. The failure to achieve 100% recovery at the more severe reaction conditions is likely due to the formation of high molecular weight products that did not elute from the GC.

**1-Ethylpyrene:** The pyrolysis of ethylpyrene led to pyrene and methylpyrene as major products, and Table II lists representative results from these experiments. The minor/trace products were diethylpyrene, methylethylpyrene, vinylpyrene, dihydropyrene and a benzene-insoluble char. The molar yield of diethylpyrene typically reached a maximum and then decreased with time. Vinylpyrene and methylethylpyrene were only observed in trace quantities, so their yields were not quantified. The lowest recovery of pyrene units in the quantified products was 72% for the reaction at 450°C and 72 minutes.

#### MECHANISTIC MODELING AND RESULTS

The development of mechanistic models for methyl- and ethylpyrene pyrolysis was guided by experimental observations, by previous mechanistic models for toluene and ethylbenzene pyrolysis, and by previous investigations into the pyrolysis of polycyclic aromatic hydrocarbons. We simulated the pyrolyses using *AcuChem*, a software package developed by the National Institute of Standards and Technology.<sup>9</sup> The program sets up and solves the differential equations that describe species' concentrations as a function of time for reactions in a constant-volume batch reactor.

**1-Methylpyrene:** The 18 elementary step free-radical reaction mechanism used to describe the pyrolysis of methylpyrene is depicted in Figure 1. Methylpyrene undergoes initiation through two possible routes: unimolecular homolytic dissociation and bimolecular reverse radical disproportionation (RRD).<sup>10,11</sup> Chain propagation proceeds via radical hydrogen transfer (RHT),<sup>12</sup> H-atom and methyl radical addition, and methyl radical and H-atom elimination. Finally, termination occurs through the recombination and disproportionation of methylpyrenyl radicals and alkyldihydropyrenyl radicals. This mechanism omits potential secondary reactions such as RRD of dimethylpyrene molecules or RHT to pyrene molecules. Thus, this model will be most valid at low methylpyrene conversions where these secondary reactions are unimportant. The Arrhenius parameters estimated for each step in Figure 1 are listed in Table III, and details of the estimation procedure are given elsewhere.<sup>4</sup>

Figure 2 displays the comparison of the model prediction and experimental observation for the temporal variation of product yields from methylpyrene pyrolysis at 425°C. The model (solid lines) predicts the experimental data (discrete points) well at conversions less than 30%. At higher conversions, however, the model tended to underpredict methylpyrene reactivity. This lack of quantitative agreement at higher conversions could be due to the model's omission of secondary reactions. For example, pyrene could serve as a hydrogen acceptor in RRD reactions, but the model does not include such steps. If it had, the predicted reactivity of methylpyrene would have increased. Overall, however, the agreement between the calculated and the experimental molar yields was reasonably good.

Figure 3 displays the model's prediction of the rates of RRD (reaction 2), RHT (reactions 4 and 5) and H-atom addition (reaction 8), reactions that add hydrogen to the ipso position in methylpyrene, as a function of conversion for the pyrolysis at 425°C. The results at 400 and 450°C were similar to those presented in Figure 3. It is apparent from Figure 3 that the rate of H-atom ipso substitution is typically lower than the rates of RHT and RRD. The rate of RHT by methylhydropyrenyl radicals (step 4) is initially faster than the rate of RRD, but at a conversion of about 0.1 the rate of RRD becomes more significant. The model predicted that this transition point occurred at methylpyrene conversions of about 0.2 and less than 0.1, respectively for pyrolysis at 400°C and 450°C, respectively. Thus, the importance of RHT by methylhydropyrenyl radicals relative to RRD decreases as temperature increases.

The rates of RHT by dimethylhydropyrenyl radicals (step 5) and H-atom substitution (step 8) are lower than those of steps 2 and 4. At 425°C, the rate of RHT by dimethylhydropyrenyl radicals is greater than the rate of H-atom substitution for methylpyrene conversions less than about 0.68. At conversions greater than 0.68, there is a shift in the

importance of these two steps as the rate of step 8 becomes greater than the rate of step 5. This behavior was also observed at the other temperatures studied. For example, at 400 and 450°C, respectively, this transition occurred at methylpyrene conversions of 0.85 and 0.48, respectively. This trend suggests that the importance of step 8 relative to step 5 increases as the temperature increases. This observation that H-atoms become more important as the temperature increases is consistent with previous work.<sup>6,13</sup>

The results of the pyrolysis simulation have revealed that the relative importance of RHT by methylhydropyrenyl radicals decreases and the role of H-atoms increases with increases in temperature. This behavior arises because high temperatures favor  $\beta$ -scission of hydropyrenyl radicals to yield a hydrogen atom rather than direct hydrogen transfer by RHT. This is because the  $\beta$ -scission step has the higher activation energy. Thus, at higher temperatures there is a greater concentration of hydrogen atoms and consequently a higher rate of H-atom ipso substitution.

**1-Ethylpyrene:** The free-radical mechanism for ethylpyrene pyrolysis is shown in Figure 4, and the estimated Arrhenius parameters for each elementary step are summarized in Table IV. Details of their estimation have been discussed elsewhere.<sup>4</sup> As was the case for methylpyrene pyrolysis, initiation in ethylpyrene proceeds through both homolytic dissociation and RRD. The resulting radicals propagate the chain through hydrogen abstraction, RHT, and addition/elimination reactions. Termination proceeds through radical disproportionation.

Figure 5 compares the model predictions and the experimental molar yields of ethylpyrene at 400, 425, and 450°C. Inspection of Figure 5 reveals essentially quantitative accord between the model calculations and the experimentally determined yields of ethylpyrene. Although the model accurately predicted the kinetics of ethylpyrene disappearance, it underpredicted the amount of pyrene and methylpyrene formed, and it overpredicted vinylpyrene formation. For example, at a batch holding time of 150 minutes and at a pyrolysis temperature of 425°C, the predicted molar yields of vinylpyrene, pyrene, and methylpyrene are 0.36, 0.36 and 0.008 respectively. Experimentally, however, vinylpyrene was not observed, and the molar yields of pyrene and methylpyrene were 0.47 and 0.08. One reason for this discrepancy is that the model, which focuses on the primary reactions, does not include the secondary decomposition reactions available for vinylpyrene. Omitted reactions include vinylpyrene polymerization, its reduction to ethylpyrene, and its decomposition to pyrene or methylpyrene. The kinetics and mechanisms of these reactions are not completely resolved and it is for this reason that they were not included in the model. If such steps were included, however, the model would predict a much lower yield of vinylpyrene and increased molar yields of methylpyrene and pyrene as observed experimentally.

Examination of Figure 6, which displays the rates of different elementary reaction steps at 425°C as a function of ethylpyrene conversion, reveals the relative importance of each of the different hydrogen addition mechanisms. Step 15, RHT by ethylhydropyrenyl radicals has the fastest rate of reaction. The next fastest hydrogenolysis step is RRD (step 2) followed by H-atom addition (step 13), RHT by ethyl radicals (step 20), and RHT by  $\alpha$ -ethylpyrene radicals (step 19). The trends that are depicted in Figure 6 were also observed for the simulations at 400 and 450°C. As was observed for the pyrolysis simulation of methylpyrene, RHT by alkylhydropyrenyl radicals and RRD are the major steps that lead to aryl-alkyl bond cleavage. The rates of the other hydrogenolysis steps, however, are not insignificant and can not be ignored. Indeed, the relative importance of H-atoms in ethylpyrene pyrolysis at high conversions stands in contrast to the model results for 1-methylpyrene where H atoms had a less significant contribution to the total hydrogenolysis rate. The increased role of H-atoms in ethylpyrene pyrolysis is likely due to their production through the  $\beta$ -scission of  $\alpha$ -ethylpyrene radicals. To summarize, the results of this simulation suggest that all of the modes of hydrogenolysis included in the simulation can be important in engendering aryl-alkyl bond cleavage in 1-ethylpyrene pyrolysis.

## CONCLUSIONS

1. Hydrogenolysis was the dominant reaction during the neat pyrolysis of methylpyrene. The major pyrolysis products were pyrene and dimethylpyrene. This experimental observation is noteworthy because radical hydrogen transfer by alkyl radicals or by  $\alpha$ -alkylpyrene radicals is not an operable mechanism in this system.

2. The pyrolysis of ethylpyrene led to pyrene and methylpyrene as the major products with pyrene being present in much higher yields. The rate of hydrogenolysis for ethylpyrene was greater than that for methylpyrene.

3. Mechanistic modeling of methylpyrene and ethylpyrene pyrolysis revealed that RRD played an important role in adding hydrogen to the ipso-position and in generating alkylhydropyrenyl radicals that then participated in radical hydrogen transfer steps. In the pyrolysis of methylpyrene, alkylhydropyrenyl radicals generated from methyl radical addition were also hydrogenolysis agents. In ethylpyrene pyrolysis alkylhydropyrenyl radicals were also largely responsible for hydrogenolysis along with contributions from H-atoms, ethyl radicals, and  $\alpha$ -ethylpyrene radicals.

#### ACKNOWLEDGEMENTS

We thank Steven Sherman and Joseph Gullo for performing the methylpyrene pyrolysis experiments. This work was supported in part by the Link Foundation, the Shell Faculty Career Initiation Fund, and the National Science Foundation (CTS-8906859). Acknowledgement is also made to the donors of the Petroleum Research Fund (ACS-PRF # 23744-AC4), administered by the ACS, for the partial support of this research.

#### LITERATURE CITED

1. Smith, C. M.; Savage, P. E. *Ind. Eng. Chem. Res.* **1991**, *30*, 331-339.
2. Smith, C. M.; Savage, P. E. *Energy & Fuels* **1991**, *5*, 146-155.
3. Smith, C. M.; Savage, P. E. *AIChE Journal* **1991**, *37*, 1613-1624.
4. Smith, C. M.; Savage, P. E. *Energy & Fuels* **1992**, *6*, in press.
5. Savage, P. E.; Jacobs, G. E.; Javanmardian, M. *Ind. Eng. Chem. Res.* **1989**, *28*, 645-652.
6. Freund, H.; Maturro, M. G.; Olmsted, W. N.; Reynolds, R. P.; Upton, T. H. *Energy & Fuels*. **1991**, *5*, 840-846.
7. Vlasnik, V. J.; Virk, P. Paper 139D *AIChE Annual Meeting*, Chicago, **1990**.
8. McMillen, D. F.; Malhotra, R.; Tse, D. S. *Energy & Fuels* **1991**, *5*, 179-187.
9. Braun, W.; Herron, J. T.; Kahanen, D. K. *Int. J. Chem. Kinet.* **1988**, *20*, 51-62.
10. Billmers, R.; Brown, R. L.; Stein, S. E. *Int. J. Chem. Kinet.* **1989**, *21*, 375-389.
11. Billmers, R.; Griffith, L. L.; Stein, S. E. *J. Phys. Chem.* **1986**, *90*, 517-523.
12. McMillen, D. F.; Malhotra, R.; Chang, S. J.; Olgier, W. C.; Nigenda, S. E.; Fleming, R. H. *Fuel* **1987**, *66*, 1611-1620.
13. McMillen, D. F.; Malhotra, R.; Nigenda, S. E. *Fuel* **1989**, *68*, 380-386.

**TABLE I: MOLAR YIELDS OF MAJOR PRODUCTS FROM 1-METHYLPYRENE PYROLYSIS**

TEMP (°C)	400	400	400	400	400	400	400
TIME (min)	30	60	90	120	150	240	300
PYRENE	0	0.01	0.01	0.01	0.02	0.05	0.06
DIMETHYLPYRENE	0	0.00	0.01	0.01	0.01	0.03	0.04
METHYLPYRENE	1.01	1.05	0.98	1.03	0.95	0.87	0.85
TEMP (°C)	425	425	425	425	425	425	425
TIME (min)	30	60	90	120	165	240	300
PYRENE	0.01	0.05	0.07	0.1	0.15	0.22	0.22
DIMETHYLPYRENE	0	0.04	0.04	0.06	0.09	0.12	0.11
METHYLPYRENE	0.97	0.90	0.90	0.83	0.67	0.57	0.54
TEMP (°C)	450	450	450	450	450	450	450
TIME (min)	30	60	90	120	150	240	300
PYRENE	0.06	0.15	0.22	0.26	0.31	0.39	0.37
DIMETHYLPYRENE	0.03	0.08	0.10	0.10	0.09	0.01	0.01
METHYLPYRENE	0.88	0.66	0.50	0.42	0.41	0.35	0.35

**TABLE II: MOLAR YIELDS OF MAJOR PRODUCTS FROM 1-ETHYLPYRENE PYROLYSIS**

TEMP (°C)	400	400	400	400	400	400	400
TIME (min)	45	70	90	110	150	200	320
PYRENE	0.20	0.47	0.13	0.37	0.44	0.61	0.60
METHYLPYRENE	0.02	0.05	0.01	0.04	0.05	0.11	0.11
ETHYLPYRENE	0.91	0.80	0.82	0.52	0.47	0.41	0.26
TEMP (°C)	425	425	425	425	425	425	425
TIME (min)	65	80	115	135	150	180	205
PYRENE	0.52	0.49	0.54	0.64	0.47	0.61	0.62
METHYLPYRENE	0.07	0.08	0.10	0.11	0.09	0.07	0.13
ETHYLPYRENE	0.55	0.41	0.32	0.33	0.18	0.13	0.17
TEMP (°C)	450	450	450	450	450	450	450
TIME (min)	20	30	42	50	60	72	80
PYRENE	0.45	0.48	0.56	0.47	0.68	0.48	0.74
METHYLPYRENE	0.08	0.08	0.10	0.10	0.14	0.11	0.13
ETHYLPYRENE	0.58	0.46	0.25	0.19	0.17	0.13	0.13

TABLE III: ARRHENIUS PARAMETERS FOR 1-METHYLPYRENE PYROLYSIS

Reaction Number in Figure 1	$\log_{10} A$ ( $s^{-1}$ or Liter mole $^{-1} s^{-1}$ )	Activation Energy (kcal mole $^{-1}$ )	Reaction Path Degeneracy
1	16	82.9	3
2	8	45.8	6
3	8	45.8	18
-3	9.5	0	-
4	8.1	16.5	2
5	8.1	16.5	1
6	8.1	16.5	3
7	10.4	2.3	3
8	10.4	2.3	1
9	8.8	4.1	3
-9	13.9	29.4	1
10	13.9	35.3	2
11	13.9	29.4	1
12	11.1	5.6	3
13	8.5	6.9	3
14	9.5	0	-
-14	16	51.2	1
15	9.5	0	-

TABLE IV: ARRHENIUS PARAMETERS FOR 1-ETHYLPYRENE PYROLYSIS

Reaction Number in Figure 4	$\log_{10} A$ ( $s^{-1}$ or Liter mole $^{-1} s^{-1}$ )	Activation Energy (kcal mole $^{-1}$ )	Reaction Path Degeneracy
1	16	69.6	1
2	8	42.8	4
3	8	42.8	12
4	14.0	53.6	3
5	13.9	35.3	2
6	14	20	1
7	12.9	38.4	3
8	11.1	5.6	2
9	8.5	5.4	2
10	8.5	8.9	2
11	8.8	15.5	2
12	10.3	2.3	3
13	10.3	2.3	1
14	9	6	3
15	8.1	16.5	2
16	8.1	16.5	1
17	8.1	16.5	3
18	8.1	25	9
19	8.1	25	3
20	8.4	14.5	3
21	8.4	14.5	9
22	9.5	0	-
23	9.5	0	-

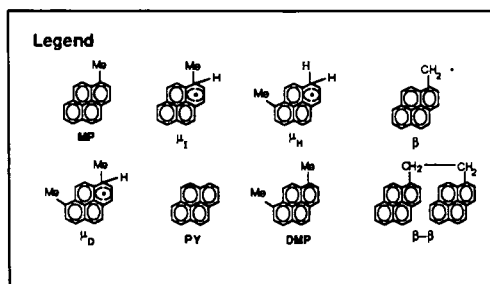
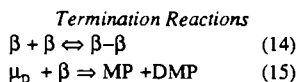
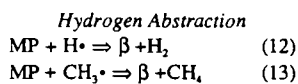
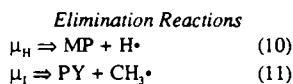
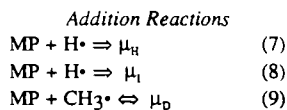
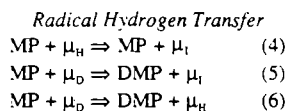
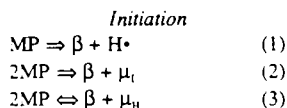


Figure 1: 1-Methylpyrene Pyrolysis Mechanism

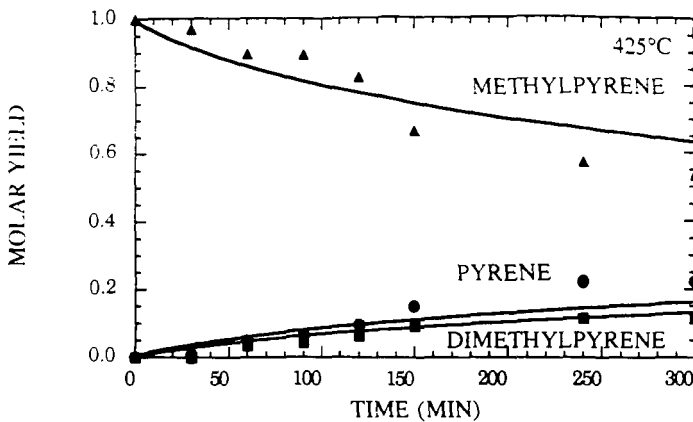


Figure 2: Model and Experimental Results for 1-Methylpyrene Pyrolysis at 425°C

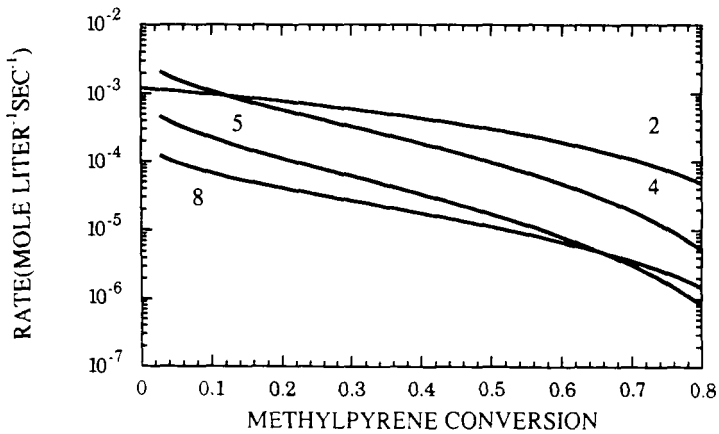


Figure 3: Hydrogenolysis Rates Calculated for 1-Methylpyrene Pyrolysis at 425°C (step 2 is RRD, steps 4 and 5 are RHT, step 8 is H atom addition)

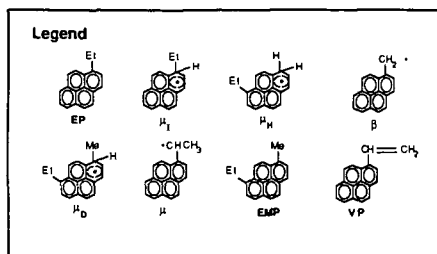
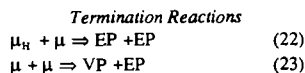
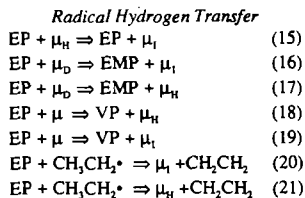
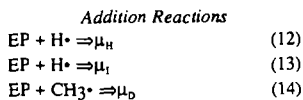
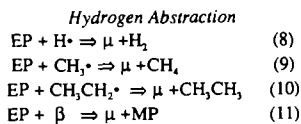
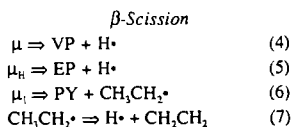
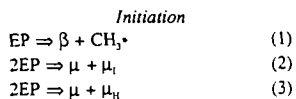


Figure 4: 1-Ethylpyrene Pyrolysis Mechanism

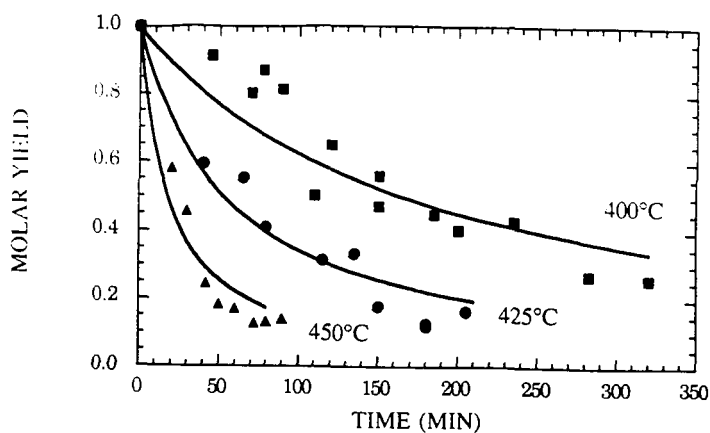


Figure 5: Model and Experimental Results for 1-Ethylpyrene Pyrolysis Kinetics

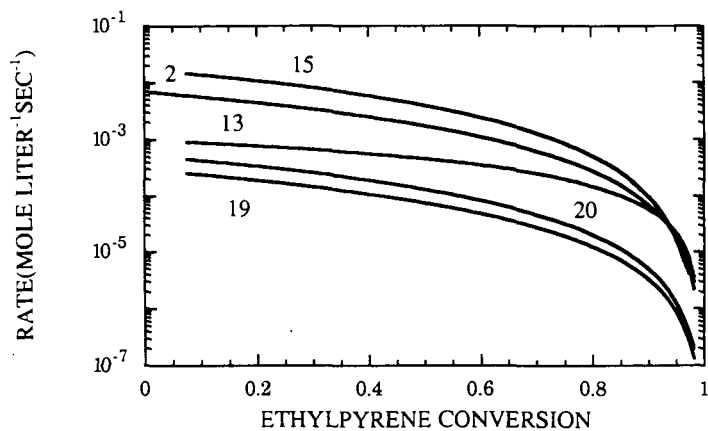


Figure 6: Hydrogenolysis Rates Calculated for 1-Ethylpyrene Pyrolysis at 425°C (step 2 is RRD, step 15 is RHT by ethylhydropyrenyl radicals, step 13 is H atom addition, step 20 is RHT by ethyl radicals, and step 19 is RHT by  $\alpha$ -ethylpyrene radicals)

## PATHWAYS FOR THERMOLYSIS OF 9,10-DIMETHYL-ANTHRACENE.

**P.S. Virk and V.J. Vlastnik**

Department of Chemical Engineering, M.I.T., Cambridge, MA 02139.

**Keywords:** Reaction Paths, Pyrolysis, Kinetics, Demethylation

**ABSTRACT.** We report experiments on thermolysis of 9,10-dimethyl-anthracene (DMA) at temperatures from 315-409 C with initial concentrations from 0.1-3.0 M. Substrate conversions ranged from 0.05 to 0.98 with quantitative assays of major products. The substrate appears to decompose primarily by two parallel pathways, namely, demethylation (major) to 9-methyl-anthracene (MA) plus methane and disproportionation (minor) to MA plus tri-methyl-anthracenes (TMA). These reactions are also associated with hydrogen transfer, as inferred from the detection of 9,10-dihydro-9,10-dimethyl-anthracenes (DHDMA). At the higher substrate conversions, the primary reaction products appear to be secondarily operated upon by a parallel pathway pair analogous to the primary pair, eventually forming anthracene (ANT). Also, minor amounts of the 1- and 2-methyl-anthracenes (1MA, 2MA) were detected, both arising subsequent to the appearance of the parent acene. A preliminary mechanism is presented for DMA thermolysis, based on elementary free-radical and molecular reactions relevant to the present conditions, combined with the experimentally observed kinetics and product selectivities. Also, frontier-orbital theory is applied to model the observed 1MA and 2MA isomer distributions.

### INTRODUCTION

The present work on DMA thermolysis is part of a continuing study of simple substrates that mimic the chemical moieties found in complex fossil materials of engineering interest. DMA was chosen for two reasons. First, its acene aromatic ring system is prototypical of the aromatic molecules found in fossil fuels, and its methyl moieties model the electron donating substituents commonly pendant on the aromatic rings of natural materials. Second, its thermal destruction is of environmental interest, the intermediate decomposition product, MA, being far more toxic than either the original DMA or the final ANT.

There appear to be no previous studies of DMA thermolysis in the literature, save for a preliminary investigation in our laboratories (Pope 1987) that is elaborated here. However, the literature does contain references to pyrolyses of the related MA (Pomerantz 1980) and ANT (Stein 1981) substrates.

In outline, we briefly describe the experimental approach and present representative results for the concentration histories and product selectivities observed during DMA thermolysis. Reaction pathways inferred from these results are then summarized, leading to a preliminary mechanism for the early stages of DMA thermolysis. Finally, frontier orbital theory is applied to understand the formation of certain minor methylated products.

### EXPERIMENTAL

The chemicals used, DMA (Aldrich 99% purity), biphenyl (BIP) (Aldrich 99% purity) and methylene chloride (EM Science omnisolv), were all obtained commercially and used as received.

Pyrolyses were conducted in batch reactors, volume 0.49 ml, made from 1/4" stainless steel Swagelok parts. The reactors, purged with inert gas, were charged with weighed amounts of biphenyl (internal standard) and DMA substrate totalling 0.30 g, sealed, and placed in an isothermal, fluidized-sand, bath for the appropriate holding time, after which they were quenched in ice-water, and their contents extracted into methylene chloride. Based on their

melting and critical properties, the biphenyl and DMA reactor contents were in the liquid phase during all experiments.

Products were identified and assayed by an HP-5890 Series II Gas Chromatograph equipped with flame ionization (FID) and thermal conductivity (TCD) detectors and on-column and split/splitless injectors. Liquid products were analysed using on-column injection, a 25m HP-101 column, and the FID. Product concentrations were calculated from experimentally determined response factors, using biphenyl as internal standard. Identified compounds typically accounted for >90% of total product mass at low fractional substrate conversions,  $X < 0.4$ , but only about 70% of total product mass at the highest conversions,  $X > 0.8$ .

Figure 1 shows the experimental grid traversed, DMA being pyrolysed at initial concentrations from 0.1 to 3.0 M, temperatures between 315 and 409 C, and holding times from 450 to 28800 s.

## RESULTS

Representative concentration histories obtained during DMA pyrolysis at  $T = 409$  C and  $[DMA]_0 = 1.0$  M are chronicled in Figure 2, with coordinates absolute mols of each identified compound,  $j$ , versus time,  $s$ . The plot clearly depicts the continuous decay of substrate DMA, the initial growth, maximum, and final decay exhibited by the primary product MA, and the initial absence and final growth of the secondary product ANT. The major thermolysis pathways evidently involve the demethylation sequence  $DMA \rightarrow MA \rightarrow ANT$ . Closer scrutiny reveals small amounts of TMA at low times, and the formation of methyl-anthracenes, with  $1MA > 2MA$ . Also, though not seen in Figure 2, small amounts of DHDMA were clearly visible at lower temperatures. The minor thermolysis pathways thus involve methylations of both the DMA substrate and the ANT final product, as well as hydrogen transfers that lead to DHDMA.

Additional insights into the operative pathways are offered by the selectivity diagram in Figure 3, which shows the selectivity  $S(j)$ , that is, (mols  $j$  formed/mol DMA reacted), versus conversion. For low  $X < 0.6$ , it is seen that both  $S(MA) \sim 0.5$  and  $S(TMA) \sim 0.1$  are essentially constant, implying that MA and TMA are both primary products of DMA thermolysis, resulting from parallel pathways that are respectively fast and slow. For high  $X > 0.6$ , the mirror-image decrease in  $S(MA)$  and increase in  $S(ANT)$  is evidence that ANT is a secondary product, arising from the primary product MA. Too,  $S(1MA)$  and  $S(2MA)$  are each essentially zero for  $X < 0.6$ , where  $S(MA)$  is large, and increase only for  $X > 0.6$ , when  $S(ANT)$  becomes appreciable. This timing implies that the 1MA and 2MA arise from methylation of ANT, and not from isomerization of MA.

## PATHWAYS

Pathways for thermolysis of DMA, inferred from results over the entire experimental grid, are summarized in Figure 4. The main demethylation sequence, shown bold, cascades from DMA to MA to ANT. Compounds in the main sequence are all subject to methylation, forming the various methyl substituted anthracenes shown to the right, but neither MA nor DMA isomerize to their positional isomers. DMA is also hydrogenated to DHDMA (cis- and trans-isomers not distinguished). In overall, unbalanced, terms, based on detected products, the primary parallel reactions of DMA are:

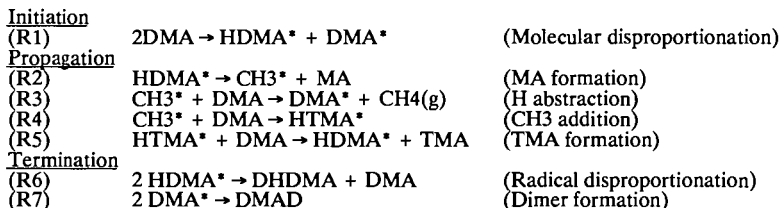
- (RO1) Demethylation      fast    **DMA  $\rightarrow$  MA (+ CH<sub>4</sub> + heavy products)**
- (RO2) Disproportionation    slow    **DMA  $\rightarrow$  MA + TMA**
- (RO3) Hydrogenation        slow    DMA  $\rightarrow$  DHDMA

A similar set of three pathways presumably operates on MA, by analogy, but we have evidence only of the demethylation step, forming ANT.

Kinetic information was also derived from the experiments that delineated the DMA thermolysis pathways. At  $T = 355\text{ C}$ , initial conversion data for  $0.1 < [\text{DMA}]_0 < 3.0\text{ M}$  suggested that the overall decomposition was  $\sim 3/2$  order in DMA. For fixed  $[\text{DMA}]_0 = 1.0\text{ M}$ , initial conversion data at temperatures  $315 < T < 409\text{ C}$ , showed an apparent activation energy  $\sim 55\text{ kcal/mol}$ .

#### MECHANISM

A possible mechanism for the early stages of DMA thermolysis, that is consistent with the present pathway and kinetic observations, is enumerated below and illustrated by the "Tolman clock" formalism in Figure 5. The elementary molecular and free-radical steps are:



The initiation reaction, (R1), involves H atom transfer from the methyl of one DMA molecule to the 9 position of another, forming the corresponding  $\text{DMA}^*$  and  $\text{HDMA}^*$  radicals. The propagation sequences involve two parallel clocks that respectively form either  $\text{MA} + \text{CH}_4$  (R2 + R3) or  $\text{TMA} + \text{MA}$  (R2 + R4 + R5); the latter slower than the former by the kinetic ratio  $R_4/R_3 \sim S(\text{TMA})/S(\text{MA}) \sim 0.2$ . Of the termination steps, (R6), the disproportionation of chain-carrying  $\text{HDMA}^*$  radicals, accounts for the observed  $\text{DHDMA}$  product. However, there is yet no independent evidence for (R7), the combination of  $\text{DMA}^*$  radicals to form dimer, although unidentified heavy products do indeed arise.

Steady-state analysis of the preceding mechanism indicates that the observed reaction orders wrt  $[\text{DMA}]$  should respectively be 1 and 2 for terminations controlled by (R6) and (R7); these bracket the experimentally observed order of  $3/2$ .

#### FRONTIER ORBITAL MODEL

The observed formations of 1MA and 2MA from ANT during DMA thermolysis at high severities invite interpretation according to frontier orbital theory, as examples of periselective methyl radical attack on the ANT nucleus. Following Fukui (1975), an interaction diagram for this system is shown in Figure 6. The corresponding expression for the FMO stabilization energy is given in the bottom line of the figure, using the coefficients and energies of the  $\text{CH}_3$  radical SOMO (singly-occupied MO) and the ANT HOMO and LUMO (highest occupied and lowest unoccupied MOs). The evaluation of these expressions is depicted graphically in Figure 7. Here each position on the ANT ring framework is decorated with its HOMO coefficients,  $C_t(\text{HO})$ , derived from MINDO calculations (Clark 1985, Dewar 1970), and then positions 9, 1, and 2 are shown interacting with the methyl radical SOMO, having  $C_u(\text{SO}) = 1$ . The resulting, favourable, nondimensional stabilization energy, denoted  $\Delta E'(\text{FMO})$ , is respectively 0.232 and 0.117 at positions 1 and 2 (position 9 is not in contention here). FMO theory thus predicts methyl radical attack favoured in the order position 1 >

position 2. The latter inequality accords with the experimental observation, from Figures 2 and 3, that  $1MA > 2MA$ .

### CONCLUSIONS

1. Thermal decomposition of DMA was experimentally studied at  $0.1 < [DMA]_0 < 3.0$  M,  $315 < T < 409$  C, covering fractional substrate conversions  $0.05 < X < 0.98$ .
2. DMA decomposition pathways included:  
 (RO1) Demethylation fast  $DMA \rightarrow MA (+ CH_4 + \text{heavy products})$   
 (RO2) Disproportionation slow  $DMA \rightarrow MA + TMA$   
 (RO3) Hydrogenation slow  $DMA \rightarrow DHDMA$
3. The MA product decomposed by pathways analogous to DMA.
4. At low conversions, DMA decomposition was  $\sim 3/2$  order in DMA, with apparent activation energy  $E^* \sim 55$  kcal/mol.
5. A mechanism was devised for DMA decomposition, comprizing 7 elementary steps. This accounted for the reaction products and kinetics observed at low DMA conversions.
6. Minor products 1MA and 2MA observed at high DMA conversions appeared to arise from ANT methylation rather than 9MA isomerization.
7. The relative amounts of 1MA and 2MA observed experimentally were interpreted by FMO theory, as periselective methyl radical additions.

### REFERENCES

- Clark, T.: "A Handbook of Computational Chemistry", Wiley, New York (1985).  
 Dewar, M.J.S.; Haselbach, E.; Worley, S.D.: *Proc. Roy. Soc. Lond.* **A315**, 431 (1970).  
 Fukui, K: "Theory of Orientation and Stereoselection", Springer-Verlag, Berlin (1975).  
 Pomerantz, M.; Combs, G.L.; Fink, R.: *J. Org. Chem.*, **45**, 143 (1980).  
 Pope, J.M.: Sc.D. Thesis, Dept. of Chem. Eng., MIT, Cambridge, MA (1987).  
 Stein, S.E.: *Carbon*, **19**, (6) 421 (1981).

### FIGURES

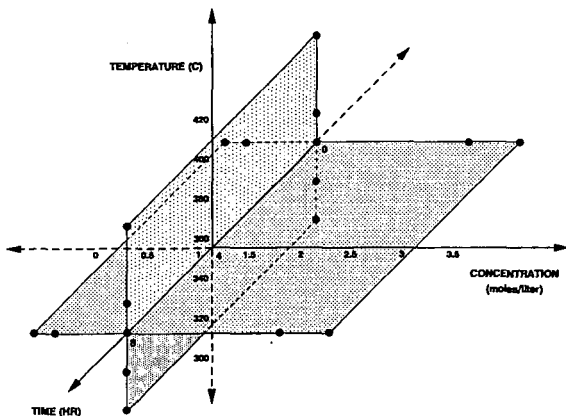


Figure 1. Experimental Grid.

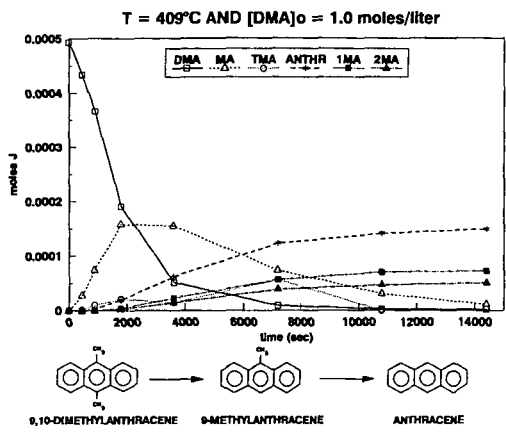


Figure 2. Concentration Histories.

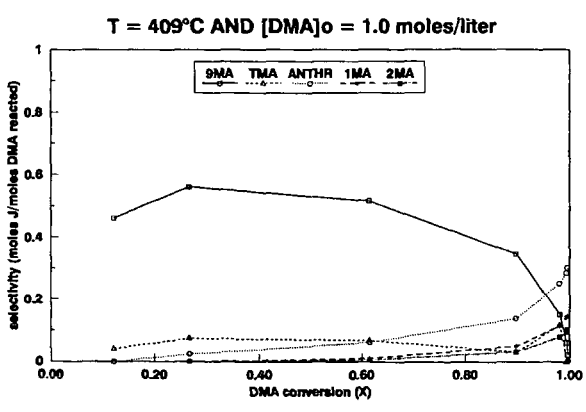


Figure 3. Selectivity Diagram.



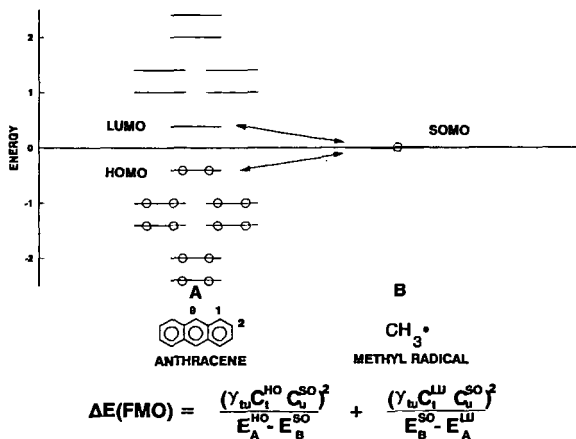


Figure 6. Frontier Orbital Interaction Diagram.

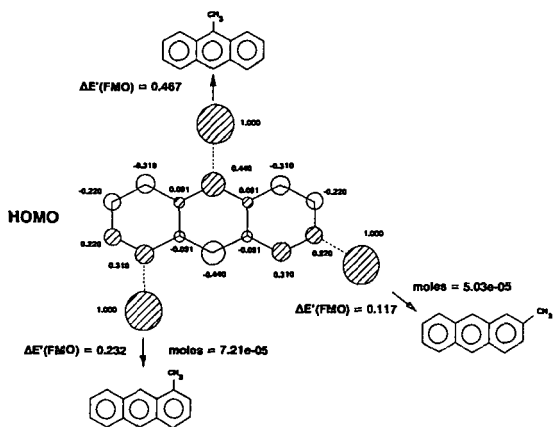


Figure 7. Periselectivity of Methyl-Anthracenes.

## HYDROGEN TRANSFER PATHWAYS UNDER RESTRICTED DIFFUSION

A. C. Buchanan, III and P. F. Britt  
Chemistry Division  
Oak Ridge National Laboratory  
P. O. Box 2008  
Oak Ridge, Tennessee 37831-6197

**Keywords:** Pyrolysis mechanisms, hydrogen transfer, restricted mobility

### ABSTRACT

The impact of restricted mass transport on the thermal processing of coal is being explored through the study of organic model compounds that are covalently anchored to an inert silica surface. Two-component surfaces are being prepared and pyrolyzed at 375 °C that contain a thermally reactive component [ $\text{Ph}(\text{CH}_2)_n\text{Ph}$ ,  $n=2-4$ ] in the presence of a second component that is either thermally inert [biphenyl or naphthalene] or contains reactive C-H bonds [diphenylmethane (DPM) or 9,10-dihydrophenanthrene (DHP)]. Reactions are found to be highly sensitive to the spatial distribution of hydrogen donors and nondonors that surround immobilized free-radical intermediates. In the presence of DPM or DHP, rapid serial hydrogen transfer steps allow radical intermediates to migrate across the surface overcoming normal diffusional limitations. Studies with DHP also reveal a minor reaction channel in which strong bond cleavage reactions occur via hydrogen transfer in these diffusionaly constrained environments.

### INTRODUCTION

Our research has been concerned with the development of model systems<sup>1-4</sup> that probe the potential perturbations in free-radical reaction pathways that may arise in coal as a result of its cross-linked, network structure.<sup>5</sup> This effect may be particularly important in thermal conversions of coals at low temperatures, e.g., 350-400°C, where bonds begin to break but most of the residual framework is retained.<sup>6</sup> Important mechanistic insights have now been gained through the study of representative organic compounds that are covalently immobilized on an inert silica surface through Si-O-C<sub>org</sub> linkages.

In order to maximize the production of hydrogen-rich products during liquefaction or pyrolysis of coal, it is important to understand and potentially control the reactions of native, reactive hydrogen-containing molecules. Our current studies employ two-component surfaces to address the influence of the structure and distribution of neighboring molecules on pyrolysis decay pathways in diffusionaly restricted environments, particularly with respect to key hydrogen transfer steps. We have focused on the thermolysis of surface-immobilized diphenylalkanes,  $\text{-Ph}(\text{CH}_2)_n\text{Ph}$  [ $n=2-4$ ], in the presence of the surface-immobilized spacer molecules, biphenyl, naphthalene, diphenylmethane, and 9,10-dihydrophenanthrene.

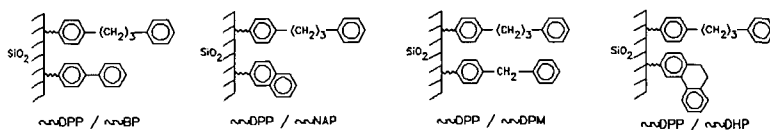
### EXPERIMENTAL

The surface immobilization, pyrolysis, and product analysis procedures have been described in detail previously.<sup>1,2</sup> The syntheses of  $p\text{-HOC}_6\text{H}_4(\text{CH}_2)_n\text{C}_6\text{H}_5$ ,  $n=2^1$ ,  $3^2$ , and  $4^3$  have also been described.

The starting materials, *p*-HOC<sub>6</sub>H<sub>4</sub>C<sub>6</sub>H<sub>5</sub>, *p*-HOC<sub>6</sub>H<sub>4</sub>CH<sub>2</sub>C<sub>6</sub>H<sub>5</sub>, and 2-HOC<sub>10</sub>H<sub>7</sub>, were commercially available, and were purified to >99.9%. A multistep synthesis was employed to prepare 3-hydroxy-9,10-dihydrophenanthrene,<sup>7</sup> which contained about 0.5% of the 3-hydroxyphenanthrene as impurity. The two-component surfaces were prepared by co-attachment in a single step, and had final purities >99.5%. Gas-phase pyrolysis products were collected in a cold trap (77K) as they formed and were analyzed by GC and GC-MS with the use of internal calibration standards. Surface-attached products were liberated as phenols following digestion of the silica in base, silylated to the corresponding trimethylsilyl ethers, and analyzed as above.

## RESULTS AND DISCUSSION

**Surface-Immobilized 1,3-Diphenylpropane (≡DPP).** Our most detailed results come from studies of the free-radical chain decomposition pathway for ≡DPP in the presence of the surface spacer molecules shown below. Pyrolysis of ≡DPP alone in sealed, evacuated (2x10<sup>-6</sup> torr) tubes at 375°C and low conversions produces the cracking products shown in Eq. 1.<sup>2</sup> No new products are detected



in the presence of the co-attached ≡BP, ≡NAP, or ≡DPM, while a minor new reaction channel is observed in the presence of ≡DHP (vide infra). The long chain, free-radical decay pathway (propagation steps shown in Eqs. 2-4) cycles through the two distinct benzylic radicals, ≡PhCH•CH<sub>2</sub>CH<sub>2</sub>Ph (1) and ≡PhCH<sub>2</sub>CH<sub>2</sub>CH•Ph (2) that undergo subsequent rapid unimolecular



decay via β-scission (Eqs. 2-3).<sup>2</sup> Selectivity in the product distribution is determined by the relative concentrations of the two benzylic radicals, [2]/[1], and is experimentally monitored by the PhCH=CH<sub>2</sub>/PhCH<sub>3</sub> yield ratio, S. In related fluid phase studies of *p*-Me<sub>3</sub>SiOPh(CH<sub>2</sub>)<sub>3</sub>Ph at 375 °C,

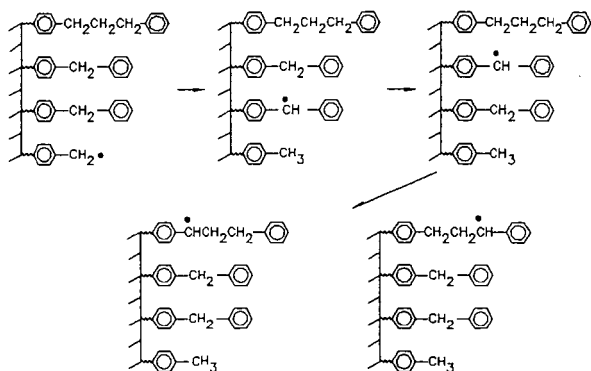


a substituent effect, S=0.91, was observed indicating a slight inherent stabilization of the benzylic radical para to the siloxy substituent.<sup>2</sup>

The initial rates and selectivities for thermolysis of ≡DPP at 375°C as a function of surface coverage and co-attached aromatic are given in Table 1.<sup>4</sup> For surfaces containing only ≡DPP, the thermolysis rate decreases dramatically with decreasing surface coverage, while S increases indicating an increasing preference for abstracting the more accessible benzylic hydrogen farthest from the surface. As shown in Table 1, the presence of ≡BP or ≡NAP results in reaction rates and selectivity values comparable with surfaces containing only ≡DPP at similar ≡DPP surface coverages. On the other hand, the

presence of  $\sim$ DPM leads to a dramatic rate acceleration compared with the  $\sim$ BP or  $\sim$ NAP spacers, and gives rate and selectivity values more typical of saturated coverages of  $\sim$ DPP (see Table 1).

These results suggest that rapid hydrogen transfer steps involving  $\sim$ DPM are occurring that allow radical centers to "migrate" on the surface as illustrated below. The result of this process is to effectively decrease the distance between a  $\sim$ DPP molecule and a radical center on the surface. This



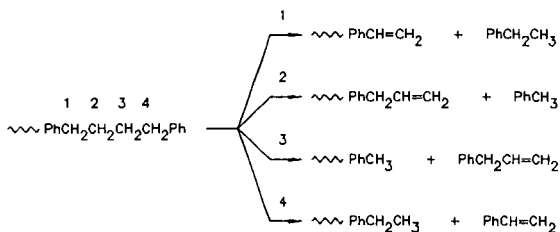
enhances the rate at which  $\sim$ DPP reacts by increasing the rate of the hydrogen transfer propagation step, which probably contains a distance dependence in the rate constant when the hydrogen abstracting radical is also surface attached. In contrast, the presence of a hydrogen donor such as tetralin<sup>8</sup> or diphenylmethane<sup>9</sup> had essentially no effect on the pyrolysis rate of liquid-phase DPP at ca. 350 °C at similar dilutions, and behaved similarly to liquid biphenyl<sup>8</sup> as diluent. The values of  $S < 1.0$  for  $\sim$ DPP/ $\sim$ DPM surfaces are also consistent with a reduced separation between  $\sim$ DPP molecules and radical centers on the surface. Radical migration effectively removes the distance dependent conformational constraints on the hydrogen abstraction reactions from  $\sim$ DPP that resulted in the unexpected regioselectivity in product formation at lower coverages.

Supporting evidence for the involvement of  $\sim$ DPM in the radical relay mechanism depicted above comes from studies of surfaces containing  $\sim$ DPP/ $\sim$ DPM- $d_2$ .<sup>4</sup> Consistent with the results for  $\sim$ DPM, we find  $S < 1.0$  and a substantial rate enhancement, although the rate enhancement is slightly less than the protium analog perhaps due to a small kinetic isotope effect. Furthermore both the gas-phase and surface-attached toluene products show substantial deuterium incorporation providing direct evidence for the involvement of H(D) transfer between  $\sim$ DPM- $h_2(d_2)$  and both chain carrying gas-phase and surface-attached benzyl radicals.

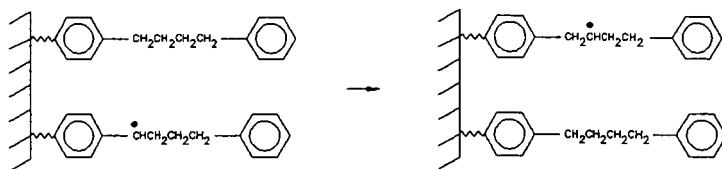
As evidenced by the rate and selectivity parameters in Table 1, the hydroaromatic  $\sim$ DHP is also very effective in promoting the radical relay pathway even for an extremely low surface coverage of  $\sim$ DPP. In addition, a second reaction channel is observed (accounting for about 2.5% of the  $\sim$ DPP reacted) that results in hydrodealkylation of  $\sim$ DPP to form  $\sim$ PhH + PhC<sub>3</sub>H<sub>7</sub>, and  $\sim$ PhC<sub>3</sub>H<sub>7</sub> + PhH in comparable amounts. This strong bond cleavage likely results from transfer of hydrogen atoms from intermediate surface-immobilized hydrophenanthryl radicals which, as opposed to diphenylmethyl

radicals, are known to possess hydrogenolysis activity.<sup>10</sup> Additional studies are in progress that examine the influence of  $\alpha$ -DHP/ $\alpha$ -DPP surface coverage and reaction temperature on the selectivity for this reaction channel.

**Surface-Immobilized 1,4-Diphenylbutane ( $\alpha$ -DPB).** A detailed analysis of the influence of restricted mobility on the pyrolysis of  $\alpha$ -DPB at 400 °C has been recently reported.<sup>3</sup> At low conversions  $\alpha$ -DPB cracks to form four main sets of products, as shown below, resulting from a long chain radical decay pathway analogous to that for  $\alpha$ -DPP that cycles through both benzylic and nonbenzylic radicals at positions 1-4.



Data for initial rates and selectivities as a function of surface coverage and co-attached spacer molecule are summarized in Table 2. The selectivities again depend on the relative concentrations of the radicals centered on carbons 1-4. The benzylic selectivity,  $C_4/C_1$ , shows the same trend with decreasing surface coverage and the type of spacer present as did the related selectivity for  $\alpha$ -DPP. The lack of selectivity between benzylic and nonbenzylic sites at high coverage (as typified by the values for  $C_1/C_2$ ), and the increase in this selectivity with decreasing surface coverage, necessitates a rapid hydrogen transfer step that interconverts benzylic and nonbenzylic radical sites prior to  $\beta$ -scission as illustrated below. This interconversion step is most efficient at high surface coverages.



The  $C_1/C_2$  product selectivity is found to be quite sensitive to the nature of the co-attached spacer present. The presence of  $\alpha$ -BP provides a barrier that inhibits the hydrogen transfer step that interconverts benzylic and nonbenzylic radicals on the surface and results in a substantially increased value of  $C_1/C_2$ . On the other hand, as in the case of  $\alpha$ -DPP, the presence of  $\alpha$ -DPM enhances the rate of radical interconversion and leads to a decreased value of  $C_1/C_2$  identical with that of a high surface coverage of  $\alpha$ -DPB alone.

## SUMMARY

Investigations of pyrolysis reactions employing two-component surfaces have provided fundamental insights into the influence of the structure of neighboring molecules on free-radical decay pathways in diffusionally constrained environments. The rates and selectivities of key hydrogen transfer steps can be profoundly effected by the structure and spatial distribution of hydrogen donors surrounding immobilized free-radical intermediates. The results give dramatic evidence that intervening molecules containing reactive C-H bonds can act as "relay catalysts" for radical intermediates allowing them to "migrate" under conditions where classical diffusion is prohibited. Diffusional limitations for similar intermediates in coal may also be overcome by similar processes. Related studies are now in progress for  $\alpha$ -BB, which has been found to primarily undergo retrogressive rearrangement and cyclization reactions when pyrolyzed under conditions of restricted mass transport.<sup>1</sup>

## ACKNOWLEDGEMENTS

We wish to thank C. A. Biggs and K. B. Thomas for their technical support. Research was sponsored by the Division of Chemical Sciences, Office of Basic Energy Sciences, U.S. Department of Energy under contract DE-AC05-84OR21400 with Martin Marietta Energy Systems, Inc.

## REFERENCES

1. Buchanan, III, A. C.; Dunstan, T. D. J.; Douglas, E. C.; Poutsma, M. L. *J. Am. Chem. Soc.* **1986**, *108*, 7703.
2. Buchanan, III, A. C.; Biggs, C. A. *J. Org. Chem.* **1989**, *54*, 517.
3. Britt, P. F.; Buchanan, III, A. C. *J. Org. Chem.* **1991**, *56*, 6132.
4. Buchanan, III, A. C.; Britt, P. F.; Biggs, C. A. *Energy Fuels* **1990**, *4*, 415.
5. Green, T. K.; Kovac, J.; Brenner, D.; Larsen, J. W., In *Coal Structure*; Meyers, R. A., Ed.; Academic Press: New York, 1982; Chapter 6.
6. Berkowitz, N. *The Chemistry of Coal, Coal Science and Technology*; Elsevier: Amsterdam, 1985; Vol. 7, Chapter 7.
7. Takaki, K.; Okada, M.; Yamada, M.; Negoro, K. *J. Org. Chem.* **1982**, *47*, 1200.
8. Poutsma, M. L.; Dyer, C. W. *J. Org. Chem.* **1982**, *47*, 4903.
9. Gilbert, K. E.; Gajewski, J. J. *J. Org. Chem.* **1982**, *47*, 4899.
10. McMillen, D. F.; Malhotra, R.; Chang, S.-J.; Ogier, W. C.; Nigenda, S. E.; Fleming, R. H. *Fuel* **1987**, *66*, 1611.

Table 1. Rate and Selectivity in Pyrolysis of -Ph(CH <sub>2</sub> ) <sub>3</sub> Ph at 375 °C			
Surface Composition	Coverage (mmol/g)	Rate x 10 <sup>4</sup> (% s <sup>-1</sup> )	S <sup>a</sup>
-DPP	0.57	18	0.96
	0.14	1.1	1.09
	0.10	0.72	1.21
-DPP / -NAP	0.12 / 0.44	1.9	1.08
-DPP / -BP	0.13 / 0.51	2.3	1.14
	0.10 / 0.51	1.2	1.18
-DPP / -DPM	0.17 / 0.42	21	0.82
	0.13 / 0.37	16	0.93
-DPP / -DPM-d <sub>2</sub>	0.16 / 0.36	13	0.98
-DPP / -DHP	0.065 / 0.47	13	0.89

<sup>a</sup> Measured by PhCH=CH<sub>2</sub> / PhCH<sub>3</sub> yield ratio.

Table 2. Rate and Selectivity in Pyrolysis of -Ph(CH <sub>2</sub> ) <sub>4</sub> Ph at 400 °C				
Surface Composition	Coverage (mmol/g)	Rate x 10 <sup>4</sup> (% s <sup>-1</sup> )	S <sup>a</sup> (C <sub>1</sub> /C <sub>2</sub> )	S <sup>b</sup> (C <sub>4</sub> /C <sub>1</sub> )
-DPB	0.485	43	1.19	0.96
	0.087	17	2.0	1.01
	0.054	9.2	2.07	1.08
-DPB / -BP	0.072 / 0.566	20	2.9	1.06
-DPB / -DPM	0.060 / 0.465	49	1.19	0.96

<sup>a</sup> Measured from PhCH<sub>2</sub>CH<sub>3</sub> / PhCH<sub>3</sub> yield ratio.

<sup>b</sup> Measured from PhCH=CH<sub>2</sub> / PhCH<sub>2</sub>CH<sub>3</sub> yield ratio.

## A SIMPLIFIED REACTION MECHANISM FOR PROPANE COMBUSTION

*J. M. Deur  
Sverdrup Technology, Inc.  
Lewis Research Center Group  
Brook Park, Ohio*

*K. P. Kundu  
National Aeronautics and Space Administration  
Lewis Research Center  
Cleveland, Ohio*

Keywords: Reduced Mechanisms, Propane Combustion, Nitrogen Oxides

### Abstract

A simplified reaction mechanism for propane combustion has been derived. This scheme is based on two competitive fuel decomposition reactions. Further, the combustion of hydrogen has been used to derive the concentrations of the intermediate reactive species, and the kinetic parameters for the rate equations are estimated through comparison of the species concentrations calculated using detailed mechanisms available in the literature. Calculated concentrations of nitrogen oxides ( $\text{NO}_x$ ) and carbon monoxide found using this mechanism agree well with previously published experimental data.

### Introduction

The principal pollutants released in hydrocarbon combustion are carbon monoxide, oxides of nitrogen, organic compounds (unburned and partially burned), and particulates, e.g., soot. In general, the observed concentrations of these various pollutant species differ from calculated equilibrium level concentrations, indicating the importance of reaction kinetics in determining pollutant emissions.

The formation and decomposition of some pollutants (carbon monoxide, organic compounds, soot, etc.) are important aspects of the overall combustion process. To understand the chemistry of these pollutant species, some knowledge of the hydrocarbon fuel combustion process is required. However, other pollutants, e.g., nitrogen oxides, form independently of the combustion process itself. Under these circumstances, it becomes possible to decouple the description of their formation from the combustion process. Even so, the reactions involving these pollutants are controlled by the environment established by the combustion process, and hence, their chemistry is still intimately connected to combustion.

Over the last decade, numerical combustion modeling has become an essential part of many research and development programs. Although combustion involves a complex coupling of chemistry and transport processes, early combustion modeling efforts treated the former in a very simplistic fashion. Unless the characteristic times for the flow field and the chemistry are widely disparate, the details of the flow field and the finite rate chemistry must be simultaneously taken into account. However, the computational burden soon becomes excessive since the level of complexity involved in such coupled calculations increases proportionately with the number of reacting species. One way to improve tractability is to reduce the number of reactions considered in a coupled solution with the flow field.

Hydrocarbon combustion is a very complex process, and any attempt to obtain a simplified reaction scheme can easily become a daunting task. During combustion, a fuel molecule breaks down into many different hydrocarbon fragments. Any reaction mechanism which aims to consider all of these fragments tends to become very large. While there have been attempts to simplify the detailed kinetic mechanisms by algebraic (1,2,3) and other techniques (4,5), it is difficult to say if any such simplified scheme can substitute the detailed mechanisms, and while a few global reaction mechanisms (6,7,8,10) have been reported, their utility in practical applications where the levels of pollutants must be calculated has not been established.

The level of detail required to obtain the concentrations of species, particularly minor constituents such as the oxides of nitrogen, is difficult to determine. Although a detailed kinetic mechanism is sometimes required to understand the process, a global reaction scheme involving a few reaction species will often suffice.

Of course, it must be emphasized that all descriptions of chemical kinetics are in real sense only approxima-

tions. Even detailed kinetic mechanisms are constructed on the basis of reproducing observable phenomena which are not necessarily singular events. Moreover, evaluation of specific rate constants over ranges of temperatures and pressures adequate for combustion modeling is a difficult problem. Thus, it cannot be assumed that any validated mechanism can be divided and the parts used to describe independent phenomena, unless the detailed mechanism was constructed in that way.

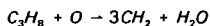
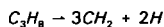
The objective here is to develop a semi-global reaction mechanism that can predict overall temperatures and concentrations of pollutants such as  $\text{NO}_x$  and  $\text{CO}$ .

#### A Simplified Reaction Mechanism

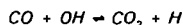
The formation of thermal  $\text{NO}_x$  is generally slow when compared to combustion itself(9). Therefore, the  $\text{NO}_x$  formation mechanism can be divided into two stages: initiation and  $\text{NO}_x$  formation.

In the initiation phase, the hydrocarbon molecule (propane in the current discussion) is broken down into hydrocarbon fragments (10), followed by hydrogen combustion reactions to generate the free radicals. For simplicity, only one type of hydrocarbon fragment, i.e.,  $\text{CH}_2$ , will be tracked in the present mechanism.

The key steps in these reactions are:

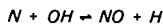


These steps generate two key radical species,  $\text{CO}$  and  $\text{H}_2$ . Further reactions of these species lead to the formation of  $\text{CO}_2$  and  $\text{H}_2\text{O}$ , the most important reaction for the disappearance of  $\text{CO}$  being:

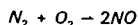


In the second stage, the  $\text{NO}_x$  is formed. The two principal sources of nitrogen oxide are: (1) oxidation of atmospheric nitrogen at high temperatures (thermal  $\text{NO}_x$ ), and (2) reactions between hydrocarbon fragments and atmospheric nitrogen (prompt  $\text{NO}_x$ ).

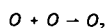
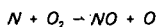
The principal reactions for thermal  $\text{NO}_x$  involve two radical species,  $\text{O}$  and  $\text{OH}$ , which are formed during the initiation stage and are near equilibrium with the corresponding molecular species.



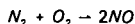
The above reactions do not correctly explain the effect of residence times on  $\text{NO}_x$  formation. To overcome this problem, the following semi-global reaction has been incorporated into the present mechanism:



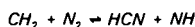
which follows from the series of reactions:



Thus, the present mechanism postulates the following reactions for thermal  $NO_x$  formation:



In fuel-rich flames, the rapid formation of NO near the flame zone cannot be explained by the equilibrium concentrations of O and OH. Although there is uncertainty in the mechanisms for such prompt  $NO_x$  formation, it is normally hypothesized that the principal product of initial reaction is HCN. In the present mechanism, it will be assumed that HCN is formed through the reaction between the hydrocarbon fragment  $CH_2$  and  $N_2$ :



The product species, HCN and NH, are subsequently transformed into other species by other reactions in the fuel rich combustion environment. In the current mechanism, these steps have not been considered. Instead, we have assumed that HCN and NH are the representative nitrogenous species themselves.

Combining the above description of the thermal and prompt  $NO_x$  formation with the previous characterization of the hydrocarbon combustion, the reduced mechanism summarized in Table I results.

#### Reaction Rates

Most reaction rates are taken from the literature with minor adjustments to match ignition delay times, flame temperatures, and concentrations of species formed during reactions. The activation energy for the fuel fragmentation reaction is taken to be equivalent to the activation energy reported by Lefebvre (11) in an ignition delay measurement.

#### Validation of Mechanism

The purpose of this mechanism is to compute  $NO_x$  emissions, which as noted earlier, depend on temperature and concentrations of radicals. To examine the fidelity of the mechanism, studies based on well stirred reactor calculations have been performed using the LSENS program (12), with sensitivity analyses generated via the decoupled direct method of Radhakrishnan (13). Flame temperatures (Fig. 1) and species concentrations (Figs. 2 through 5) for various test conditions have been compared with results found with a standard detailed mechanism of Miller and Bowman (14).

However, since agreement between experimental data and computed results using the Miller and Bowman mechanism is less than satisfactory in the case of  $NO_x$  formation, direct comparisons between calculations based on the present mechanism and experimental data obtained by Anderson (15) have been made (Figs. 6 and 7). These experiments were conducted at an initial pressure of 5.5 atmospheres and initial temperatures of 600 K and 800 K, although comparisons are only shown at 800 K in the above figures.

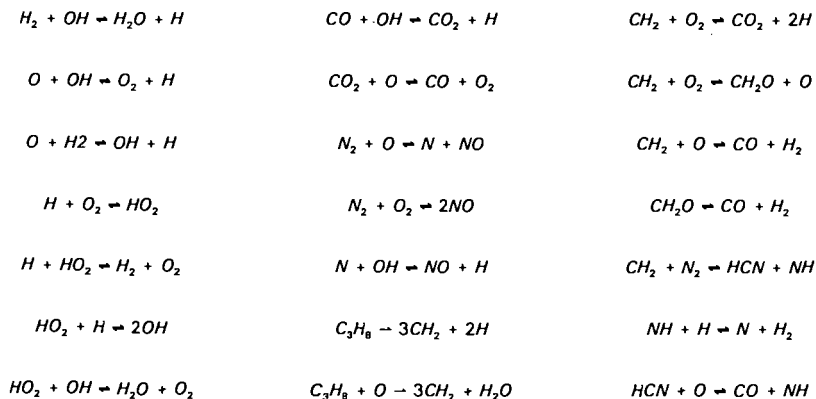
Finally, since the ultimate use of the reduced mechanism is multi-dimensional reacting flow field calculations, the Anderson burner geometry has been modeled using KIVA-II (16) with the current mechanism. Favorable comparisons (Fig. 8) have been obtained with regards to the  $NO_x$  emission levels over the range of equivalence

ratios and residence times reported by Anderson.

#### References

1. Peters, N., and Kee, R. J., *Comb. and Flame*, Vol. 68, 1987, p. 7.
2. Paczko, G., et. al., *21st Sym. (Intl.) Comb.*, 1988, p. 739.
3. Chen, J. Y., and Dibble, R. W., *SAND-90-8447*, 1990.
4. Lam, S. H., *Recent Advances in Aerospace Sciences (C. Casci, Ed.)*, Academic Press, 1985.
5. Lam, S. H., and Goussis, D. A., *MAE Report No. 1799*, Princeton U., 1988.
6. Ying, S. J., and Nguyen, H. L., *AIAA Paper No. 90-0546*, 1990.
7. Westbrook, C.K., and Dryer, F. L., *Comb. Sci. Tech.*, Vol. 27 (1-2), 1989, p. 31.
8. Reitz, R. D., and Bracco, F. V., *Num. Fluid Mech.*, Vol. 5, 1982, p. 130.
9. Bowman, C. T., *Fossil Fuel Combustion (W. Bartock and A.F. Sarofim, Eds.)*, Wiley, 1991.
10. Kiehe, T. M., et. al., *Comb. Sci. Tech.*, V. 54, 1987, p. 1.
11. Freeman, G. and Lefebvre, A. H., *Comb. and Flame*, V. 58, 1984, p. 153.
12. Radhakrishnan, K., *Prog. in Astro. and Aero.*, V. 135, 1991, p. 83.
13. Radhakrishnan, K., *NASA-CR-179636*, 1987.
14. Miller, J. A., and Bowman, C. T., *Prog. in Energ. and Comb. Sci.*, V. 15, 1989, p. 287.
15. Anderson, D. A., *NASA-TM-X-71592*, 1975.
16. Amsden, A. A., et. al., *LA-11560-MS*, 1989.

Table I. Reduced Reaction Mechanism for Propane Combustion.



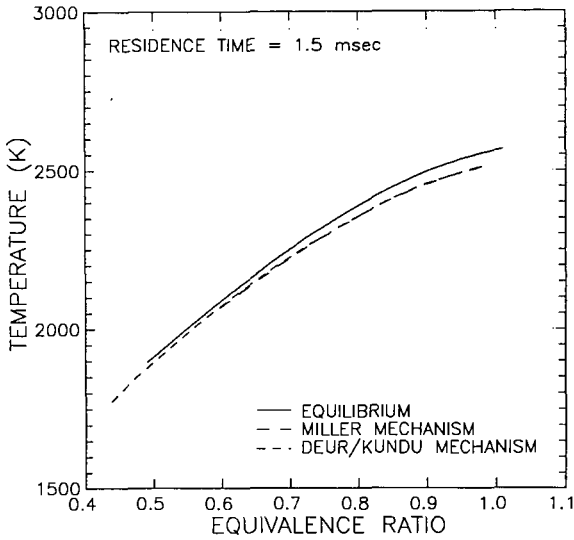


Figure 1. Equilibrium and Adiabatic Flame Temperature Comparison.

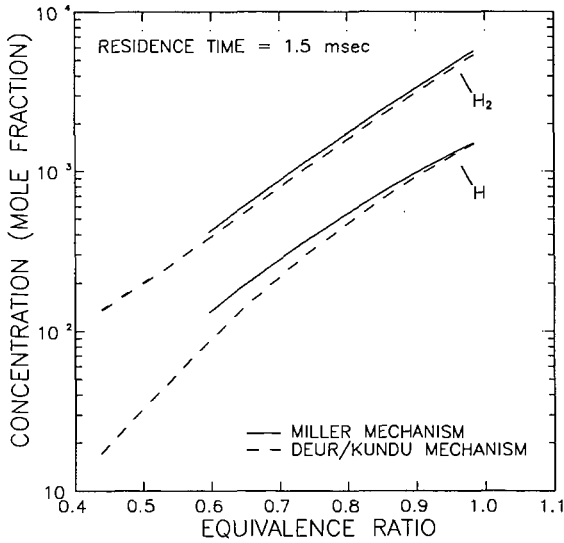


Figure 2. H and H<sub>2</sub> Species Concentration Comparison (Residence Time = 1.5 msec).

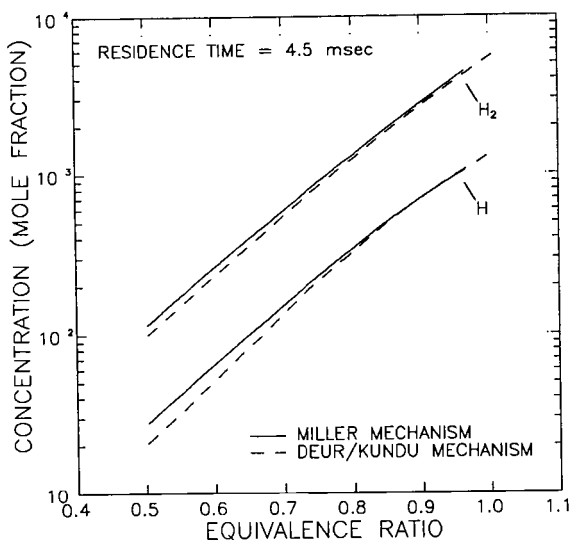


Figure 3. H and H<sub>2</sub> Species Concentration Comparison (Residence Time = 4.5 msec).

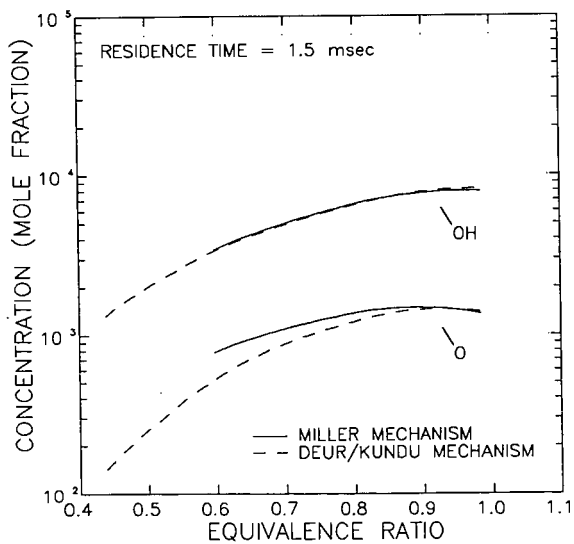


Figure 4. O and OH Species Concentration Comparison (Residence Time = 1.5 msec).

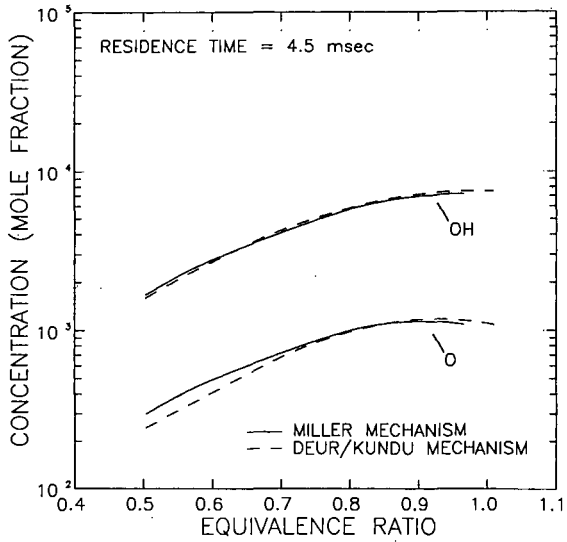


Figure 5. O and OH Species Concentration Comparison (Residence Time = 4.5 msec).

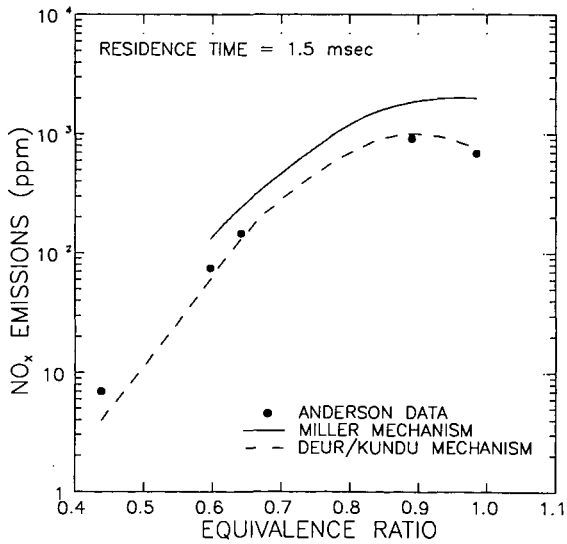


Figure 6.  $\text{NO}_x$  Emissions Comparison (Residence Time = 1.5 msec).

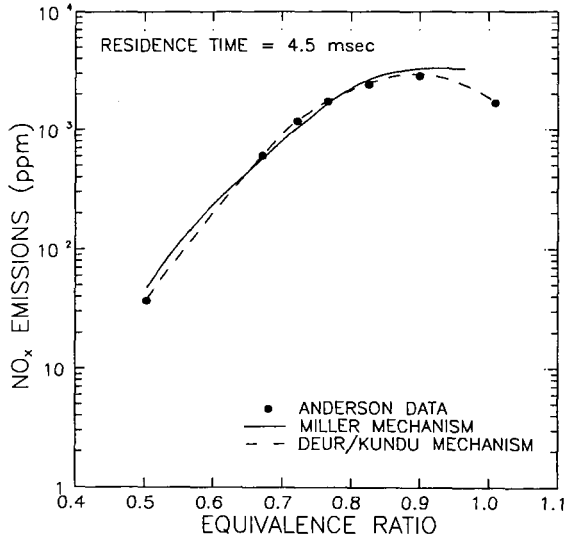


Figure 7. NO<sub>x</sub> Emissions Comparison (Residence Time = 4.5 msec).

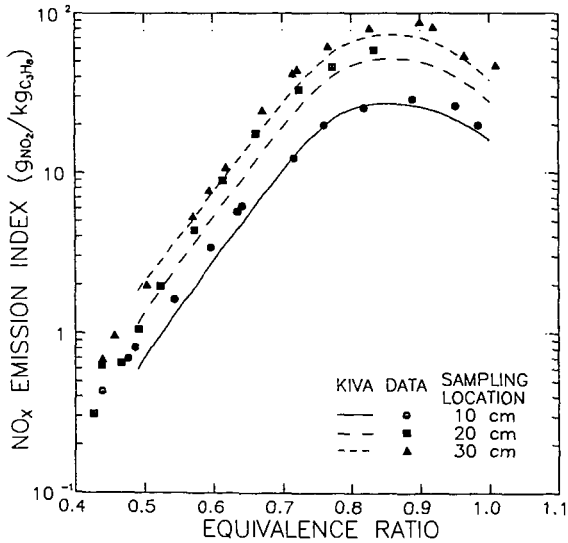


Figure 8. NO<sub>x</sub> Emissions Comparison: Anderson Experimental Data vs. KIVA-II Predictions.

Mechanisms of Hydrogen Donation from Cyclic Olefins  
to Pittsburgh No. 8 Coal

Michael W. Bedell, Exxon Research and Development Laboratories  
Baton Rouge, LA 70821  
Christine W. Curtis, Chemical Engineering  
Auburn University, AL 36849-5127

**Keywords:** Hydrogen Donation, Cyclic Olefins, Coal Liquefaction

## INTRODUCTION

Hydrogen donation is considered to be an important mechanism by which hydrogen is transferred from the solvent to coal during coal liquefaction (Bockrath, 1982). Hydrogen donation from cyclic olefins such as 1,4,5,8,9,10-hexahydroanthracene (HHA) and 1,4,5,8-tetrahydronaphthalene or isotetralin (ISO) to coal has been shown to be both rapid and effective (Bedell and Curtis, 1991). This investigation examined the mechanisms and kinetics by which HHA and ISO transfer their hydrogen to Pittsburgh No. 8 coal and compared these effects with those of hydroaromatic donors. The cyclic olefins readily converted to hydroaromatics at liquefaction conditions but still remained more effective than most conventional hydroaromatic donors in converting coal. Combinations of cyclic olefins and conventional hydroaromatic donors produced effective hydrogen donor combinations providing hydrogen rapidly and sustaining hydrogen donation throughout the reaction time. The universality of the effectiveness of the cyclic olefin donation was examined with a set of eight coals from the Argonne Premium Coal Bank that are of different rank and reactivity. The cyclic olefins effectively converted the coals of different rank, being most effective with the coals of intermediate reactivity.

Efficient coal liquefaction processing requires that hydrogen be transferred to the dissolving coal matrix at the rate that it can be accepted by the reacting coal molecules and effectively used donors. A key to obtaining high coal conversion in liquefaction through donation from solvent is the matching of the rate that hydrogen is released by the donor and accepted by the coal. When these rates are not matched, inefficient usage of the hydrogen results. When hydrogen is released by the donor too quickly, the hydrogen is not used by the dissolving coal and forms gaseous hydrogen; when hydrogen is released too slowly, retrogressive reaction of the dissolving coal molecules can occur forming refractory coke precursors.

The goals of this research were to evaluate the effects of different rates of hydrogen donation by evaluating the hydrogen donation from a cyclic olefin, 1,4,5,8,9,10-hexahydroanthracene (HHA) in combination with the hydroaromatic, 9,10-dihydroanthracene (DHA). The acceptor used in this study was Pittsburgh No. 8 coal. Liquefaction reactions were performed with the combined donor system as well as with individual cyclic olefins, HHA and ISO, and hydroaromatic donors, DHA, octahydroanthracene (OHA) and tetralin (TET). The rate of hydrogen acceptance by Pittsburgh No. 8 coal was determined in terms of coal conversion to THF solubles after different reaction times.

These same hydrogen donors were evaluated with eight coals from the Argonne Premium

Coal Sample Bank. These coals were of different rank and reactivity. The various degrees of hydrogen acceptability and, hence, reactivities of the coals were evaluated.

## EXPERIMENTAL

**Reactions with Pittsburgh No. 8 Coal.** The reactions of cyclic olefins, HHA and ISO, and hydroaromatic donors, DHA, OHA, and TET were performed with Pittsburgh No. 8 coal from the Argonne Premium Coal Sample Bank. Information concerning Pittsburgh No. 8 coal properties is given in Table 3. Reactions were performed in 50 cm<sup>3</sup> stainless steel tubular reactors that were agitated at 700 cpm. The reaction conditions used were 30 minutes reaction time, 1250 psig H<sub>2</sub> atmosphere at ambient temperature, 380°C reaction temperature, 2.0g coal, 4.0g total solvent mixture including 0.5 weight percent donable hydrogen of the donor with the balance being hexadecane as the diluent solvent.

**Reactions with Argonne Coals.** Reactions were performed with the hydrogen donors, both cyclic olefins and hydroaromatic donors, and eight Argonne Premium Sample Bank coals. Another coal, Western Kentucky No. 9, from the PSU/DOE sample bank was used for comparison. The reactions were performed using the same type of reactor and conditions as those with Pittsburgh No. 8 coal.

**Materials and Analysis.** The hydrogen donors used were obtained from the following manufacturers and were used as received: tetralin, 1,4,5,8,9,10-hexahydroanthracene, 1,2,3,4,5,6,7,8-octahydroanthracene, 9,10-dihydroanthracene, and hexadecane from Aldrich Chemical Co.; 1,4,5,8-tetrahydronaphthalene (isotetralin) from Wiley Organics Inc.; and Pittsburgh No. 8, Illinois No. 6, Upper Freeport, Pocahontas No. 3, Lewiston Stockton, Blind Canyon, Wyodak and Beulah Zap coals from the Argonne Premium Coal Sample Bank. Western Kentucky No. 9 coal was obtained from the PSU/DOE Coal Sample Bank.

The hydrogen donor compounds and their products produced during coal liquefaction were analyzed by gas chromatography using a Varian 3400 gas chromatograph equipped with a HT-5 column from SGE and FID detection. The internal standard method with biphenyl as the internal standard was used. The peaks were identified by comparing retention times with authentic compounds and by GC mass spectrometry using a VG 70EHF mass spectrometer.

Coal conversion is defined as

$$\text{Conversion} = [1 - [\text{IOM (maf)}] / \text{coal charge (maf)}] \times 100$$

where IOM is the THF insoluble organic matter remaining after reaction and maf is defined as moisture and ash free.

## RESULTS AND DISCUSSION

Cyclic olefins, as donors for coal liquefaction, have been shown to release their hydrogen readily and quickly to the dissolving coal matrix. The conversion of cyclic olefins occurred very rapidly at liquefaction temperatures, forming a number of reactions products including

hydroaromatic and aromatic compounds (Bedell and Curtis, 1991). HHA converted quickly at temperatures of 380°C and above, forming reaction products of DHA, OHA, and anthracene (ANT). DHA has also been shown to be very effective in converting coal at liquefaction temperatures (Bedell, 1991); however, the conversion and subsequent release of hydrogen from DHA was not nearly as rapid as that from HHA. The purpose of this research was to investigate the possible synergism between the hydrogen donating rate of HHA and DHA on coal conversion. The idea being explored was that HHA released its hydrogen very quickly making it readily available to the coal as it initially began to dissolve while DHA released its hydrogen more slowly making hydrogen available to the less reactive components of the coal.

The reactions performed as shown in Table 1 were comprised of varying amounts of HHA and DHA. The reactions were configured to maintain a constant level of 0.5 weight percent donable hydrogen. Hence, the amount of donable hydrogen remained the same although the relative amount of each donor was varied from 75% HHA and 25% DHA to 75% DHA and 25% HHA. The reaction that produced the highest coal conversion to THF solubles contained equal levels of donable hydrogen from HHA and DHA. Nearly 12% more coal conversion was obtained from the combined HHA/DHA system than with HHA alone, while nearly 7% more conversion was obtained with the combined system than with DHA alone. The reactions containing 75% HHA and 25% DHA produced more coal conversion than the reaction with HHA alone, and nearly equivalent coal conversion as the reaction with DHA alone. The reaction containing 75% DHA and 25% HHA produced more conversion than either HHA or DHA alone.

These increases in coal conversion with the combined systems suggested that combining the two donors provided a synergism in both the amount and rate of hydrogen released in the system. Additional reactions were performed to evaluate the effect of time on the behavior of the hydrogen donors. Reactions were performed with the combined HHA and DHA system and with the individual donors of HHA, DHA, OHA, ISO and TET for reaction times of 5, 15, 30 and 60 minutes. Hydrogen donation was monitored by evaluating the reaction products from the donors. Hydrogen acceptance was measured by evaluating coal conversion to THF solubles. At the short reaction time of 5 minutes, HHA produced the most coal conversion, producing slightly more than the HHA/DHA combined system, 5% more than the DHA system, and 16% more than OHA. Analysis of the reaction products from hydrogen donors showed that more than 70% HHA converted while less than 25% DHA converted after 5 minutes of reaction. In the combined system, almost all of the HHA had converted after 5 minutes. Comparison of the cyclic olefin, ISO, to the hydroaromatic donor, TET, again showed much higher coal conversion at short reaction time. ISO converted very rapidly forming a reaction products of 1,2-dihydronaphthalene (DHN) and naphthalene (NAP) while TET remained essentially unreacted. These experimental results indicate that the rapid release of hydrogen by cyclic olefins promoted coal conversion at shorter reaction times compared to the slower hydrogen release by the hydroaromatic donors.

The liquefaction reactions of Pittsburgh No. 8 coal at 15, 30 and 60 minutes with the two types of donors are also compared in Table 2. At the short reaction time of five minutes, the cyclic olefin HHA produced the highest coal conversion to THF solubles. At longer reaction times of 15 and 30 minutes, the combined HHA/DHA reaction produced the highest coal

conversion. At the longest reaction of 60 minutes, the combined HHA/DHA and the individual DHA and HHA systems all produced similar coal conversions. Even in the system with no hydrogen donor present, the amount of coal conversion increased with time. Hence, coal conversion in a hydrogen atmosphere increased with time regardless of the presence or type of hydrogen donor present. However, the presence of the hydrogen donor increased the amount of coal conversion achieved by 13 to 22% at the long reaction time. Greater benefits were observed with some of cyclic olefin donors or the combined cyclic olefin/hydroaromatic donors at shorter reaction times.

Each of the hydrogen donors underwent reactions that released hydrogen from themselves. HHA showed the most reactivity while OHA showed the least amount of reactivity for the conversion of the donor to other species. In the reaction times of 15 minutes and longer, HHA formed OHA, DHA, and ANT; OHA formed DHA and ANT and DHA formed OHA and ANT. At short reaction time of 5 minutes, tetrahydroanthracene (THA) was observed in the individual reactions of OHA, HHA and DHA.

The reactions using the two ring donors, ISO and TET, yielded the same trends. ISO converted coal much more quickly than did TET and showed substantial increases in coal conversion compared to the amount produced by TET. However, at longer reaction times of 15 and 30 minutes, both ISO and TET showed similar coal conversion which was substantially more than without any donor. ISO was highly reactive forming TET and naphthalene (NAP) at reaction times of 15 minutes and longer, but forming 1,2-DHN rather than TET at the short reaction time (5 min.). TET converted very little and only formed small amounts of NAP.

**Argonne Coals.** Cyclic olefins have been shown to be effective hydrogen donors for bituminous coals, Western Kentucky (Bedell and Curtis, 1991) and for Pittsburgh No. 8 coal. To establish the universality of these donors, a series of reactions was performed in which cyclic olefins were reacted with eight coals from the Argonne Premium Coal Sample Bank. The efficacy of the hydrogen donation from the cyclic olefins to coals of different rank was compared to the efficacy of hydrogen donation from hydroaromatic donors. These reactions were performed using an equivalent amount of donable hydrogen for each hydrogen donor species and a reaction time of 30 minutes. The efficacy of hydrogen donation for each hydrogen donor for each coal was evaluated in terms of coal conversion to THF solubles.

The coals, themselves, had considerably different reactivities. Reactions in hydrogen and hexadecane without an added hydrogen donor ranked the reactivity of the coals for conversion as Illinois No. 6 > Western Kentucky No. 9 > Pittsburgh No. 8 > Blind Canyon > Wyodak-Anderson and Upper Freeport > Beulah-Zap and Lewiston-Stockton >> Pocahontas No. 3. The reactivity ranking of the coals became less distinct when the different donors were added to the reaction system. The addition of hydrogen donors to the system increased the amount of coal conversion obtained for most of the coals. The most active donors were the cyclic olefins, HHA and ISO, and the hydroaromatic donor, DHA. The hydroaromatic donors, OHA and TET, contributed less hydrogen to the system and resulted in less coal conversion.

The coals of high inherent reactivity, Kentucky No. 9, Illinois No. 6, and Pittsburgh No. 8 showed similar coal conversions with DHA and HHA. These coals were evidently sufficiently

reactive to be able to utilize the hydrogen that was quickly released from the cyclic olefin, HHA. The coals of lower reactivity, Upper Freeport, Lewiston-Stockton, Blind Canyon, Wyodak, and Beulah Zap, showed a much wider disparity between the coal conversion obtained with DHA and that from HHA. For these coals, the quick release of hydrogen from HHA was not effective in promoting coal conversion, most probably because these coals were slow to react and could not utilize the hydrogen released from the cyclic olefin quickly enough to promote coal conversion.

### SUMMARY

The combination of the cyclic olefin, HHA, with the hydroaromatic donor, DHA, was the most effective hydrogen donor system, producing the most coal conversion in the least amount of time. HHA released its hydrogen rapidly to produce high initial levels of coal conversion to THF solubles. Although coal conversion increased with increasing reaction time, the combined HHA/DHA yielded a high level of coal conversion at very short time with only small increases being observed with increased time. The high level of reactivity of the cyclic olefins resulted in quick release of hydrogen that could then be incorporated into the dissolving coal matrix of the reactive coals. However, the coals of lesser reactivity did not benefit to nearly the same degree to the quick release of the hydrogen by the cyclic olefin. The slower release of DHA was more effective in promoting the desired reactions between donated hydrogen and the less reactive coals.

### REFERENCES

- Bedell, M.W. and Curtis, C.W., *Energy and Fuels*, 1991, 5, 469.  
 Bedell, M.W., Ph.D. Dissertation, Auburn University, 1991.  
 Bockrath, B., *Coal Science*, Vol. 2, Academic Press, New York, NY, 1982.

Table 1. Effect of Hydrogen Donor Content on Coal Conversion

Percentage of Hydrogen Donor		Coal Conversion
Dihydroanthracene	Hexahydroanthracene	
%	%	%
100	0	56.4 ± 0.1
75	25	60.8 ± 1.6
50	50	63.7 ± 0.1
25	75	55.5 ± 0.3
0	100	51.8 ± 0.6
0	0	20.1 ± 3.3

Reaction Conditions: Pittsburgh No. 8 coal, hexadecane as solvent, 1250 psig H<sub>2</sub> at ambient temperature, 380°C, 30 minute reaction time.

Table 2. Effect of Time and Hydrogen Donor Content on Coal Conversion

Hydrogen Donor	Coal Conversion (%) at Specific Reaction Times (min)			
	5	15	30	60
HHA + DHA*	30.9±0.3	58.0±0.5	63.1±1.0	63.7±0.1
DHA	27.5±1.1	55.2±0.3	56.4±0.1	67.7±1.6
HHA	32.3±1.4	44.6±4.0	51.8±0.6	65.0±0.7
OHA	15.5±1.2	25.9±0.9	38.8±1.0	58.5±0.9
ISO	19.1±0.6	37.1±1.6	42.3±5.2	58.8±0.2
TET	6.0±0.4	17.4±1.0	30.5±3.8	56.9±2.6
No Donor	7.9±0.2	20.9±0.1	20.1±3.3	44.2±3.1

Reaction Conditions: Pittsburgh No. 8 coal, hexadecane as solvent, 1250 psig H<sub>2</sub> at ambient temperature, 380°C.

\*HHA and DHA present in a 1 to 1 weight ratio.

Table 3. Proximate Analysis of the Argonne Premium Sample Coals

Coal	Moisture %	Ash %	Volatile Matter %	Sulfur %	BTU	Rank
Kentucky No. 9	7.12	10.97	35.77	4.50	11936	HVB
Illinois No. 6	7.97	14.25	36.86	4.45	10999	HVB
Upper Freeport	1.13	13.03	27.14	2.29	13315	MVB
Pocahontas No. 3	0.65	4.74	18.48	0.66	14926	LVB
Pittsburgh No. 8	1.65	9.10	37.20	2.15	13404	HVB
Lewiston Stockton	2.42	19.36	29.44	0.69	11524	HVB
Blind Canyon	4.63	4.49	43.72	0.59	13280	HVB
Wyodak	28.09	6.31	32.17	0.45	8426	Sub B
Beulah Zap	32.24	6.59	30.45	0.54	7454	LIG

All values are weight percents for the as-received coals.

HVB = high volatile bituminous  
MVB = medium volatile bituminous  
LVB = low volatile bituminous  
Sub B = subbituminous  
LIG = lignite

Table 4. Coal Conversion for Reactions of Argonne Coals with Hydrogen Donors in Hexadecane

Coal Reacted	Coal Conversion: (%) with						No Donor Added
	DHA	HHA	OHA	ISO	TET		
Kentucky No. 9	68.3(1.0)	65.0(3.3)	49.7(1.0)	37.2(0.4)	29.8(0.2)	25.6(1.8)	
Illinois No. 6	69.6(2.0)	67.7(0.2)	66.1(2.8)	65.5(1.6)	62.1(2.0)	55.7(0.1)	
Upper Freeport	47.1(2.0)	15.8(1.2)	13.0(1.7)	20.9(2.5)	8.3(0.7)	11.4(0.5)	
Pocahontas No. 3	4.5(0.1)	-4.4(0.1)	-6.1(2.0)	-6.7(1.5)	-3.1(1.0)	-5.7(1.7)	
Pittsburgh No. 8	56.4(0.1)	51.8(0.6)	38.8(1.0)	42.3(5.3)	30.5(3.8)	20.1(3.3)	
Lewiston Stockton	41.7(1.9)	25.2(2.1)	19.6(1.2)	20.9(1.1)	9.1(2.6)	6.0(3.1)	
Blind Canyon	64.8(3.9)	41.6(1.6)	27.9(0.7)	25.3(0.2)	15.2(2.0)	17.4(0.4)	
Wyodak (dried)*	50.6(0.6)	40.5(1.3)	21.4(1.2)	21.1(2.9)	14.9(1.5)	11.7(1.5)	
Beulah Zap (dried)*	35.6(3.0)	20.8(3.0)	13.3(1.0)	13.8(0.1)	5.0(2.5)	8.1(2.1)	

Reaction Conditions: hexadecane as solvent, 1250 psi, hydrogen at ambient temperature, 30 minute reaction time, 380°C

\* dried to approximately 4% moisture content

# Temperature-Programmed Liquefaction of Low-Rank Coals in H-Donor and Non-Donor Solvents

Chunshan Song and Harold H. Schobert

Fuel Science Program, Department of Materials Science and Engineering,  
209 Academic Projects Building, The Pennsylvania State University,  
University Park, PA 16802

Keywords: Temperature-programming, Coal Liquefaction, H-donor

## Introduction

U.S. production of low-rank coals including lignite and subbituminous coals has increased tenfold over the last two decades, and production is poised for a further step increase [1]. Recently there has been increasing interest in finding ways to improve conversion of low-rank coals, which are often less readily liquefied than bituminous coals [2]. In coal liquefaction, the thermally derived reactive fragments (radicals) must be stabilized to achieve molecular weight reduction, otherwise they will promptly recombine or crosslink to form more refractory materials [3]. The rate of thermal fragmentation is mainly determined by coal reactivity, temperature, and time, while its balance with the rate of radical capping by hydrogen-donation is a critical factor [3,4]. It is now recognized that low-rank coals are more reactive than had been thought previously, and their conversion in high-severity processes is accompanied by significant retrogressive reactions [5].

Due to the presence of various C-O and C-C bonds in coals, there may be a relatively broader distribution of dissociation energies of bonds connecting the structural units in low-rank coals, as can be visualized from the dissociation energies of various C-O, C-C and C-H bonds that are believed to be relevant to coal and coal conversion processes [6]. The concept of distribution of bond energies for coals is also supported by the results of temperature-programmed pyrolysis (TPP) of coals ranging from brown to bituminous coals [6,7]. TPP data show that more bonds in low-rank coals are thermally broken at lower temperatures as compared to bituminous coals [6]. The question that arises for liquefying low-rank coals is how to balance the rates of bond cleavage with the rates of hydrogen transfer to the radicals. Of some importance to the present work are several recent reports showing that using relatively slow heating rates [3,4,8] is effective for liquefying low-rank coals. In catalytic liquefaction, temperature-staged conditions have been shown to improve coal conversion and oil yields [9-11], even in the aqueous liquefaction system [12].

For a given reaction system, controlling the conditions is important for maximizing the yield and quality of products and minimizing retrogressive reactions. The retrogressive reactions may include the crosslinking of thermally generated radicals and condensation of thermally sensitive compounds. The temperature-programmed liquefaction (TPL) reported here seeks to efficiently liquefy low-rank coals by controlling the rate of pyrolytic cleavage of weak bonds while minimizing the retrogressive crosslinking of radicals and thermally sensitive groups. In preliminary communications, we reported that temperature-programming appears to be promising for more efficient conversion of low-rank coals in tetralin [13,14]. This paper reports on the temperature-programmed and non-programmed liquefaction (N-PL) of a subbituminous coal and a lignite in H-donor and non-donor solvents. Reported separately are the solid-state  $^{13}\text{C}$  NMR and pyrolysis-GC-MS studies of coal structure and the TPL reactions [15], and catalytic TPL of a low-rank coal using dispersed Mo catalyst [16].

## Experimental

The coals used were a Montana subbituminous coal and a Texas lignite obtained from the DOE/Penn State Coal Sample Bank (DECS-9 / PSOC-1546; DECS-1 / PSOC 1538). Table I shows the characteristics of these coals. The coals were recently collected and stored under argon atmosphere in heat-sealed, argon-filled laminated foil bags consisting of three layers (polyethylene plus aluminum foil plus polyethylene) [17]. The coals were crushed to less than 60 mesh and dried in vacuo at 95°C for 2 h (before use) by placing a flask containing the fresh coal into a preheated vacuum oven. Our preliminary data showed that vacuum dried coal gave similar or slightly higher conversion than the fresh coal. The H-donor vehicle used was tetralin, a known H-donor. As non-donor, naphthalene and 1-methylnaphthalene were used. The products from low temperature runs with naphthalene at  $\leq 350^\circ\text{C}$  were rock-like and

difficult to remove from the reactors. However, there were no such experimental problems with 1-methylnaphthalene because it is a liquid. Liquefaction was carried out in 25 mL microautoclaves using 4 g coal (< 60 mesh) and 4 g solvent under 6.9 MPa H<sub>2</sub> using a given temperature program. The liquid and solid products were separated by sequential Soxhlet extraction with hexane, toluene and THF for about 24 h. The THF-insoluble residues were washed with acetone, then with pentane to remove THF completely, and subsequently dried in a vacuum oven at 100°C for over 6 h before weighing. The conversions of coal into THF-solubles were determined from the amount of THF-insoluble residues and are based on the dmmf basis. The yields of preasphaltene (THF soluble but toluene insoluble) and asphaltene (toluene soluble but hexane insoluble) are given as the yields of recovered products, and the yields of oil plus gases are determined by difference between total conversion and the sum of preasphaltene and asphaltene yields.

## Results and Discussion

### Temperature-Programming

Figure 1 shows the reactor heat-up profiles for temperature programmed liquefaction. Although the temperature inside the reactor was not measured, the pressure change of the reactor during the heat-up can give a direct measure of the temperature change. Figure 2 shows the change of sandbath temperature and pressure of the reactor for a TPL run of DECS-9 in tetralin with 6.9 MPa cold H<sub>2</sub> at final temperature of 400°C. The sandbath temperature was controlled manually such that the heating ramp would be the same for all the runs. It can be seen from Figures 1 and 2 that the programming was successfully achieved. The t-p profile in Figure 2 is typical for a thermal run, but a catalytic run shows a different t-p change pattern [6]. No catalyst was used in the present work. The selected temperature program consisted of a low-temperature soak at 200°C for 15 min, programmed heating to a final temperature at about 7°C/min, followed by a 30 minute hold at the final temperature (300, 350, 375, 400, and 425 °C). We expect few chemical reactions to occur at 200°C. The rationale for selecting such a low temperature for soaking is to allow the solvent molecules to penetrate into the interior of coal particle (diffusion and swelling), before they are needed as hydrogen donors for stabilizing the radicals and thermally labile compounds in the subsequent heat-up period and high temperature stage.

### Temperature-Programmed Liquefaction

Figure 3 shows the yields of THF-, toluene- and hexane-soluble products plus gas from duplicate runs of Montana coal, as a function of final TPL temperature. At 300°C, the yield of THF-solubles is only slightly higher than that of the original coal. It should be noted that the low temperature TPL did not cause considerable increase in coal conversion, but did result in some desirable change in coal structure. As shown in Figure 3, the conversion of coal to THF-solubles increased significantly with increasing final temperature from 300 °C (9%) to 400 °C (about 79%), but rose to a much lesser extent from 400 to 425°C (about 82%). On the other hand, the conversion to toluene solubles displayed a monotonic increase from 300 to 425 °C.

Figure 4 shows the product distribution from TPL runs in tetralin as a function of final temperature. It is clear from Figure 4 that from 300 to 350°C, the increase in conversion was due mainly to gains in preasphaltene and asphaltene yields, while the oil yields rose substantially with increasing temperature from 350 to 425°C. It is likely that under the TPL conditions, increasing temperature up to 350°C contributed to cleavage of the weak bonds that released the larger molecules of asphaltene and preasphaltene classes from macromolecular network; increasing temperature from 350 to 400 directly promoted the formation of oil from coal; and further increasing temperature from 400 to 425°C further enhanced oil formation from both coal depolymerization and the thermal cracking of preasphaltene and asphaltene.

We also conducted the control runs under the conventional non-programmed (N-PL) conditions (rapid heat-up from 23°C to reaction temperature in 2-3 minutes) at the temperatures of 350-425°C. Figure 5 compares the TPL and N-PL data for DECS-9 coal in tetralin. As can be seen from Figure 5, relative to N-PL, TPL afforded more preasphaltene at low temperatures between 350-375°C, and more toluene solubles and more oil between 375-425°C. It should be noted that the data in Figure 5 are average of duplicate runs for both TPL and N-PL. The raw data from the duplicate runs show the same trend. For example, the THF conversions from duplicate experiments of N-PL are 70.6 and 72.2% for runs at 400°C, and 75.0, 75.7 and 78.4% for runs at 425°C in tetralin under H<sub>2</sub>. A longer N-PL run at 400°C for extended time period (60 min) only increased the THF conversion by about 2-3 % as compared to the 30 min N-PL run. However, the THF conversions from duplicate TPL runs are 77.0 and 81.4% for TPL at 400°C, and 81.4 and 83.1% for TPL at 425°C. In the case of DECS-1 Texas lignite, TPL runs also gave considerably higher conversions than N-PL runs in tetralin. The average values from duplicate runs of DECS-1 in tetralin are shown in Table 2.

In order to understand the beneficial effects of TPL in H-donor tetralin, we also conducted both TPL and N-PL runs in

non-donor solvents. The data in Table 2 and Table 3 shows that temperature-programming in a non-donor solvent such as naphthalene or 1-methylnaphthalene does not appear to have any significant impact on coal conversion and product distribution. This indicates that beneficial effects of TPL as compared to N-PL in tetralin solvent are closely associated with hydrogen transfer from tetralin.

The above results demonstrated that in the presence of H-donor solvent, TPL can afford considerably higher conversion than the conventional run at the same or even higher final temperatures. This comparison clearly showed that the programmed heat-up is superior to the rapid heat-up for conversion of the low-rank coals in tetralin under H<sub>2</sub>, although it is known that in coal pyrolysis ultrarapid heating increases tar yields [18]. These results indicate that the temperature-programming is a promising approach for converting low-rank coal in H-donor solvent, and further improvement may be achieved by finding the optimum program and by using a catalyst. In fact, we also demonstrated that catalytic TPL of DECS-9 is superior to N-PL in the presence of a dispersed Mo catalyst and a process solvent which has much lower H-donating ability compared to tetralin [16]. Analytical characterization of the residues using CPMAS <sup>13</sup>C NMR and pyrolysis-GC-MS [15] points to the progressive loss of oxygen functional groups and aliphatic species from the macromolecular network of the subbituminous coal during its depolymerization in tetralin under TPL conditions. The higher conversions in TPL runs (relative to the conventional runs in tetralin) suggest that the removal of carboxylic and catecholic groups from the coal during the programmed heat-up in tetralin may have contributed to minimizing the retrogressive crosslinking at higher temperatures.

### Mechanistic Considerations

Comparative examination between the TPL and N-PL runs using different solvents established that the beneficial effects of temperature-programming in tetralin are not due to thermal treatment but are closely associated with low temperature hydrogen-transfer during programmed heat-up. Although H-transfer is a chemical process, both the physical and chemical mechanisms can be responsible for the desirable effects of TPL as compared to N-PL in tetralin. Our initial idea in designing the temperature program was to meet the physical as well as chemical requirements for conversion of coals which are macromolecular in chemical nature but are microporous in physical nature. The rationale of selecting a low temperature soak is associated with the characteristics of coal pore structure. A large part of pore volume of low-rank coals is located in mesopores (20-500 Å in diameter) and macropores (>500 Å). However, most of the surface area of coals is enclosed in the micropores (<20 Å); hence rates of reaction are limited by rates of diffusion through the micropores [19,20]. Spears et al. [20] reported that the micropore walls contain polar functional groups, and their abundance is higher for low-rank coals. It is considered that soak at 200°C for 15 min will facilitate the diffusion of tetralin into the micropores (< 20 Å) and smaller mesopores (>20 Å). Also, possibility exists that tetralin could induce swelling at 200°C which may open up some pores that are solvent-inaccessible at room temperature. However, such physical effects would be smaller for liquefaction of bituminous coals.

The chemically beneficial effect of TPL compared to N-PL in H-donor lies in the programmed heat-up. The H-transfer from H-donor could stabilize the thermally derived radicals and thermally sensitive groups. Because of the bond dissociation energy distribution, one could selectively break certain bonds at certain temperature range by using temperature programming, which would provide time for radical to abstract H from H-donor. Low-rank coals are characterized by low aromaticities and high oxygen functionalities [21]. Suuberg et al. [22], Solomon et al. [18] and Lynch et al. [23] have indicated that during coal pyrolysis, decarboxylation is accompanied by crosslinking reactions and the formation of CO<sub>2</sub>. McMillen et al. [24] have provided some insights into the retrogressive reactions involving polyhydroxy structures. It is likely that the retrogressive reactions occurring during liquefaction of low-rank coals under conventional high-severity conditions are, at least in part, associated with the reactions of their oxygen functional groups. It seems possible from comparative examination of the coal conversion data that the TPL conditions may facilitate the reduction of crosslinking reactions of the thermally sensitive groups such as oxygen-functional groups at low temperatures in H-donor. Both the present and previous results [3,4,8] strongly suggest that very fast heating would result in too fast a thermal fragmentation of low-rank coals at high temperatures to be balanced by H-donation, which consequently leads to enhanced retrogressive reactions.

### Acknowledgements

Financial support for this work was provided by the Cooperative Program for Coal Research (Fund No. 424-04-2404 LG-4-91) at Pennsylvania State University. We gratefully acknowledge the assistance of Mr. J. McConnie in liquefaction experiments. We also wish to thank Dr. A. Davis and Mr. D.C. Glick for providing the samples and data of the coals from Penn State Coal Sample Bank.

## References

- Sondreal, E.A., Paper presented at the *Information Transfer Session*, Cooperative Program in Coal Research, The Pennsylvania State University, Nov. 18-19, 1991.
- Derbyshire, F.; Davis, A.; Lin, R., *Energy & Fuels* 1989, 3, 431.
- Song, C., Hanaoka, K. and Nomura, M., *Fuel* 1989, 68, 287.
- Song, C., Nomura, M. and Hanaoka, K., *Coal Sci. Technol.* 1987, 11, 239.
- DOE COLIRN Panel, "Coal Liquefaction", Final Report, DOE-ER-0400, Vol. I & II, 1989
- Song, C.; Nomura, M.; Ono, T., *Am. Chem. Soc. Div. Fuel Chem. Prepr.* 1991, 36(2), 586
- Song, C.; Nomura, M., *Fuel*, 1986, 65, 922.
- Masunaga, T and Kageyama Y. *Proc. 1989 Int. Conf. Coal Sci.*, Tokyo, 1989, 819.
- Derbyshire, F.J.; Davis, A.; Epstein, M.; Stansberry, P.G. *Fuel* 1986, 65, 1233
- Derbyshire, F.J.; Davis, A.; Schobert, H.; Stansberry, P.G. *Am. Chem. Soc. Div. Fuel Chem. Prepr.* 1990, 35, 51.
- Burgess, C.E. and Schobert, H. *Am. Chem. Soc. Div. Fuel Chem. Prepr.* 1990, 35, 31.
- Stenberg, V.I., Gutenkurt, V., Nowok, J. and Sweeny P.G. *Fuel* 1989, 68, 133.
- Song, C.; Schobert, H.H.; Hatcher, P.G., *Proc. 1991 Int. Conf. Coal Sci.*, 1991, UK, p.664.
- Song, C.; Schobert, H.H.; Hatcher, P.G., *Energy & Fuels* 1992, in press.
- Song, C.; Schobert, H.H.; Hatcher, P.G., *Am. Chem. Soc. Div. Fuel Chem. Prepr.* 1992, 37, in press.
- Huang, L.; Song, C.; Schobert, H.H., *Am. Chem. Soc. Div. Fuel Chem. Prepr.* 1992, 37, in press.
- Davis, A.; Glick, D.C.; Mitchell, G.D., Proceedings of DOE Liquefaction Contractors' Review Meeting, Sept. 3-5, 1991, Pittsburgh, p.398-410.
- Solomon, P.R.; Serio, M.A.; Despande, G.V.; Kroo, E. *Energy & Fuels* 1990, 4, 42.
- Mahajan, O.P.; "Porosity of Coals and Coal Products", in *Analytical Methods for Coal and Coal Products*, Vol. I, C. Karr, Ed., Academic Press, New York, 1978, p.125-162.
- Spears, D.R.; Sady, W.; Kisper, L.D., *Am. Chem. Soc. Div. Fuel Chem. Prepr.* 1991, 36 (2), 1277.
- Schobert, H.H., *Resources, Conservation and Recycling* 1990, 3, 111.
- Stuoberg, E.M.; Unger, P.E.; Larsen, J.W. *Energy & Fuels* 1987, 1, 305.
- Lynch, L.J.; Sakurovs *Proc. 1991 Int. Conf. Coal Sci.*, Newcastle upon Tyne, 1991, 592.
- McMillen, D.F.; Chang, S.; Nigenda, S.E.; Malhotra, R. *Proc. 1985 Int. Conf. Coal Sci.*, Sydney, 1985, 153.

**Table 1.** Representative Analyses of DOE / Penn State Coal Samples

Sample No.	DECS-9 or PSOC 1546	DECS-1 or PSOC 1538
<b>Proximate (wt%)</b>		
Volatile Matter	33.5 (47.1) <sup>a</sup>	33.2 (55.5) <sup>a</sup>
Fixed Carbon	37.1 (52.9) <sup>a</sup>	25.8 (44.5) <sup>a</sup>
Moisture	24.6	30.0
Ash	4.8	11.1
<b>Ultimate (wt%, dmmf)</b>		
Carbon	76.1	76.1
Hydrogen	5.1	5.5
Nitrogen	0.9	1.5
Organic Sulfur	0.3	1.1
Oxygen (by diff)	17.6	15.8
<b>Source &amp; Rank</b>		
State	Montana	Texas
County	Bighorn	Freestone
City	Decker	Fairfield
Seam	Dietz	Bottom
Age of Seam	Paleo	Eocene
ASTM Rank	Subbit B	Lig A / Sub C
Sampling Date	6/12/90	12/1/89

a) On a dry, mineral matter free (dmmf) basis.

**Table 2.** Temperature-Programmed (TPL) and Non-programmed Liquefaction (N-PL) with H-Donor Teralin and Non-donor 1-Methylnaphthalene (1-MN) Solvents at 400 °C for 30 min

Coal	DECS-9	DECS-9	DECS-1	DECS-1	DECS-9	DECS-9
	Mont Sub	Mont Sub	Texas Lig	Texas Lig	Mont Sub	Mont Sub
	TPL	N-PL	TPL	N-PL	TPL	N-PL
Solvent	Tetralin	Tetralin	Tetralin	Tetralin	1-MN	1-MN
<b>Prod. dmmf wt%</b>						
THF-Conv <sup>a</sup>	79.2	71.4	78.0	69.8	34.1	32.2
Tolue-Conv <sup>b</sup>	55.5	50.1	66.1	58.0	27.1	25.4
Oil + Gas	34.4	29.4	48.5	45.1	18.9	16.0
Asphaltene	21.1	20.6	17.5	12.9	8.2	9.4
Preasphaltene	23.7	21.4	11.9	11.8	7.0	6.8

a-b) Total conversion to a) THF-solubles and b) toluene-solubles plus gas.

**Table 3.** Temperature-Programmed (TPL) and Non-programmed Liquefaction (N-PL) with H-Donor Teralin and Non-donor Naphthalene Solvents at 350 °C for 30 min

Coal	DECS-9	DECS-9	DECS-9	DECS-9
	Mont Sub	Mont Sub	Mont Sub	Mont Sub
	TPL	N-PL	TPL	N-PL
Solvent	Tetralin	Tetralin	Naphthalene	Naphthalene
<b>Prod. dmmf wt%</b>				
THF-Conv <sup>a</sup>	42.0	31.9	21.3	21.4
Tolue-Conv <sup>b</sup>	19.2	17.0	13.7	14.2
Oil + Gas	2.7	4.0	9.3	7.9
Asphaltene	16.5	13.0	4.4	6.3
Preasphaltene	22.8	14.9	7.6	7.2

a-b) Total conversion to a) THF-solubles and b) toluene-solubles plus gas.

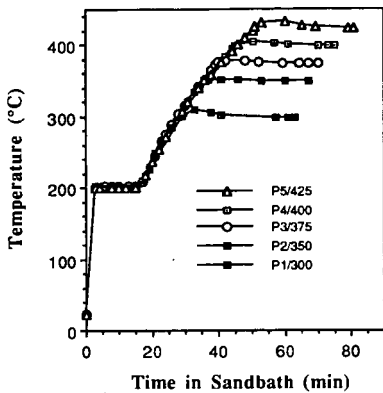


Figure 1. Temperature programs examined in TPL of DECS-9 coal.

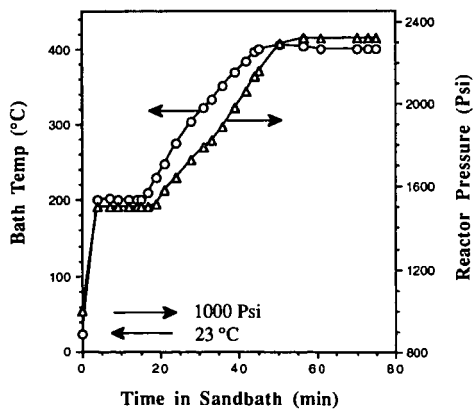


Figure 2. Typical temperature-pressure profile during programmed heat-up and holding for non-catalytic TPL of DECS-9 coal in tetralin at a final temperature of 400 °C.

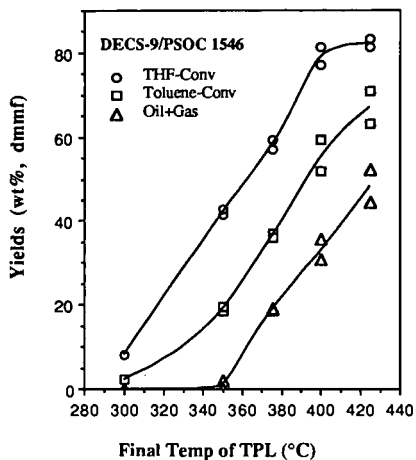


Figure 3. Relationship between final temperature of TPL and coal conversion to THF-, toluene- and hexane-solubles plus gases.

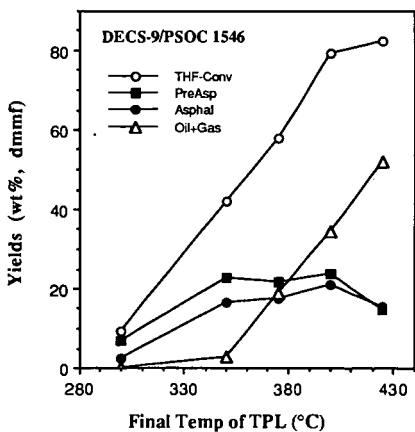


Figure 4. Product distribution from TPL of DECS-9 in tetralin at different final temperatures ranging from 300 to 425°C.

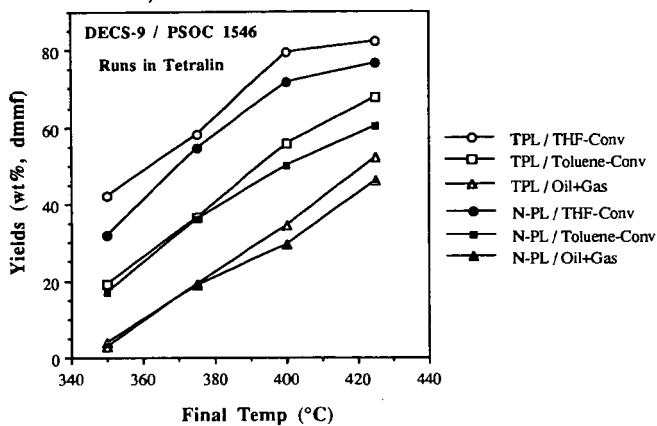


Figure 5. Comparison between temperature-programmed (TPL) and non-programmed (N-PL) runs of DECS-9 coal in tetralin solvent.

STUDIES OF THE REACTIONS OF DIBENZYL ETHER UNDER  
PRECONVERSION PROCESSING CONDITIONS\*

Frances V. Stohl and Richard J. Kottenstette  
Process Research Division 6212  
P.O. Box 5800  
Sandia National Laboratories  
Albuquerque, NM 87185

Keywords: retrogressive reactions, dibenzyl ether, pyrite, kaolinite

INTRODUCTION

The occurrence of retrogressive reactions during direct coal liquefaction processing is harmful because these reactions result in the formation of high molecular weight material that is refractory to further processing. Therefore, the yields of desired products are decreased, downstream processing conditions must be more severe than if retrogressive reactions did not occur, and in some cases, an accumulation of solids causes process shutdown.<sup>(1)</sup> The objectives of this research project are 1) to determine the causes of retrogressive reactions during the initial processing of coal (known as preconversion processing) in direct liquefaction and 2) to devise methods for minimizing these undesired reactions. The first objective involves evaluating the effects of process conditions and additives on retrogressive reactions. The approach to completing this objective is twofold. Initial scoping studies have been done using the model compound dibenzyl ether (DBE). Subsequent work will use coal. Work on the second research objective will be performed in conjunction with the evaluation of the effects of process variables and additives on coal. Research for completing the second objective will involve several different approaches such as the use of cleaned coals, and the use of different coal pretreatments.

DBE was chosen for the initial scoping studies for three reasons: 1) ether linkages represent one type of bonding reported to be present in coal<sup>(2)</sup>; 2) other investigators have analyzed the kinetics and mechanism of thermolysis of DBE<sup>(3,4)</sup> and have also used DBE to study effects of process variables in coal liquefaction<sup>(5)</sup>; and 3) DBE is known to undergo retrogressive reactions. In the work reported here, experiments have been performed to evaluate the impacts of different types of mineral matter (including low temperature ash (LTA) separated from Illinois #6 coal, kaolinite (a clay mineral commonly found in coal), and pyrite) on the reaction of DBE. The preconversion processing conditions used in this work are similar to those that occur between the time the coal is mixed with recycle solvent and the time the coal slurry enters the first-stage reactor at the Wilsonville Advanced Direct Coal Liquefaction R & D Facility. This includes the preheating step in which the coal slurry is heated up to first-stage reaction temperatures. The initial temperature for preconversion processing is about 180°C (the temperature of the solvent-coal mixture just prior to entering the preheater at Wilsonville). The final temperature has not been reported because the temperature of the feed to the

\* This work was supported by the U.S. Department of Energy at Sandia National Laboratories under contract DE-AC04-76DP00789.

first-stage reactor is proprietary. However, it must be less than the average first-stage temperature, which is approximately 425°C. The slurry blend tank and feed tank are both at atmospheric pressure; pressurization with hydrogen occurs prior to the slurry entering the preheater.

## EXPERIMENTAL

### Materials

The commercial hydrotreating catalyst used in these experiments was Shell 324N, a NiMo/Al<sub>2</sub>O<sub>3</sub> catalyst with 12.4 wt% Mo and 2.8 wt% Ni. Prior to use, this catalyst was presulfided with a 10 mol% H<sub>2</sub>S/H<sub>2</sub> mixture at 380°C and atmospheric pressure for 2 h, and was then ground to -200 mesh. Three types of fine-grained mineral matter were utilized: coal-derived mineral matter, kaolinite (Al<sub>2</sub>Si<sub>2</sub>O<sub>5</sub>(OH)<sub>4</sub>), and a coal-derived pyrite sample. The coal-derived mineral matter was separated from Illinois #6 coal, which was obtained from the Argonne Premium Coal Sample Program, by using an LFE Corp. low temperature ashier (model LTA 504). The kaolinite, in the form of a Georgia kaolin, was used as received. The pyrite sample was obtained by beneficiation of coal at the Robena Laboratory of the U. S. Steel Corporation and was subsequently pulverized under nitrogen to a particle size of -5 microns by means of a four inch orbital "Micron-Master Jet Pulverizer" at the Jet Pulverizer Co., Palmyra, New Jersey. The pyrite sample was cleaned by low-temperature ashing to oxidize the associated organic matter. After low-temperature ashing, the pyrite was separated from the other mineral matter by using the acid cleaning procedure, which consists of washing and filtration using hydrochloric acid, followed by hydrofluoric acid, and a repeat of the hydrochloric acid treatment, reported by Bishop and Ward<sup>(6)</sup>. X-ray diffraction was used to check the purity of pyrite samples.

### Hydrotreating Experiments

All reactions with DBE were performed in 26 cm<sup>3</sup> 316 stainless steel microautoclaves. The heat up time and quench time for each reaction were less than 2 minutes each. Nominal reactant and catalyst loadings for most experiments (unless otherwise noted) were 100 mg DBE, 50 mg catalyst, and 50 mg mineral matter. The microautoclaves for all experiments were charged with 1000 psig H<sub>2</sub> cold charge pressure. Reaction times at temperature for all experiments were 15 minutes; reaction temperatures ranged from 180°C to 300°C.

### Product Analyses

Products from the microautoclave experiments were dissolved in carbon disulfide (CS<sub>2</sub>) and analyzed using a combination of gas chromatography (GC) and GC/mass spectrometry (GC/MS). Recoveries of products from runs were determined quantitatively by GC using dodecane as an internal standard and response factors determined for DBE and toluene. Recoveries of products from the DBE reactions included quantitation of all non-CS<sub>2</sub> related peaks that were detected by GC (Figure 1). Unidentified compounds with GC retention times less than DBE are classified as low molecular weight unknowns, i.e. the molecular weight (MW) is less than 198, which is the MW of DBE. The total amount of low molecular weight material is equal to the sum of DBE, additional identified compounds (all of which have MWs less than DBE), and the low molecular weight unknowns. The unidentified compounds with retention times greater than DBE represent compounds with MWs greater than DBE, which were formed by retrogressive reactions. The total amount of high molecular weight material (HMWM) formed by retrogressive reactions is defined in this work as the sum of the amount of unidentified compounds detected by GC that had higher retention times than DBE

and the amount of material that was not detectable by GC. This non-detectable material, which did not elute from the GC column, was determined by difference.

Field Ionization Mass Spectrometry (FIMS) analyses, which provide molecular weight distributions for products vaporized using a mild ionization source, were performed on the products from several of the experiments. These analyses were done by Ripu Malhotra of SRI International.

## RESULTS and DISCUSSION

### The Impact of Low Temperature Ash from Illinois #6 Coal on DBE Reactions

Results of an experiment performed at 300°C with the low temperature ash separated from the Illinois #6 Argonne coal are shown in Figure 2. This reaction had a DBE:LTA ratio of 2.25:1. The total recovery of all products detectable by GC analysis was only about 9 wt%, of which about 4 wt% was low molecular weight products (including toluene, diphenyl methane (DPM), and C<sub>14</sub>H<sub>14</sub> compounds) and about 5 wt% was unidentified material with a MW greater than DBE. The remainder of the reaction product (91 wt%) did not elute from the GC column. Therefore, the total amount of HMWM in the product was about 96 wt% indicating the occurrence of significant retrogressive reactions. The results of this experiment were compared to those of a similar experiment with Shell 324M catalyst. The experiment with Shell 324M had a 2:1 DBE:Shell 324M ratio; other conditions were the same. The total recovery of all products detectable by GC was 83 wt%, of which about 71 wt% was low molecular weight material (42 wt% toluene, 1 wt% DPM, 11 wt% bibenzyl, 9 wt% other C<sub>14</sub>H<sub>14</sub> compounds, 8 wt% low molecular weight unknowns). The presence of a catalyst and no mineral matter yields a significant improvement in recoveries of low molecular weight material. (Previous work has shown that the presence of a good hydrogen donor with the Shell 324M would give a significantly higher yield of low molecular weight material.) A similar thermal reaction with no additives gave about 98 wt% recovery of low molecular weight material of which 89 wt% was DBE.

The results of the experiment with Illinois #6 LTA showed that mineral matter in coal can produce significant amounts of retrogressive reactions with DBE. Since coal-derived mineral matter contains many different components, additional experiments were performed with several of the components.

### The Effects of Pyrite on DBE Reactions

The effects of pyrite on the reaction of DBE were studied because it has known catalytic activity in direct coal liquefaction. Results of an experiment with freshly cleaned Robena pyrite and DBE are shown in Figure 3. The DBE:pyrite ratio was 2:1. Results show that pyrite yields about the same total recovery of material on the GC (about 84 wt%) as Shell 324M. However, the pyrite gives more low molecular weight material than Shell 324M (77 wt% versus 71 wt%), and the distribution of low molecular weight material is significantly different; pyrite gave about 60% more toluene than Shell 324M. Both of these reactions were run in duplicate and showed excellent reproducibility.

An additional experiment was performed with an oxidized sample of Robena pyrite. This sample had been low temperature ashed and acid cleaned in 1980 using the same procedures as the freshly cleaned pyrite. It was stored under air in a glass sample vial without any special precautions to prevent oxidation. A comparison of the DBE reaction product distributions from experiments with these two pyrite samples is shown in Figure 4. The aged pyrite yielded about 95 wt% HMWM whereas the freshly cleaned pyrite gave only

23 wt% HMWM. X-ray diffraction analyses of both pyrite samples showed that the aged sample had significant amounts of iron sulfate hydrate present, whereas the freshly cleaned sample was pure pyrite.

#### The Effects of Kaolinite on DBE Reactions

Kaolinite was also chosen for additional experiments because it is a clay mineral present in coal, and clays usually are the most abundant minerals in coal. In addition, a previously reported study<sup>(7)</sup> has shown that the acidic components of coal mineral matter enhance DBE conversion. Figure 5 shows the product distributions for five reactions of DBE with varying amounts of kaolinite present. These results show that retrogressive reactions occur for all the experiments. With the least amount of kaolinite only about 15 wt% of the product is HMWM. However, for higher concentrations of kaolinite, as much as 93 wt% of the product can be HMWM. An additional set of experiments was performed to determine the impact of reaction temperature on product distribution with 36 wt% kaolinite on a weight of DBE basis (Figure 6). The results show that even at a temperature of 180°C significant retrogressive reactions occur with about 75 wt% HMWM formed. A FIMS analysis of the product from the 180°C reaction is shown in Figure 7. The number average MW for the product was 804, significantly higher than the MW of DBE (198). The spectrum shows that the reaction product had compounds with MWs greater than 1300 amu. In addition, it shows groups of peaks that are separated by 90 amu. This distribution is indicative of the occurrence of benzylation reactions, which are known to occur in the presence of strong Lewis acids.

Three experiments were performed to determine the impact of water on the reaction of DBE with kaolinite. These results, shown in Figure 8, indicate that water does decrease the formation of HMWM. However, the effect is not very large and large amounts of water are required.

#### CONCLUSIONS

The results of these experiments indicate that the mineral matter in coal can have a significant effect on retrogressive reactions. Kaolinite yields high amounts of retrogressive reactions that occur down to reaction temperatures at least as low as 180°C. These retrogressive reactions are due to benzylation reactions. Pyrite, in contrast, can be either beneficial or harmful. If the pyrite is unoxidized, it can give high yields of desired product. However, if the pyrite is oxidized, it can yield significant amounts of retrogressive reactions. It has been demonstrated that retrogressive reactions can occur under currently used preconversion processing conditions and that improved processing techniques need to be developed to prevent these harmful reactions. Coal cleaning involving removal of the clays and readdition of unoxidized pyrite may be one technique for improving coal liquefaction.

#### REFERENCES

1. Gollakota, S. V., Vimalchand, P., Davies, O. L., Lee, J. M., Corser, M. C., Cantrell, C. E., Proc. Liquefaction Contractors' Review Meeting, 504-531, Pittsburgh, PA, September 3-5, 1991.
2. Shinn, J.H., Fuel 63(9), 1187-96, 1984.
3. Korobkov, V.Y., Grigorieva, E.N., Senko, O.V., Kalechitz, I.V., Fuel Proc. Tech. 19, 243-52, 1988.
4. Cronauer, D.C., Jewell, D.M., Shah, Y.T., Modi, R.J., Ind. Eng. Chem. Fundam. 18(2), 153-162, 1979.

5. Panvelker, S.V., Shah, Y.T., Cronauer, D.C., Ind. Eng. Chem. Fundam. 21, 236-42, 1982.
6. Bishop, M., Ward, D. L., Fuel 37, 191-200, 1958.
7. Kamiya, Y., Nagae, S., Oikawa, S., Fuel 62, 30-3, 1983.

LOW MOLECULAR WEIGHT MATERIALS

- TOLUENE Cc1ccccc1
- ADDITIONAL IDENTIFIED PRODUCTS
  - BENZALDEHYDE O=Cc1ccccc1
  - BENZYL ALCOHOL Oc1ccccc1
  - BIBENZYL c1ccccc1Cc2ccccc2
  - DIPHENYL METHANE c1ccccc1Cc2ccccc2
- UNIDENTIFIED GC PEAKS (RT < DBE)

HIGH MOLECULAR WEIGHT MATERIALS

- UNIDENTIFIED GC PEAKS (RT > DBE)
- NOT DETECTABLE BY GC

Figure 1. Distribution of reaction products used for quantification.

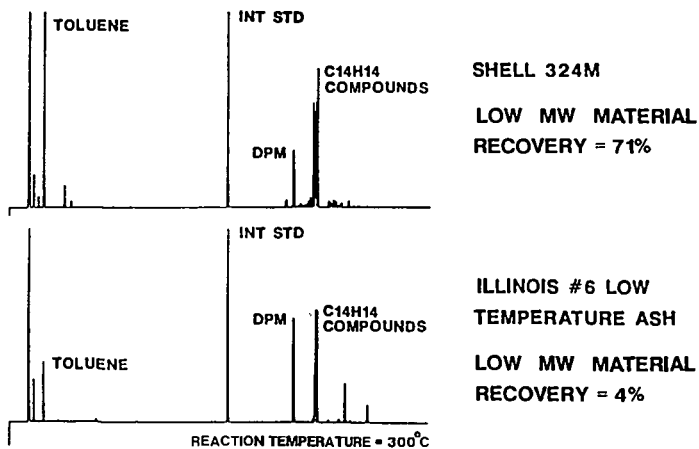


Figure 2. Mineral matter addition gave much higher yields of HMWM than Shell 324M.

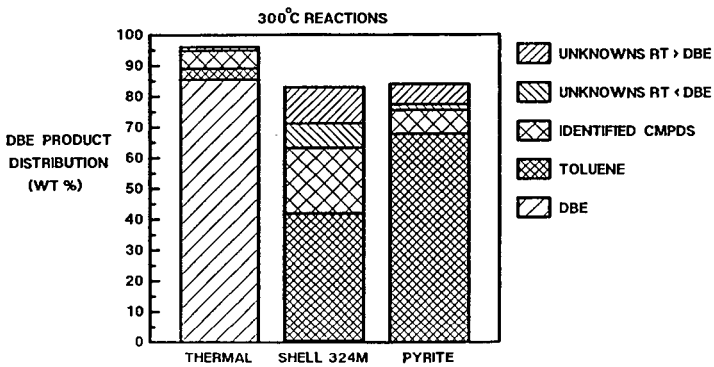


Figure 3. Pyrite addition gave 60% more toluene than Shell 324M at 300°C.

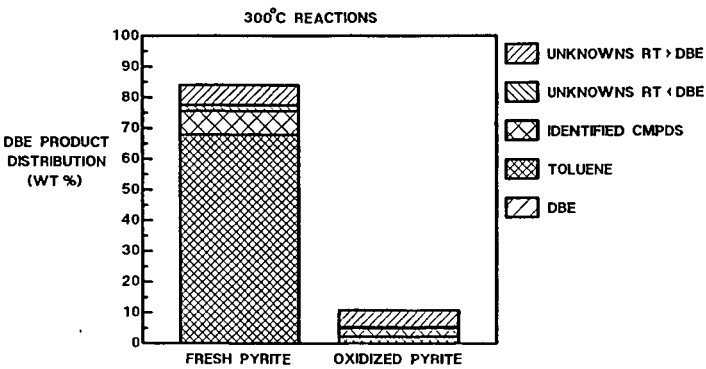


Figure 4. Oxidized pyrite causes significantly more retrogressive reactions than fresh pyrite.

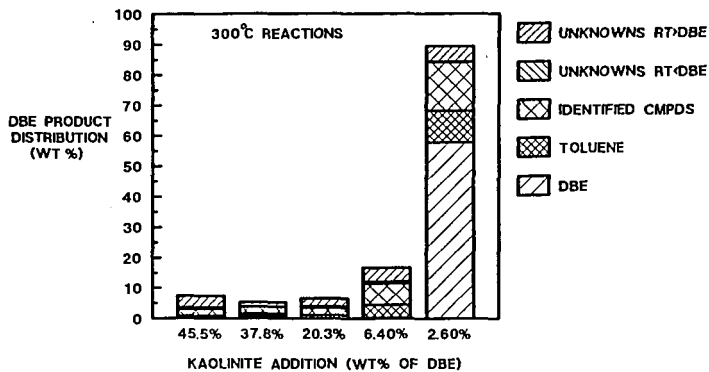


Figure 5. Kaolinite addition at 300°C causes the formation of HMWM.

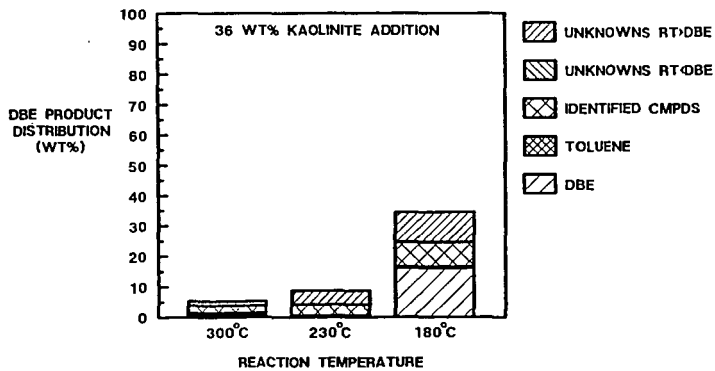


Figure 6. Kaolinite addition causes retrogressive reactions at temperatures as low as 180°C.

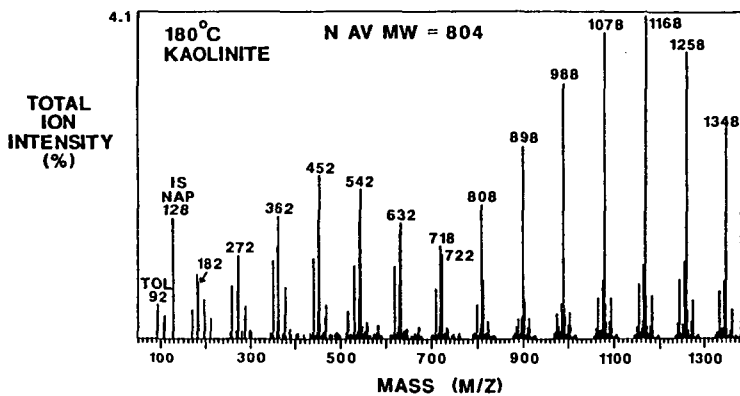


Figure 7. At 180°C, kaolinite gives benzylated products with molecular weights greater than 1300 amu.

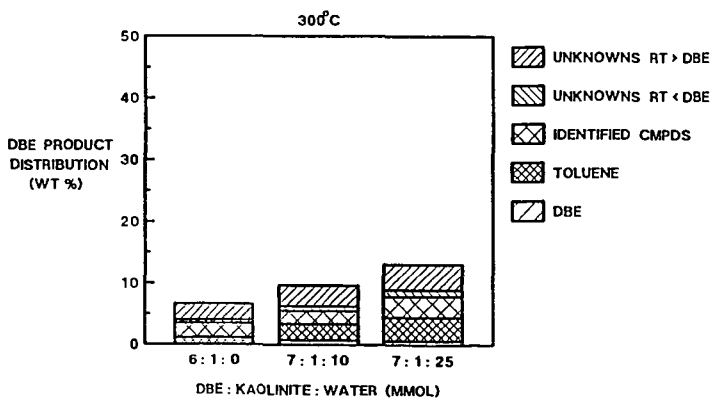


Figure 8. Addition of water appears to decrease the effect of kaolinite on retrogressive reactions.

## CATALYSTS FOR AQUEOUS/CO LIQUEFACTION OF SUBBITUMINOUS COAL

Ramesh K. Sharma and Edwin S. Olson

University of North Dakota Energy and Environmental Research Center  
Grand Forks, ND 58202

Key Words: Aqueous/CO liquefaction, homogeneous catalysts, sodium aluminate

### ABSTRACT

Coal liquefaction has been effectively carried out with carbon monoxide reductant in an aqueous solvent (CO steam process). Australian workers demonstrated that sodium aluminate is able to catalyze the conversion of Australian coals in the CO/H<sub>2</sub>O system and in water/hydrogen donor solvent mixtures. To demonstrate an economical process for liquefaction of Wyodak subbituminous coal, aqueous sodium aluminate has been utilized as the catalyst. High conversions comparable with those obtained with hydrogen donor solvents and hydrogen sulfide were obtained. The product consists of a large distillate fraction composed of oxygenated compounds and many aromatics. The asphaltene and oil fractions are suitable for second-stage catalytic hydrogenation. Reactions utilizing hydrogen as the reductant gave low conversions with sodium aluminate. The nature of the reductive reactions catalyzed by the sodium aluminate in aqueous/carbon monoxide systems are currently being investigated with various model compounds.

### INTRODUCTION

The goal of the UNDEERC coal science group is the development of new homogeneous catalysts for first-stage coal liquefaction. These catalysts are expected to aid in solubilization and preliminary reduction of low-rank coals to a high quality intermediate product that can be easily converted to distillate fuels with low heteroatom content.

Catalysis of the first stage of coal liquefaction involves improving the rates of bond cleavage reactions leading to improved solubility and of preliminary reduction reactions so that oils and asphaltene are produced without extensive retrogressive reactions. These materials should be able to interact effectively with the solid and colloidal coal matter, catalyzing the conversion to soluble oils at moderate temperature, while minimizing problems with low surface areas or mass transfer. Thus various inorganic agents that are soluble in the reaction vehicle or solvent are being investigated. Some of these (e.g., sodium aluminate) are polymeric at the reaction conditions and are precursors for the clays and zeolites that are currently under investigation as second-stage liquefaction catalysts.

### EXPERIMENTAL

#### Catalytic Liquefaction of Coal

A slurry consisting of 5.0 g of coal (as received Wyodak-Clovis Point) and a solution of the desired catalyst in 20 g solvent (water) was placed in a 70-ml

Parr reactor. The reactor was evacuated and charged with a mixture of 1000 psi of desired gas. The reactor was heated to 400°C in a rocking autoclave (initial heatup time = 11 minutes) and left at this temperature for 30 minutes. At the end of the reaction, the reactor was cooled to room temperature, and the gases were removed. The reactor was attached to a set of two traps cooled in ice and liquid nitrogen. The product slurry was distilled to remove water. The distillate was saturated with NaCl and extracted with ether. The extract was mixed with appropriate internal standard and analyzed by GC and GC/FTIR/MS.

The residue was extracted with pentane, toluene, and tetrahydrofuran (THF). The pentane-soluble fraction was mixed with appropriate internal standard and analyzed by GC. The toluene-soluble, THF-soluble, and THF-insoluble fractions were dried in vacuo at 110°C overnight and weighed. The percent conversion was calculated on the basis of the coal (maf) that did not appear in the THF-insoluble fraction. The conversion and yield data are given in Table 1.

#### Catalytic Hydrotreating of Model Compounds

In a typical run, 0.5 g of model compound, 2 g of solvent (water), and the desired amount of catalyst (if needed) were placed in a tubing bomb (12-mL microreactor). The microreactor was evacuated, pressurized with 1000 psig of carbon monoxide, placed in a rocking autoclave, and heated to 400°C. At the end of the specified reaction period, the microreactor was cooled in a dry ice-acetone slurry, degassed, and opened. The resulting slurry was acidified with dilute HCl. The desired amount of the internal standard was added to the product slurry, and the product slurry was extracted with methylene chloride. The methylene chloride extract was dried over molecular sieves (4Å) and analyzed by GC/FID and GC/FTIR/MS.

#### Instrumentation

Quantitative GC/FID analyses were performed with a Hewlett Packard 5880A gas chromatograph equipped with a Petrocol capillary column. A mixture of iso-octane and n-octadecane was the internal standard. GC/FTIR/MS was performed on a Finnigan 800 ITD ion trap detector with a HP 5890A gas chromatograph and a J&W 30-m x 0.32-mm (ID), 1.0-micron film of DB-5. A 15-m x 0.25-mm (ID), 0.25-micron DB-5 film capillary column was used for the analysis of high boiling components.

### **RESULTS AND DISCUSSION**

In the first part of our study of homogeneous catalysts for first-stage coal liquefaction, catalysts for improving the conversion and product quality of liquefactions carried out in aqueous systems were investigated. Aqueous reactions that utilize carbon monoxide as the reductant gas have been extensively investigated in this and other laboratories over many years (1-3). Basic catalysts have been employed to achieve higher conversions. The aqueous/CO reduction has been shown to be superior to hydrogen for the first stage of liquefaction.

Little is understood about the mechanism of the aqueous/CO reaction with coal or even with model organic compounds. Jones and others have shown that an aryl ketone (benzophenone) and an aryl carbinol are reduced (4). Bases were required for reduction of the ketone, and higher conversions were obtained for the carbinol reduction in the presence of base. Reduction of anthracene and quinoline were also effected with aqueous CO; however, higher conversions of

anthracene were obtained in the absence of base (5). The reduction of ketones with CO in aqueous sodium carbonate can be explained by sodium ion activation of the CO to give an intermediate such as formate that can donate hydride to the carbonyl. Reduction of anthracene or other hydrocarbons would appear to proceed by a different mechanism.

In screening a number of candidates for improving the conversion in aqueous/CO liquefaction processing, Jackson and others (6,7) found that aqueous sodium aluminate gave good conversions of brown coal to oils at temperatures of 350° to 400°C. Factors such as pH and concentration in aqueous systems of the materials are critical in determining the actual aluminate structures present; however, Jackson did not report the pH of his system. Being amphoteric, the polymeric aluminate form may have Lewis acid sites at moderate pH values of 8-12 that would be effective in cleavage of covalent bonds in coals. Whether the sodium aluminate is able to activate the carbon monoxide so as to produce a hydride- or hydrogen-donating intermediate or some other form of activated hydrogen is still not certain.

The first priority in our work was to verify that sodium aluminate is also effective in improving the aqueous-CO liquefaction of low-rank western U.S. coals and to measure the solubilities and product qualities of the reaction products from these U.S. coals. Since high conversions to THF solubles are easily obtained at 400°C without any promoter or catalyst with the low-rank coals, the conversion to oils, asphaltenes, and distillate needs to be accurately determined. The composition of the distillate, oil, and asphaltene product obtained after first-stage liquefaction in aqueous CO must be determined for comparison with that obtained in organic solvents with CO or with hydrogen. Previous studies have indicated that the volatile first-stage product from aqueous liquefaction should contain large amounts of phenolics rather than hydrocarbons, as for organic solvent liquefaction. If this is the case, the distillate can be removed and used elsewhere, so that hydrogen is not wasted in deoxygenation of phenols.

The conversion of Wyodak subbituminous coal to THF solubles in the aqueous/CO liquefaction with sodium aluminate was 89% (Table 1). This was substantially higher than that obtained with no added sodium aluminate (78%). The high conversion with sodium aluminate is consistent with that observed by Jackson and others for Australian brown coals (6,7). Conversion in an aqueous/CO liquefaction experiment with sodium hydroxide catalyst was actually much lower than expected on the basis of previously reported work. Under the same conditions as the sodium aluminate experiments, only 72% of the Wyodak coal was converted to THF solubles with sodium hydroxide catalyst. After stirring the sodium aluminate and sodium hydroxide solutions with the coal at room temperature, the pH of the reactions was measured, and both reactions were at a pH of 11. At the end of the reactions, the pHs of the aqueous portions of the products were between 6 and 7 as a result of carbon dioxide generation during the liquefaction from decarboxylation and water-gas shift reactions. It is likely that the sodium aluminate is polymeric during the reaction, but further information is needed to understand the nature of the aluminate catalyst under these conditions.

The liquefaction product quality as determined by the distribution of solubility fractions was good for the sodium aluminate-catalyzed reaction. As shown in Table 1, the toluene solubles amounted to 20% of the maf coal, and 42% of the coal was converted pentane solubles, CO<sub>2</sub>, and H<sub>2</sub>O. The major products in the distillate were oxygenated compounds, such as methanol, 2-propanol (from

acetone), and phenolics. In addition, there were hundreds of hydrocarbon components that are typically found in coal-derived products. A similar distribution was obtained for the NaOH-catalyzed reaction, but the amounts in each of the fractions were much lower.

Reactions were conducted to verify that carbon monoxide was the most effective gas for the liquefaction of Wyodak under the mildly basic conditions. Hydrogen (1000 psi at room temperature) gave only a 43% conversion to THF solubles. Since nitrogen (1000 psi) gave a similar conversion (41%) and a similar product solubility distribution, it is unlikely that hydrogen had any effect at all in the liquefaction and was not activated by the sodium aluminate.

The second priority in our program was to understand something about the nature of the sodium aluminate catalysis. Sodium aluminate could probably activate CO for hydride reduction as well as sodium carbonate, perhaps better. But does it also activate CO so that hydrogenation of hydrocarbons occurs? Can it lower activation energies for cleavage of bonds such as in ether and carboxylate groups? The reactions of several model compounds were investigated in aqueous/CO conditions, and the results were compared with those obtained in the absence of the sodium aluminate.

Anthracene was heated in water at 400°C (2 hr) with 1000 psi of carbon monoxide (measured at room temperature). In the reaction with no promotor, a 79% conversion of the anthracene was observed (Table 2). The main reaction product was 9,10-dihydroanthracene, with 1,2,3,4-tetrahydroanthracene being a minor product. When sodium aluminate (1.25 mmole/g of substrate) was added, the conversion of anthracene increased to 82%. An anthracene reaction carried out with an equivalent amount of sodium hydroxide gave a lower conversion (64%). The lower anthracene conversion with sodium hydroxide is consistent with the lower conversion Stenberg and others reported for reactions of anthracene carried out with added sodium carbonate (5). Stenberg's results were obtained at more severe conditions (425°C, 1500 psi CO at room temperature), and the main product was tetrahydroanthracene, rather than dihydroanthracene. Dihydroanthracene may be an intermediate in the formation of tetrahydroanthracene, and more transformation of the initial dihydroanthracene may occur at the higher temperature. The sodium aluminate can, therefore, promote the reaction of carbon monoxide with polynuclear aromatic hydrocarbons somewhat better than water in a process that is retarded by the presence of other basic compounds and, in addition, can catalyze the reaction of carbon monoxide in the reduction of carbonyl groups in a process that is catalyzed by sodium carbonate or hydroxide.

Substituted naphthalenes were not significantly reduced by CO with the sodium aluminate promotor under the same conditions used for anthracene. Sodium 1-naphthoate was converted to naphthalene with complete decarboxylation and only 2% reduction to tetralin and to 1-methylnaphthalene. Sodium 1-naphtholate and 1-naphthol were recovered mostly unreacted, with 3% reduction to naphthalene and to tetralin. Increasing the amount of sodium aluminate tenfold in the naphthol reduction resulted in only a slight increase in the yield of tetralin.

Further work on the mechanisms and nature of the intermediates involved in these reactions is in progress.

#### ACKNOWLEDGEMENT

The support of the US Department of Energy is gratefully acknowledged.

## REFERENCES

1. Appell, H.R.; Wender, I.; Miller, R.D. Prep. Pap.--Am. Chem. Soc., Div. of Fuel Chem. 1969, 13, 39-44.
2. Sondreal, E.A.; Knudson, C.L.; Schiller, J.E.; May, T.H. Proc. 9th Biennial Lignite Symp.: DOE/GFERC/IC-77/1, 1977, 129-158.
3. Ross, D.S.; Green, R.K.; Monsani, R.; Hum, G.P. Energy Fuels 1987, 1, 287.
4. Jones, D.; Baltisberger, R.J.; Klabunde, K.J.; Woolsey, N.F.; Stenberg, V.I. J. Org. Chem. 1978, 43, 175-177.
5. Stenberg, V.I.; Wang, J.; Baltisberger, R.J.; Van Buren, R.; Woolsey, N.F. J. Org. Chem. 1978, 43, 2991-2994.
6. Jackson, W.R.; Lim, S.C.; Stray, G.J.; Larkins, F.P. Proc. 1989 Internat. Conf. on Coal Sci.; Tokyo, Dec. 1989, Vol. II, pp 815-818.
7. Hughes, C.P.; Sridhar, T.; Chuan, L.S.; Redlich, P.J.; Jackson, W.R.; Larkins, F.P. USA/Australia Workshop on Use of Low-Rank Coals; Billings, MT, May 1991.

Table 1 Catalytic Liquefaction of Wyodak Coal

Reaction Temp. = 400°C, Reaction Time = 30 min Coal (as rec.) = 5.0 g, Reductant gas = 1000 psi (at room temp.)					
Catalyst (mmol/g coal)	Reductant	Conv. (%)*	Products (%)		
			Tol.-S	THF-S	Pent.-S#
NaAlO <sub>2</sub> (0.5)	CO	89	20	27	42
NaOH (0.5)	CO	72	16	22	34
None	CO	78	n	44	34
NaAlO <sub>2</sub> (0.5)	N <sub>2</sub>	41	n	18	23
NaAlO <sub>2</sub> (0.5)	H <sub>2</sub>	43	n	17	25

\* = Conversions are based upon the amount of initial coal (maf).

# = Pentane solubles are by difference, also includes the products extracted by ether from the distillate.

n = Not determined.

Table 2 Reactions of Anthracene

Reaction Temperature = 400°C, Reaction Time = 2 hours Solvent (Water) = 2 g, CO = 1000 psig			
Catalyst (mmol/g substr)	Substr. (mmol)	Conv. (%)	Major Products (mmol)
None	2.77	79	9,10-Dihydroanthracene (2.02) Tetrahydroanthracene (0.11)
NaAlO <sub>2</sub> (1.25)	2.81	82	9,10-Dihydroanthracene (2.19) Tetrahydroanthracene (0.13)
NaOH (1.25)	2.79	64	9,10-Dihydroanthracene (1.70) Tetrahydroanthracene (0.10)

DRYING OF BEULAH-ZAP LIGNITE.  
PRETREATMENT WITH SOLVENTS AND REHYDRATION

Karl S. Vorres  
Chemistry Div., Bldg. 211  
Argonne National Lab.  
Argonne, IL 60439

Keywords: Drying, Solvent pretreatment, Rehydration

ABSTRACT

Lignite (-100 mesh from the Argonne Premium Coal Sample Program) was dried in nitrogen under various conditions in a Cahn 121 thermobalance as part of a program on drying low rank coals for liquefaction. Samples were pretreated with solvents to determine the solvent's ability to displace water from the pores. Toluene had little effect. Acetone and methanol, selected because of water miscibility, were examined also. The methanol accelerated the drying, apparently because it was able to diffuse into the pores. The effect of drying on reactivity was examined by determining the rate of rehydration. Hysteresis was also examined. Rehydration is slow, and incomplete within a 23 hour period. The ability of carbon dioxide to substitute for nitrogen was examined. The behavior was similar with slight advantages for using nitrogen.

INTRODUCTION

Liquefaction of coals at low severity conditions is an important goal of coal research to maintain an economical, stable, long term supply of liquid fuels. Lignite is an abundant and reactive U. S. coal. One of the detracting properties of lignite is the high moisture content. Drying is usually carried out to minimize the impact of this constituent in the conversion process. Drying affects the reactivity of the coal. This effect is thought to be due to physical changes, such as irreversible pore collapse and/or other structural changes. Earlier work has indicated changes in the oil yield derived from raw, partly dried and more completely dried lignite samples (1).

Comments by some speakers to the effect that carbon dioxide can more effectively displace moisture from coal than nitrogen, reminiscent of use for surface area measurements or oil displacement from source rock, led to tests of the substitution of carbon dioxide for nitrogen in drying experiments.

It has also been suggested that the use of light oil to agglomerate coal prior to liquefaction may be beneficial in terms of moisture removal. There are benefits in terms of mineral reduction. Some added experiments were carried out to determine the capability of a light aromatic hydrocarbon and some other small hydrophilic molecules to accelerate drying rates.

The reactivity of the product coal is always of concern. A loss in reactivity due to a drying method, even though drying is improved, may preclude the use of the drying method. A standard

test adopted here for comparison of reactivity has been the ability to rehydrate the sample, as measured by the rate under a standard set of conditions.

#### EXPERIMENTAL

Coal drying was done with a Cahn model 121 thermobalance attached to an IBM PC/XT microcomputer. Vendor-supplied software was used to monitor the progress of individual runs, and convert data files to a form that could be further studied with Lotus 123.

The data were obtained as files of time, temperature and weight at 10 second intervals. Run times varied from 7-23 hours. Sample sizes started as about 80 mg. Temperatures were 30 or 40 C. The gas velocity past the sample was typically 80 cc/min in the 25 mm diameter tube. The sample was placed in a quartz flat bottom pan. The sample was the -100 mesh Argonne Premium Coal Sample - Beulah-Zap lignite (5).

Samples were quickly transferred from ampoules which had been kept in constant humidity chambers with water at room temperature (293°K). In the thermobalance system a period of about 5 minutes was used to stabilize the system and initiate data acquisition. A condenser was made to replace the usual quartz envelope that surrounds the sample. An antifreeze solution was circulated from a constant temperature bath through the condenser to maintain constant temperature during the experiments. This was more stable than the original furnace and provided very uniform temperature control during the experiments.

The gas atmosphere for the nitrogen gas runs was cylinder nitrogen (99.99%) or "house" nitrogen from the evaporation of liquid nitrogen storage containers used without further purification. For the carbon dioxide the gas was 99.9% carbon dioxide from a gas cylinder. The gas velocity was measured with a float-type flowmeter and adjusted for the density difference between carbon dioxide and air.

Data were analyzed as reported earlier (1,2,3,4). The best fit was obtained with a first order or unimolecular expression. Regression analysis was used to obtain the kinetic constants. Lotus 123 was used for analysis of individual run data. Approximations to a first and second derivative of the rate expressions were made in Lotus 123 by averaging over 20 of the 10 second time intervals before and after the point of interest. These derivatives were plotted with the rate data for further interpretation of the data.

Experiments with solvents were carried out by weighing the samples as usual and then adding solvent so that the sample was just covered with liquid. This was done on a balance to determine the amounts of solvent. The sample was then transferred to the TGA and a drying run was carried out in nitrogen as with earlier samples. There was about five minutes of contact time before the beginning of the drying run.

The reactivity of the sample was checked by measuring the rate of hydration. Tests of rehydration or humidification involved switching the gas atmosphere by passing the same gas flow through a coarse fritted gas bubbler filled with distilled water at room temperature (293°K). Typical times for the change were about 5 minutes. Finally hysteresis checks were made by redrying the humidified sample following the procedure for the initial drying.

#### RESULTS AND DISCUSSION

Earlier work by the author with higher rank coal samples (3,4) included studies of humidification of dried samples to determine hysteresis, observe consistency or changes in mechanism of reaction and compare rates of moisture loss and gain.

#### Basis for Comparison

The solvent based runs were carried out at 30°C and the runs with carbon dioxide were carried out at 40°C and a gas flow rate of 80 cc/min with sample sizes of about 80 mg. Runs with nitrogen at those conditions were used for comparison. The sets of runs include 135-7, 145-146, 150-2.

In this series of runs the sample was initially dried in nitrogen, then the gas atmosphere was changed to humid nitrogen to allow humidification to take place, and then the sample was redried to compare with the original drying. Three series of runs are summarized in Table 1.

Table 1. Runs in Nitrogen for Comparison

Run #	Coal type	$k_1$ dry	Moisture	$k_{humid}$	$k_{redry}$	Temp
135-7	raw	.00269	31.86%	.00264	not run	30 C
145-6	equil	.00323	29.6%	.00445	not run	30 C
150-2	equil	.00503	32.25%	.0092	.00367	40 C

MC?

A typical run series in which the three runs are superimposed is shown in Figure 1. The runs indicate that the raw coal (fresh from the ampoule) does not lose moisture as rapidly as the sample which has been allowed to equilibrate with water in a desiccator chamber at room temperature for at least a few days. Under similar conditions the equilibrated coal does not lose as much moisture as the fresh one. The rate of hydration of the equilibrated coal is greater than the rate for the raw coal. The indicated rate reflects the speed of approach to the final state for the system. The final state for rehydration or humidification involves a significantly lower moisture content than the starting material (i.e. 5% vs 31%). Therefore a comparison, per unit time, of the mass of water initially lost with the amount regained by the coal indicates that the rate of loss in the initial drying surpasses the rate of rehydration by a significant amount.

The rate of humidification of the dried coal from experiments at 40 C increases more than the rate of drying compared to the rates at 30 C. The shape of the rate function versus time curve is different for the redrying of the humidified coal than for the

original drying of the coal, implying a change, probably to a desorption mechanism. A slightly higher amount of moisture is removed by drying at higher temperature.

#### Drying in Carbon Dioxide

Two samples (about 80 mg) were each placed through a series of three runs without removing them from the TGA. The purpose was to establish the drying rate, rehydration rate and hysteresis by measuring the redrying rate of the humidified sample (one was at 57 cc/min gas flow, while the other was at 80 cc/min). These rates were to be compared to those in nitrogen.

A comparison of the data with that indicated above using nitrogen indicated that the drying behavior in carbon dioxide is very similar. The CO<sub>2</sub> drying rate (run 166) was .00398 based on mg water/gm sample per 10 second interval at 40°C with a gas flow rate of 57 cc/min. The weight loss amounted to 30.12% moisture removal. The indicated rate followed an induction period of about 1800 seconds while the rate slowly increased from .00333 to .00398. Following the initial 4,200 seconds of the run the rate gradually slowed so that in the period from 28,000 to 44,000 seconds the rate was .00056 based on mg water/gm sample/10 second interval. The rate slowed even further after that and the run was ended after 68,040 seconds.

Following a five minute changeover to humid CO<sub>2</sub>, data on hydration were obtained. The rate of hydration (run 167) following drying in carbon dioxide also followed a first order expression. About 200 seconds were needed for the moist carbon dioxide to displace the dry gas. The rate gradually increased over about 1600 seconds until it became constant at about .00521 mg water/gm sample/10 second interval at the 57 cc/min flow rate. After 3600 seconds the rate gradually decreased. It should be noted that the rate of rehydration was greater than the rate of drying. The moisture addition resulted in restoration of the moisture content to only 4.45% compared to 30.1% originally.

The humidified sample was redried in run 168 to compare the behavior with the raw sample and establish hysteresis effects. The weight loss data no longer followed a first order expression, so a direct comparison of rates was not possible. The data appear to be closer to a desorption kinetic form, indicating a significant change in mechanism. Figure 2 shows the weight change data for the three runs.

Another sample was run through the same three steps of drying, rehydration and redrying to check the reproducibility of results and compare the behavior at 80 cc/min gas flow. Runs 169-171 showed the same behavior and the weight curves superimpose very well.

When the gas flow rate was 80 cc/min the drying rate increased from .00326 to .00403. The duration of the interval for the high rate was about 3,300 seconds and then the rate gradually decreased to .00177, about three times the rate for run 166.

The rate constant for humidification in run 170 at 80 cc/min was initially .0053 and increased to .0062.

The redrying of the humidified sample in run 171 indicated that the mechanism has again shifted as the rate constantly decreased if a first order plot was attempted. Again, desorption kinetics seem more appropriate.

The initial changes in the rate during the first drying prompted a re-examination of a number of runs to determine if the rate change might be due to some induction step or thermal lag as the sample changed temperature or possibly induced by the gas flow. Runs 135 at 30°C in nitrogen and 150 at 40°C in nitrogen were studied for this purpose. Each of these involved sample sizes of about 80 mg with the same flat bottom quartz bucket and 80 cc/min gas flow past the sample.

A superposition of Figures 1 and 2 indicates that similar runs in nitrogen show a more rapid loss of moisture.

#### Drying with Solvents

Several solvents were used to explore the effects of treatment with volatile hydrocarbons and water miscible solvents (toluene, acetone and methanol). A run using water in place of a solvent was carried out for a check on the experimental procedure. The experimental results are indicated in Table 2.

The rates of drying for the toluene treated sample appear to be less than that for the others. Treatment with acetone is essentially similar to the base water case. Treatment with water appears to cause a slight increase. The addition of methanol apparently permits diffusion of the miscible solvent into the pores such that the measured mass change is accelerated. The change can be due to a combination of a real rate increase and the increase in mass of methanol compared to water (neglecting volume effects).

The solvents rapidly evaporated following a linear weight loss with time. The drying then appeared to be similar to normal drying in mechanism and in terms of rates, except as noted above. Humidification and redrying were similar also to the cases of nitrogen drying of normal samples.

Table 2. Drying Lignite After Exposure to Solvents at 30°C

Solvent	Run #	$k_1$ dry	Moisture
Toluene	137-9	.00317	29.0%
Acetone	140-2	.00333	30.3%
Methanol	142-4	.00397	31.1%
Water	147-8	.00363	30.4%

#### Drying in Humid Nitrogen

A series of runs were carried out in humid nitrogen to determine the limits of water reabsorption, and search for changes in rate or mechanism. Runs 154-5 at 40°C and 156 at 60°C are summarized in Table 3.

Table 3. Drying Lignite in Humid Nitrogen

Run #	Temp°C	$k_{\text{humid}}$	Moisture Loss	$k_{\text{dry N}}$	$k_{\text{humid 2}}$
154	40	.00414	23.7%		
156	60	.01227	28.5%	.00531	.01736

It is no surprise that the rates of drying are less than those under dry conditions, in this case about 80% of the rate at 40°C. The amount of moisture lost at 40°C is about 7-8% less than that lost using dry nitrogen.

#### CONCLUSIONS

A base set of rates is available to compare the results of thermogravimetric analysis (TGA) experiments over the temperature range of interest.

The curves for drying and humidification with moist nitrogen or carbon dioxide are very similar.

The curves for redrying humidified samples are different from the drying of the original sample, implying a different mechanism for the second moisture loss, probably following a desorption rate control.

The use of solvents to accelerate the rate of drying does not seem to be beneficial with a non-miscible aromatic light hydrocarbon like toluene. A water miscible solvent like acetone was not beneficial either when the contact time before the experiment was only five minutes. A smaller water miscible molecule did have an effect, indicating that the rate would increase.

The use of humid nitrogen in place of nitrogen reduces the amount of moisture that will be removed in an initial drying. The amount that can be restored in humidification at a given temperature is also reduced indicating a limited reactivity compared to a nitrogen dried material.

#### ACKNOWLEDGMENTS

The author gratefully acknowledges the support of the U. S. Department of Energy, Pittsburgh Energy Technology Center.

#### REFERENCES

1. Vorres, K. S., Wertz, D., Joseph, J. T. and Fisher, R., Am. Chem. Soc. Preprints Fuel Chem. Div. 36 (3), 853 (1991).
2. Vorres, K. S., Molenda, D., Dang, Y. and Malhotra, V. M., Am. Chem. Soc. Preprints Fuel Chem. Div. 36 (1), 108 (1991).

3. Vorres, K. S., R. Kolman, and T. Griswold, Am. Chem. Soc. Preprints Fuel Chem. Div. 33 (2), 333 (1988).
4. Vorres, K. S. and R. Kolman, Am. Chem. Soc. Preprints Fuel Chem. Div. 33 (3), 7 (1988).
5. Vorres, K. S. Energy & Fuels, 4 (5) 420 (1990).

**Fig. 1, Lignite in N<sub>2</sub>, 40 C**

ND150-2, -100 mesh, 81 mg, 80 cc/min, fbb

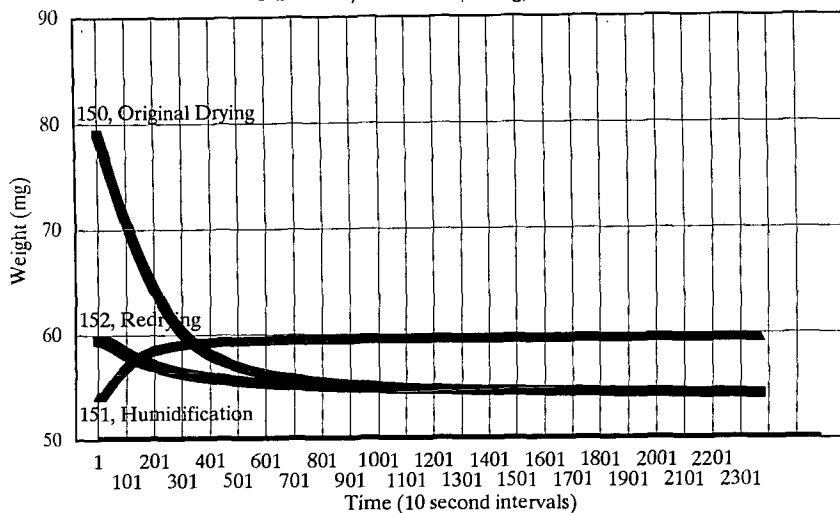
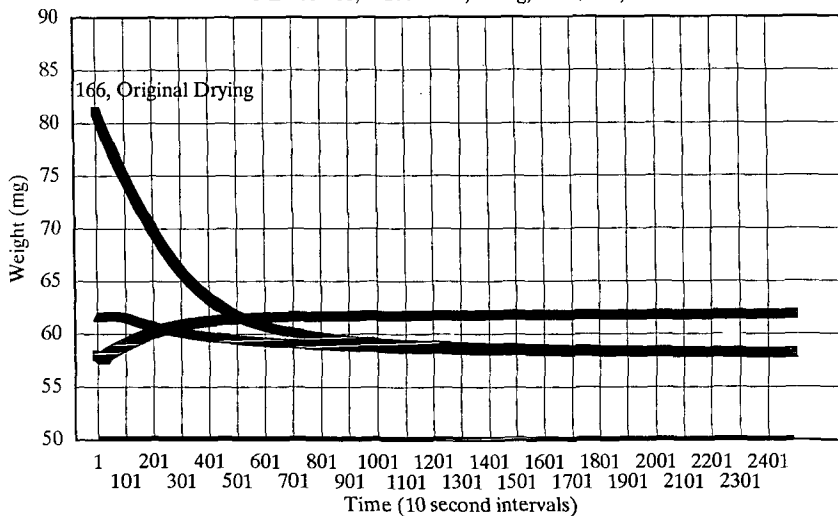


**Fig. 2, Lignite in CO<sub>2</sub>, 40 C**

ND166-68, -100 mesh, 83 mg, 57 cc/min, fbb



## HOT VAPOR TREATMENT OF GULF PROVINCE LIGNITES

Stanley D. Merritt, John P. Wagner, Tibor G. Rozgonyi and Jerome H. Zoeller, Jr. Engineering Biosciences Research Center, Texas Engineering Experiment Station, College Station, Texas TX 77843-2476

Keywords: Coal, desulfurization, fluidized bed.

### INTRODUCTION

Fluidized steam beds are used in Germany ( 1, 2 ), Australia ( 3 ), Hungary ( 4 ) and more recently in The United States ( 5 ) for the drying of low rank coal. The technologies developed for this process can be carried out on a continuous mode, and provides an economical alternative to dewatering the fuel before, or during, the combustion operation. Fuels which contain sulfur do produce sulfurous effluent gases under steam drying conditions. It has long been known that treatment of coals with hot hydrogen produces hydrogen sulfide, and sulfur dioxide with hot oxygen. In fact, sulfurous fumes are sometimes noted when sulfur-containing coals are heated in air at temperatures below 200 °C. The present work is to study conditions under which this effect could be enhanced. The possibility of achieving significant desulfurization under the comparatively mild thermal conditions in a fluidized steam bed - typically 160 °C. with a wide range of residence times - prompted a search for vapor phase reagents that would induce chemical desulfurization of coal under hot vapor conditions.

Studies of chemical reagents for coal desulfurization are of several types. Chemicals of promise to us are the redox reagents, studied in water solution. Notable examples of these include the CO/H<sub>2</sub>O water gas shift couple ( 6 ), numerous mineral acids ( 7, 8 ), alkali bases ( 9, 10 ), transition metal cations ( 11 ), peroxy radical generators ( 12, 13 ), and the HBr/Br<sub>2</sub> redox couple ( 14 ). Perchloroethylene is a reagent that has demonstrated desulfurization potential ( 15 ), and can be vaporized. EPRI has in fact sponsored research into the behavior of coals under hot vapor treatment ( 16 ). For our initial experiments, nitrous oxide, trimethylamine and dimethyl ether were selected. All three are well-documented electron transfer reagents.

Two reactors were constructed for the study ( 17 ). A fixed bed reactor was made from stainless steel tubing. The reactor is fed with premixed hot vapor, heated continuously, and monitored for temperature and pressure. It is the results of these experiments that will be discussed here. A fluidized bed was made from a section of tubing seven cm. in diameter, to study the process under more realistic conditions. Three typical Gulf province lignites were used. The hot vapor reagents consisted of nitrogen or air mixed with 0.2 % steam and 15 to 30 % of the reagent.

## EXPERIMENTAL

**Reactors** A fixed bed reactor was fabricated from stainless steel tubing 1.9 cm. in diameter by 15.2 cm. long. Sintered stainless steel plates threaded at the bottom ( 100 um. pores ) and top ( 90 um. pores ) of the unit contain the sample and the fines that are generated. Line connections leading to and from the reactor are 1.27 cm. in diameter. Figure 1 is a diagram of the apparatus. Close to the entrance and exit ports to the reactor are thermal wells for thermocouples, and ports for the differential flow meter probes. The reactor is wrapped with heating tape. Gases are led through flowmeters into a section of 3/4" stainless steel tubing wrapped with heating tape. Water is also metered into this preheater. The heated vapors are led into the bottom of the reactor.

A fluidized bed system was made from a stainless steel tube 7 cm. in diameter and 12 inches high, fitted at the bottom with a removable distributor plate of sintered stainless steel. A 90 um. pore filter at the exit contained the fines. This unit takes a much larger gas volume than the fixed bed unit. The preheater is a series of parallel tubes positioned inside of a Lindberg tubular furnace. The reactor itself is heated by a tubular furnace as well.

**Lignites** Yegua sequence lignite was a polydisperse run-of-mine sample from the Texas Municipal Power Authority generating plant at Gibbon Creek. Particals as large as 7 mm. are present with intermediate and fine particals. Wilcox sequence lignites were also provided by TMPA, from their mines in Freestone County and Martin Lake. These two lignites were sieved to 16 X 30 mesh and 30 X 200 mesh respectively, and deslimed. Table 1 lists the properties of these lignite samples.

**Reagents** Nitrous oxide was obtained from the Nitrous Oxide Corporation. Trimethylamine and dimethyl ether were supplied by the Aldrich Chemical Company. The gas mixtures consist of nitrous oxide in moist air, trimethylamine in moist nitrogen, and dimethyl ether in moist nitrogen. The composition of the gases is given in Table 2.

**Hot Vapor Treatment** Temperatures under which the lignites were treated are shown in Table 3. Also shown here are the sulfur contents and calorific values of the untreated, nitrogen control, and treated lignites. Treated samples were sealed under nitrogen until their analyses.

**Analysis** Proximate analysis were done on all samples, with analysis for total sulfur. In selected experiments, samples of the effluent gases were analysed by gc-ms.

## RESULTS AND DISCUSSION

Results from the gas mixtures in Table 2, at the temperatures listed in Table 3, for the three lignites treated in the fixed bed reactor, are listed in Table 3. Here is listed the total sulfur content, calorific value and the sulfur emissions parameter. Although none of these experiments show significant desulfurization, some aspects of the data deserve note. None of the Gibbon Creek samples show a change in their calorific value, but both the Freestone County and Martin Lake samples increase in calorific value by 15 to 20%.

Analysis of selected samples of the effluent gases ( Freestone County,  $N_2$  ; Martin Lake,  $NMe_3$  and Martin Lake  $Me_2O$  ) showed that hydrogen sulfide is evolved. The apparent increase in the sulfur content of the treated lignites indicates that mass loss is occurring. The volatile matter yield of the treated samples is never more than 3 to 4% higher than the values given in Table 1. Tar does collect in the effluent gas tubing. All this suggests that mass loss from the samples, by decarboxylation or resin devolatilization, is larger than any desulfurization effect.

When heated at 110 °C. for an hour, all the treated samples show an increase in mass, typically from 2 to 5%. The treatment of Martin Lake lignite in the fluidized bed at 110 °C. results in the formation of dust, which is not present in the original lignite.

## ACKNOWLEDGEMENTS

This research is made possible through the support of the Texas Higher Education Coordinating Board, through their Texas Advanced Technology Program. The continuing support of the Center for Energy and Mineral Resources, of Texas A&M University, is also gratefully acknowledged.

## REFERENCES

1. Wolf, B., Energietechnik 1988, 7, 245
2. Militzer, K.-E., and Nebelung, M., Drying Technology 1988, 4, 675
3. Huggins, R.S., Allerdice, D.J. and Perry, G.J. "Upgrading Experience and Studies on Australian Brown Coals" In Proceedings of the Opportunities in the Synfuels Industry, University of North Dakota Energy and Minerals Research Center; Bismark, North Dakota, August 28-31, 1988

4. Rozgonyi, T.G. and Szigeti, L.Z. (1985) , Fuel Processing Technology 1985, 1
5. Land, G.W. and Brown, G.J., "The First Commercial Application of Fluid Bed Drying to Subbituminous Coal", COALPREP 89 the sixth International Coal Preparation Exhibition & Conference, May 2-4, 1989; Lexington, Kentucky
- 6.. Ross, D.S., Blessing, J.E., Nguyen, Q.C. and Hum, G.P. Fuel 1984, 9, 1206
7. Salem, G.F. and Schmidt, A.M. "Chemical Beneficiation of Coal", U.S. Patent 4,741,741 to Standard Oil Company, Cleveland, May 3, 1988, Filed Oct 17, 1977
8. McGowan, C.W., Cates, K.Q. and Markuszewski, R (1988) "The Conversion of Organic Sulfur in Coal to Sulfate using Perchloric Acid", Prepr. Pap. - Div. Fuel Chem., Amer. Chem Soc. 1988, 1, 225
9. Markuszewski, R., Miller, L.J., Strazheim, W.E., Fan, C.W., Wheelock, T.D. and Greer, R.T., "Evaluation of the removal of Organic Sulfur from Coal", pp 401-414 in New Approaches to Coal Chemistry, ACS Symp. Series 169
10. Mazumder, B., Saikia, P.C., Baruah, B.D. and Bordolo, C.S., Fuel 1989, 5, 610
11. Janikowski, S.K., Skrobbutt, A.T. and Vorres, K.S. "Ultrafine Coal Cleaning with Metal Salt Solutions", In Processing and Utilization of High Sulfur Coals, Y. P. Chugh and R. D. Caudle, Editors. Proceedings of the Second International Conference on Processing and Utilization of High Sulfur Coals, Sept. 28 - Oct. 1, 1987, Carbondale, Illinois.
12. Venkata Swamy, Y. and Chandra, D. J. Inst. Fuel 1986, 107, 120
13. Brubaker, I.M. and Stoicos, T. "Precombustion Coal Desulfurization with Sodium Hypochlorite", In Processing and Utilization of High Sulfur Coals, Y. A. Attia, Editor. Proceedings of the First International Conference on Processing and Utilization of High Sulfur Coals, Columbus, Ohio, Oct. 13 - 17, 1985. pp 311
14. Schuetz, G.H. and Serrini, G., Fuel 1988, 12, 1595
15. Buchanan, D.H. "Coal Desulfurization using Perchloroethylene", Quarterly Reports for the period ending May 31, 1989, July 17, 1989, to The Center for Research on Sulfur in Coal.
16. Tewksbury, T.L., Carlton, H.E. and Oxley, J.H. (1988) "Progress Report on the Selective Oxidation of Pyrites in Coal", Proceedings: Twelfth Annual EPRI Contractors' Conference on Fuel Science and Conversion, Report AP-5460-SR, 1988 pp4-1 to 4-16, Palo Alto, California, May 13-14, 1987, Electric Power Research Institute, Palo Alto
17. Merritt, S.D., "Development and Evaluation of Two Reactors Designs for Desulfurization of Texas Lignites", M.S. Thesis submitted to Texas A&M University, May, 1991.

Table 1: Properties of the Lignites Studied.

Lignite	H <sub>2</sub> O % Whole	S <sub>tot</sub> % Dry	Ash Yield % Dry	Volatile Matter % DAF	Calorific Value Btu/#
Gibbon Creek	30.5	1.45	37.0	58.7	7630
Freestone County	12.2	0.73	9.2	50.0	9421
Martin Lake	11.8	1.79	10.7	51.0	9219

Table 2: Hot Vapor Treatment Conditions. Temperatures are listed in Table 3.

Label	Treatment	Vapor Composition	Residence Time, Min.
UN	Untreated Lignite	-	-
N <sub>2</sub>	Wet Nitrogen Control	N <sub>2</sub> /H <sub>2</sub> O = 99.8/0.2	20
N <sub>2</sub> O	Nitrous Oxide	N <sub>2</sub> O/Air/H <sub>2</sub> O = 24.8/75.0/0.2	20
NMe <sub>3</sub>	Trimethyl Amine	NMe <sub>3</sub> /N <sub>2</sub> /H <sub>2</sub> O = 19.2/80.6/0.2	20
Me <sub>2</sub> O	Dimethyl Ether	Me <sub>2</sub> O/N <sub>2</sub> /H <sub>2</sub> O = 23.9/75.9/0.2	20

Table 3: Treatment temperatures, Sulfur contents and calorific values for the untreated lignites ( UN ), wet nitrogen controls ( N<sub>2</sub> ), and representative samples of the treated lignites.

Lignite	Treatment (Table 2)	Temp. °C.	S <sub>tot</sub> % Dry	Calorific Value, BTU/#	#SO <sub>2</sub> MBTU
<b>Gibbon Creek</b>	UN	-	1.45	7630	3.8
	N <sub>2</sub>	220	1.33	7666	3.5
	N <sub>2</sub> O	220	-	-	-
	NMe <sub>3</sub>	130	1.36	7666	3.6
	Me <sub>2</sub> O	220	1.44	7623	3.8
<b>Freestone County</b>	UN	-	0.73	9421	1.6
	N <sub>2</sub>	220	1.00	11335	1.8
	N <sub>2</sub> O	220	1.27	11466	2.2
	NMe <sub>3</sub>	130	0.91	11063	1.7
	Me <sub>2</sub> O	220	0.93	11213	1.7
<b>Martin Lake</b>	UN	-	1.79	9219	3.9
	N <sub>2</sub>	120	2.15	10909	3.9
	N <sub>2</sub> O	110	2.39	10784	4.4
	NMe <sub>3</sub>	110	2.29	10837	4.2
	Me <sub>2</sub> O	120	2.09	10919	3.8

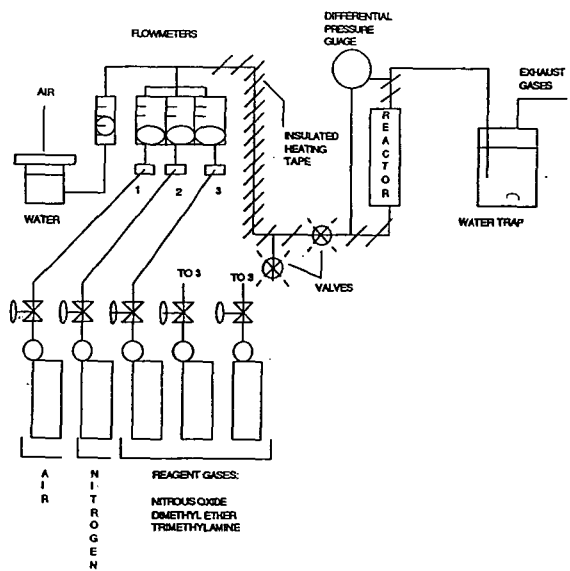


Figure 1: Diagram of the Fixed Bed Reactor. In the Fluidized Bed Reactor, the preheater and Reactor are heated by Lindberg tubular furnaces.

## COAL SOLUBILIZATION USING METAL ALKOXIDES IN REFLUXING ALCOHOLS

Kuntal Chatterjee, Sao Jiralerspong and Leon M. Stock  
Department of Chemistry, The University of Chicago  
5735 South Ellis Ave., Chicago, IL 60637

### INTRODUCTION

The inability to quantitatively solubilize coal in common organic solvents has been a detriment to the use and study of this vast fuel resource. Our efforts in the past few years have been directed toward its solubilization through O- and C-alkylation and base-promoted depolymerization.<sup>1</sup> O-Alkylation, which completely disrupts intermolecular hydrogen bonding, only increases the solubility of low rank coals such as Wyodak and Illinois No. 6 coals to the 35% level.<sup>1</sup> C-Alkylation, which can be extremely effective for the solubilization of high rank coals, is only moderately more effective for these coals than O-alkylation alone.<sup>2</sup> We were intrigued by the possibility that their solubilization could be improved by basic reagents without alkylation when we found that two high rank coals were rendered about 40% soluble merely by treatment with strong bases (most notably Lochmann's base).<sup>3</sup> We concluded that this procedure was effective because the carbanions generated by the strong bases underwent carbon-carbon bond cleavage and produced smaller, more soluble coal fragments.<sup>3</sup> Our prior work with basic reagents did not convert the two low rank coals to soluble products and we reasoned that the carbanions that are produced by very strong bases also undergo condensation reactions to retrogressively increase the size of the coal molecules. We, therefore, sought to eliminate this undesirable reaction by trapping the carbanions with a proton donor. The present study describes an approach to solubilize Illinois No. 6 coal (APCSP 3) by base treatment with metal alkoxides in refluxing proton donating alcohols.

### EXPERIMENTAL SECTION

*Materials.* The Illinois No. 6 coal (APCSP 3) was obtained from the Premium Sample Program at Argonne National Laboratory.<sup>4</sup> Elemental analysis (wt.%) of moisture-free coal: C, 65.7; H, 4.2; N, 1.2; S, 4.8; O (by difference) 9.8; Ash, 14.3. Pyridine was purified by distillation over barium oxide. Sodium, potassium, sodium methoxide, *n*-octanol, and benzyl alcohol were used as received from Aldrich Chemical Company. Methanol, *n*-butanol, and *tert*-butanol were used as received from J.T. Baker Inc.

*General Reaction Procedure.* In general, the alcohol (420 mmol) and solid potassium (80 mmol) were added to a flame-dried round-bottom flask and stirred under dinitrogen at room temperature for 30 to 45 minutes to form the metal alkoxide. The coal (2 g) was then added and the reaction mixture was stirred for 5 minutes before heating to reflux. Usually, a small pool of potassium was visible when the coal was added. The reaction mixture was refluxed for 24 hours. It was cooled in a 0 °C bath and any remaining base was diluted with *tert*-butanol followed by methanol and water. It was then acidified with dilute hydrochloric acid (2 M) until the pH was less than 1. This acidified mixture was stirred under dinitrogen for 48 hours and the solvents were removed from the reaction product either by rotary evaporation or by vacuum distillation, depending upon the boiling points of the solvents. The reaction product was then washed under dinitrogen on a Nucleopore polycarbonate membrane filter (pore size 0.8 mm) with dilute hydrochloric acid (2 M, 5 L), with methanol until the filtrate was colorless (8 L), and with aqueous methanol (50% by

volume) until the filtrate was free of halide ions (12 L). Finally, the reaction product was dried at 110°C under high vacuum for 48 hours. A sample was submitted for elemental analysis.

A portion of the product was subjected to pyridine extraction and unless otherwise mentioned, the solubility of the reaction product was determined from the weight of the insoluble portion.

*Analysis of Products.* Elemental analyses were performed by Commercial Testing and Engineering Company of South Holland, Illinois. Infrared spectroscopy was carried out on a Nicolet 20SXB FTIR spectrometer. <sup>2</sup>H NMR spectroscopy was carried out on a Varian XL-400 spectrometer.

## RESULTS AND DISCUSSION

Significant work has been done with alcohols as solvents and reagents for the liquefaction of coal. Use of low boiling alcohols under super critical conditions or in hydrogen donor solvents in the presence or absence of bases has been investigated by a number of workers.<sup>5-7</sup> Ross *et al.* have investigated potassium isopropoxide in isopropanol and potassium hydroxide in methanol at 400 °C.<sup>5</sup> More recently, Ouchi and his coworkers have reported the reactions of coals with ethanolic sodium hydroxide at temperatures ranging from 260 to 450 °C.<sup>6</sup> Similar reactions were also performed with ethylene glycol as solvent by Winans *et al.*<sup>7</sup> The yields of the liquified coals in these studies were high but the conditions were also severe. We sought milder conditions for the conversion so that the side reactions, if any, could be minimized. Also, some investigators have neglected the possibility that alcohols transform and adduct to coal molecules. Accordingly, we measured the conversion exclusively on the basis of the weight of the insoluble coal residue.

Potassium or sodium alkoxides, as described in the Experimental Section, were used in different alcohols at reflux for 24 hours and then the products were quenched with dilute acid. The results are presented in Table 1.

The reaction of Illinois no. 6 coal with sodium methoxide in refluxing methanol yielded a product which was only 33% soluble in pyridine. The pyridine solubility of the raw coal is 27%. Treatment with potassium *n*- and *tert*-butoxide in *n*- and *tert*-butanol with boiling points 118 and 83°C, respectively, increased the solubility of the coal to 42%. There was no significant difference between the effectiveness of the two isomeric butanols. Potassium *n*-octoxide in *n*-octanol (b.p. 196°C) gave an even more soluble product, 53%. Finally, potassium and sodium benzoxide in refluxing benzyl alcohol (b.p. 205°C) provided more than 70% soluble material.

We also briefly investigated the optimum conditions. There were differences in the yields at 6 and 24 hours, so we adopted the 24 hour reaction time for all our reactions. Selected other results are shown in Table 2. With sodium benzoxide, concentrations from 40 to 120 mmol per gram of coal gave good results and the product obtained was about 70% soluble in pyridine. However, higher concentrations of the base resulted in reaction products with masses much greater than those of the starting materials. Thus, it was evident that at higher base concentration, chemical addition reactions take place.

The results also show that the extent of solubilization does not depend on the basicity of the alkoxides. Rather, the differences in their effectiveness apparently arise as a consequence of the differences in their boiling points. There are two lines of evidence. First, the two higher-boiling alcohols, benzyl alcohol and *n*-octanol with boiling point near 200°C, gave more soluble products than the lower-boiling alcohols. Second, the use of sodium methoxide in refluxing benzyl alcohol was as effective as sodium benzoxide in the same solvent (Table 1). These results strongly suggest that there is a significant activation energy for the key conversion reaction.

We believe that there are two underlying reasons for the success of this strategy. First, hydrogen is probably transferred from the solvent to the coal. Previous work performed by the Argonne group demonstrated that the aromatic rings in coal underwent reduction in proton donor solvents with alkali hydroxides.<sup>7</sup> In this study, benzaldehyde was detected among the reaction products. The microanalytical data for the reaction products, however, indicate that the increase in

the hydrogen content is modest. Second, subtle base-catalyzed carbon-oxygen, carbon-sulfur and carbon-carbon bond cleavage reactions fragment the low rank coals. It has been shown previously that strong bases such as Lochmann's base, can cleave carbon-carbon bonds in hydrocarbons if the resulting carbanions are stable.<sup>1</sup> Also, it has been shown that sulfidic carbon-sulfur bonds undergo cleavage under basic conditions.<sup>8</sup> In presence of proton donor solvents, the anions formed in such bond scission processes are trapped and the possibility for their recombination to yield a condensation product is reduced.

A major point of interest was the large decrease in the total sulfur content of the products.<sup>8</sup> The reduction ranged from 16% for *tert*-butoxide in *tert*-butanol (4.1 wt% S) to 80% for benzoxide in benzyl alcohol (1.0 wt% S). This result implies that all the pyrite and at least 50% of the organic sulfur were removed. The extent of sulfur removal for the various alkoxides in the corresponding alcohols paralleled their ability to solubilize the coal.

### CONCLUSIONS

Treatment of Illinois No. 6 coal with alkoxides in refluxing alcohols yields products that are 40 to 70% soluble in pyridine, compared to 27% for the starting material. The extent of solubilization depends upon the boiling point of the alcohol and not upon the structures of the alkoxide and the alcohol. The best results were obtained with 40 mmol of sodium or potassium benzoxide per gram of coal in benzyl alcohol. Significant sulfur removal was achieved, an 80% reduction from 4.8 to 1.0 wt% S by using the benzoxide. Thus, base-catalyzed reactions at temperatures near 200 °C solubilize and desulfurize this Illinois No. 6 coal.

### ACKNOWLEDGEMENTS

The authors wish to acknowledge support of this work from the United States Department of Energy under contract no. DOE/AG22-87PC79938.

### REFERENCES

1. Chatterjee, K., Ph.D Dissertation, The University of Chicago, 1991.
2. Chatterjee, K.; Miyake, M.; Stock, L. M., *Energy and Fuels*, 1990, 4, 242.
3. Chatterjee, K. and Stock, L. M., manuscript in preparation.
4. Vorres, K.S. *Energy and Fuels*, 1990, 4, 420.
5. Ross, D.S. and Blessing, J. E., *Fuel*, 1979, 58, 433; 58, 438.
6. Makabe, M., Hirano, Y., Ouchi, K. *Fuel*, 1978, 57, 289; 57, 801; Makabe, M., Ouchi, K. *Fuel*, 1979, 58, 43.
7. Winans, R.E.; Hayatsu, R.; Mcbeth, R. L.; Scott, R. G.; Moore, L. P. and Studier, M. H. Ed. M.L.Gorbaty and K.Ouchi. *Advances in Chemistry Series* 1981, 192, pp 133.
8. Chatterjee, K. and Stock, L. M. *Energy and Fuels*, 1991, 5, 704.

TABLE 1.  
RESULTS FOR ALKOXIDE TREATMENT OF ILLINOIS NO. 6 COAL IN REFLUXING  
ALCOHOLS. DETERMINING THE OPTIMUM REACTANT-SOLVENT SYSTEM.

reaction conditions: base, solvent, time	reaction temperature, °C	coal recovered, wt%, db	pyridine solubility, wt%
raw coal	-	-	27
NaOMe (40 mmol/g), MeOH, 24 h, protonation	65	86	33
KO <i>n</i> -Bu (40 mmol/g), <i>n</i> -BuOH, 24 h, protonation	118	76	42
KO <i>r</i> -Bu (40 mmol/g), <i>t</i> -BuOH, 24 h, protonation	83	83	42
KO <i>n</i> -Oct (40 mmol/g), <i>n</i> -OcOH, 24 h, protonation	196	79	53
KOBz (40 mmol/g), BzOH, 24 h, protonation	205	43 <sup>a</sup>	82
NaOBz (40 mmol/g), BzOH, 24 h, protonation	205	51 <sup>a</sup>	74
KOBz (40 mmol/g), BzOH, 24 h, protonation	205	95	66
NaOMe (40 mmol/g), BzOH, 24 h, protonation	205	68 <sup>a</sup>	64

<sup>a</sup>The recovery of the products after the reaction was low since a significant portion of the coal was soluble in the alcohol, and this material was removed during washing and filtration.

TABLE 2.  
 RESULTS FOR SODIUM BENZOXIDE TREATMENT OF ILLINOIS NO. 6 COAL IN  
 REFLUXING BENZYL ALCOHOL AT 205 °C. EFFECT OF CHANGING THE BASE  
 CONCENTRATION.

concentration of sodium benzoxide (mmol/g coal)	coal recovered, wt%, db	pyridine solubility, wt%
raw coal	-	27
40	51 <sup>a</sup>	74
74	77 <sup>a</sup>	52
121	63 <sup>a</sup>	70
253	285	31
486	457	35

<sup>a</sup>The recovery of the products in these experiments was low since a significant portion of the coal was soluble in the alcohol and this material was discarded in these experiments.

## ENHANCED LOW SEVERITY COAL LIQUEFACTION USING SELECTIVE CALCIUM REMOVAL

K. Shams, R.L. Miller, and R.M. Baldwin

Chemical Engineering and Petroleum Refining Department  
Colorado School of Mines  
Golden, Colorado 80401

### ABSTRACT

This paper reports results from an on-going process development study in which coal is converted to liquid products at relatively mild reaction conditions. The process consists of three main steps: 1) mild pretreatment of the feed coal at ambient conditions using methanol (or other common organic solvent) and a trace amount of hydrochloric acid to enhance dissolution reactivity and dry the coal, 2) low severity thermal dissolution to obtain a very reactive coal-derived residual intermediate product amenable to upgrading, and 3) catalytic upgrading of the residual products to distillate liquids. We have found that mild pretreatment of Wyodak subbituminous coal using methanol/HCl can provide an improvement in THF conversion of greater than 30 wt% at 350° C reaction temperature. Analysis of treated Wyodak and Illinois #6 coal samples indicates that no organic phase alteration such as alkylation occurs during pretreatment, but that over 90 wt% of the calcium is removed from each coal. Calcium is thought to catalyze retrogressive reactions during coal pyrolysis, and thus calcium removal prior to low severity liquefaction minimizes the production of THF-insoluble products.

### INTRODUCTION

Much of the recent research in direct coal liquefaction seeks to develop methods for dissolving coal at low reaction severity (defined as temperatures below 350° C and pressures of 1000-1500 psi). The incentives for developing a viable low severity liquefaction process are numerous; they include: 1) reduced hydrocarbon gas production resulting in reduced feed gas consumption and enhanced hydrogen utilization efficiency, 2) suppressed retrogression of primary coal dissolution products resulting in enhanced distillate and residuum product quality, 3) production of high boiling residuum which is less refractory and thus more amenable to catalytic upgrading in a conventional second-stage hydrocracker, 4) substitution of less expensive off-the-shelf vessels, piping, valves, pumps, etc. in place of expensive, custom-designed units, and 5) less severe slurry handling and materials of construction problems as a result of lower operating temperatures and pressures.

However, as shown schematically in Figure 1, lowering the liquefaction severity reduces coal conversion and liquid product yields unless the intrinsic coal reactivity can be sufficiently enhanced using some method of physical or chemical pretreatment. The main challenge to developing a viable low severity liquefaction process scheme involves finding an efficient and inexpensive means of coal pretreatment which will provide high levels of conversion and liquid product yields at low reaction severity. Researchers at several locations including the Pittsburgh Energy Technology Center (1), the University of North Dakota Energy and Environmental Research Center (2), Carbon Resources, Inc. (3), and the Colorado School of Mines (4) have investigated various methods for improving coal reactivity and liquid yields at mild reaction conditions. These studies showed that coal can be readily converted to tetrahydrofuran (THF) soluble products via selective chemical attack rather than thermal bond scission, but that the rate and extent of coal dissolution at mild conditions is strongly dependent upon intrinsic coal reactivity.

Numerous chemical treatments including reductive and non-reductive alkylation (5,6), acylation (7), partial oxidation (8), alkali hydrolysis (9), and solvent swelling (10) have been used to disrupt the coal's organic structure and increase solvent solubility. Limited work has been reported in which the liquefaction reactivity of alkylated coals has been studied. Schlosberg et al. (11) measured the reactivity of alkylated Wyodak subbituminous and Illinois #6 bituminous coals in tetralin at 427° C, 1500 psi hydrogen pressure and 130 min. reaction time. A 10-21 wt% (maf and alkyl group-free basis) increase in cyclohexane conversion was noted for the alkylated coals.

More recently, the effect of chemical pretreatment on the inorganic constituents of coal via a vis liquefaction reactivity has been studied. Mochida (12) reported that hydrochloric acid can be used to destroy cationic bridges present in low rank coals, thereby reducing coordination between oxygen-containing functional groups and allowing better contacting between coal and solvent during the initial stages of dissolution. Joseph (13) reported that removal of sodium, potassium, and calcium from low rank coals enhances liquefaction reactivity. He attributes this effect to inhibited hydrogen transfer in the presence of these cations.

The objective of this paper is to present experimental results from a study in which mild chemical pretreatment using methanol and hydrochloric acid was used as a method to improve intrinsic coal reactivity at low liquefaction reaction conditions. Possible explanations for the observed reactivity enhancement will also be discussed.

## EXPERIMENTAL PROCEDURE

The entire suite of eight coals from the Argonne Premium Coal Sample Bank was used as the source of feed coals for this study. Ultimate analyses for these coals are listed in Table I (14). Coal samples were stored under argon in sealed ampules prior to pretreatment and liquefaction experiments.

Coal was pretreated by suspending 5 g of undried coal in 40 cm<sup>3</sup> of methanol and 0.6 cm<sup>3</sup> of concentrated hydrochloric acid in a 100 cm<sup>3</sup> round bottom flask and continuously stirring the coal/methanol slurry on a magnetic stirring plate for 3 hrs. The flask was connected to a cooling water condenser to reduce solvent losses by evaporation. Several experiments were completed in which dry nitrogen was used to blanket the coal/methanol slurry; elemental analyses of the treated coals showed no difference in the extent of oxidation when the system was purged with nitrogen and when it was vented to the atmosphere. Several experiments using hexane or acetone in place of methanol were also completed.

After pretreatment, most of the organic solvent was decanted off and the moist coal sample washed with three 50 cm<sup>3</sup> aliquots of fresh solvent to remove residual acid. Any remaining solvent was recovered by vacuum drying (50° C, 10-20 millitorr pressure, 24 hrs.). Untreated coal samples were vacuum dried at the same conditions before liquefaction. After drying, all treated and untreated coal samples were stored at room temperature in a vacuum desiccator (0.1 torr) before analysis or liquefaction. Reactor runs were scheduled so that each coal sample was stored for less than 12 hours before use. Portions of each untreated coal and pretreated coal were subjected to elemental analysis and ash analysis, as well as <sup>1</sup>H CRAMPS and <sup>13</sup>C CP/MAS NMR, FTIR, Mossbauer, and XRD spectroscopy.

Liquefaction experiments were conducted in a 20 cm<sup>3</sup> tubing bomb reactor attached to an agitator and immersed in a fluidized sandbath. Low severity reaction conditions were set at 350° C reaction temperature, 1000 psig initial cold hydrogen pressure, and 30 min. reaction time. Dihydrophenanthrene (DHP) was used as hydrogen donor solvent (2/1 solvent/coal wt. ratio) in these runs. Coal conversion was measured using THF extraction data corrected for the intrinsic THF solubilities of treated and untreated coals. Solubility measurements were conducted at ambient conditions and consisted of three steps: 1) sonicating the liquid products from the tubing bomb reactor (or feed coal sample) in excess THF for 10 min., 2) centrifuging the mixture at 2000 rpm for 15 min., and 3) decanting THF-soluble products and excess THF from the THF-insoluble residuum. This procedure was repeated at least two times until no additional THF-soluble products were recovered. Remaining THF-insolubles were dried at 100° C for 24 hours to remove residual THF, weighed, and finally ashed. Coal conversion to THF-soluble products was computed on a moisture and ash-free basis, correcting for the intrinsic solubility of the feed coal.

## RESULTS AND DISCUSSION

Effect of pretreatment on low severity liquefaction reactivity. Reactivity data for the untreated and treated Argonne coals are shown in Figure 2. Each of these data points represents the average of 2-3 reactor experiments; conversion differences of 2.1 wt% or greater (maf basis) represent statistically significant differences in liquefaction reactivity at the 95% confidence level. At the low severity reaction conditions studied, three of the high volatile bituminous coals [Illinois #6

(72.1 wt%), Blind Canyon (69.6 wt%), and Pittsburgh #8 (57.0 wt%)] gave the highest THF conversions. Wyodak subbituminous coal was the next most reactive coal (44.4 wt%), while Pocahontas low volatile bituminous coal was the least reactive sample studied (15.6 wt%). These reactivity data follow the same trends reported for the Argonne coals by other investigators (15).

Pretreatment with methanol and HCl using the procedure described earlier enhanced low severity liquefaction reactivity for all eight Argonne coals. The absolute increase ranged from only 5.5 wt% for Blind Canyon coal to 31.5 wt% for Wyodak coal, and averaged 18.0 wt% for the eight coals. No simple trends in reactivity improvement with chemical or physical properties of the coals were obvious, although the reactivity of pretreated low rank coals (Wyodak and Beulah-Zap) increased much more than reactivity of the six bituminous coals.

Although vapor phase methanol/HCl mixtures have been shown to partially alkylate bituminous coals (16), NMR and FTIR measurements indicated no alkylation occurred during our pretreatment experiments. This result was confirmed by replacing methanol with hexane or acetone (two solvents which cannot participate in acid catalyzed alkylation chemistry) during pretreatment; the reactivity of coals pretreated with hexane/HCl and acetone/HCl was also enhanced.

In an attempt to separate the effects of methanol and HCl on reactivity enhancement, a series of experiments was completed in which samples of Wyodak subbituminous coal and Illinois #6 bituminous coal were pretreated using methanol only (no HCl addition) and HCl only (1.5 wt% HCl in distilled water, no methanol addition). Results of low severity liquefaction experiments using these treated coals are summarized in Figure 3. As expected, no reactivity enhancement occurred when coal samples were pretreated with only methanol. However, coal samples treated with HCl/water exhibited significant reactivity improvement, although less than observed using methanol/HCl. Blank pretreatment using only distilled water did not affect the low severity reactivity of either coal. Thus, we can conclude that, while the presence of a small concentration of HCl is essential for successful pretreatment, the addition of methanol or other organic solvent such as hexane or acetone improves pretreatment effectiveness. Mochida (12) attributes this effect to improved wettability of the coal surface by the organic solvent and thus better contacting between coal and acid.

Effect of pretreatment on coal composition. To begin elucidating the cause of the reactivity enhancement shown in Figure 2, we used several analytical techniques to study changes in the organic and inorganic phases of Wyodak and Illinois #6 coals during pretreatment. NMR and FTIR analyses indicated no measurable organic phase alterations with one exception. The Wyodak FTIR spectra indicated formation of carboxylic function groups during pretreatment, probably as a result of divalent (Ca,Mg) cationic bridge destruction (12,13). Mossbauer spectroscopy results demonstrated that pyrite was largely unaffected by treatment with methanol and HCl, eliminating the possibility that  $FeCl_3$ , a known coal dissolution catalyst, was being formed in the treated coal.

X-ray diffraction measurements were conducted on the low temperature ash (LTA) from untreated and treated Wyodak and Illinois #6 coals. These results indicated that over 90 wt% of the calcium was leached from each coal during pretreatment. In these spectra, calcium was observed only as  $CaCO_3$  with no  $CaO$  or  $CaSO_4$  present. This observation agrees with a report by Miller and Givens (17) that organically-bound calcium will convert to  $CaCO_3$  rather than  $CaO$  during low temperature ashing. Elemental analyses of treated coal samples confirmed the extent of calcium loss during pretreatment, and also showed that a lesser amount of magnesium was also extracted.

Effect of calcium content on low severity liquefaction reactivity. To study further the effect of calcium content on liquefaction reactivity, Wyodak and Illinois #6 coal samples with varying calcium contents were prepared by varying the amount of acid used during pretreatment. Other pretreatment conditions were the same as described earlier. Results of low severity liquefaction runs using these samples are shown in Figure 4. The reactivity of both coals was enhanced as calcium was removed; once again, the effect was more pronounced for Wyodak coal, particularly at a calcium content of less than about 0.2 wt%.

Several low severity liquefaction experiments were completed in which calcium as  $\text{CaCO}_3$  was added back to the reactor prior to liquefaction. In each experiment, the amount of calcium added was equivalent to the amount extracted during pretreatment. Results of these experiments are summarized in Figure 5. As these data show, the beneficial effect of  $\text{MeOH}/\text{HCl}$  pretreatment was almost completely negated by adding  $\text{CaCO}_3$  to the liquefaction reaction system. A similar effect was observed when  $\text{CaO}$  was added during low severity liquefaction of pretreated Wyodak and Illinois #6 coals.

The mechanistic role of calcium during low severity coal dissolution is not completely understood. Mochida (12) attributed accelerated rates of low rank coal dissolution to the destruction of calcium dicarboxylate structures and therefore, less coordination of oxygen-containing function groups. Joseph (13) speculated that calcium and other exchangeable alkaline and alkaline earth cations impeded hydrogen transfer during coal dissolution; removal of these cations would improve the rate of hydrogen transfer to coal free radicals as they form, and thus improve the extent of coal conversion. Joseph also cited the propensity of calcium dicarboxylate structures to undergo cross-linking reactions during the initial stages of coal dissolution.

We hypothesize that, in addition to the effects cited above, the presence of calcium can directly catalyze retrogressive reactions involving coal-derived free radical species during low severity liquefaction. Numerous studies have cited the role of calcium (as  $\text{CaCO}_3$  or  $\text{CaO}$ ) in increasing char yields and reducing tar yields during coal pyrolysis; the char yield enhancement has been attributed to catalysis of metaphast recombination prior to devolatilization (18) and catalysis of repolymerization and secondary cracking reactions (19). We are presently conducting a series of model compound studies to help elucidate the mechanistic effects of calcium during low severity liquefaction.

#### ACKNOWLEDGMENT

We wish to acknowledge financial support from the U.S. Department of Energy under Contract Nos. DE-AC22-88PC88812 and DE-FG22-90PC90289.

#### LITERATURE CITED

1. Bockrath, B.C.; Illig, E.C.; Finseth, D.H.; Sprecher, R.F. Prepr. Pap. - Am. Chem. Soc., Div. Fuel Chem., **29**, 5, 76, 1984.
2. Farnam, S.A.; Wolfson, A.C.; Miller, D.J.; Gaides, G.E.; Messick, D.D. Prepr. Pap. - Am. Chem. Soc., Div. Fuel Chem., **30**, 2, 354, 1985.
3. Porter, C.R.; Knudson, C.L.; Rindt, J.R. Prepr. Pap. - Am. Chem. Soc., Div. Fuel Chem., **31**, 4, 70, 1986.
4. Miller, R.L.; Baldwin, R.M. Prepr. Pap. - Am. Chem. Soc., Div. Fuel Chem., **31**, 4, 152, 1986.
5. Sternberg, H.; Delle Donne, C.L. Fuel, **53**, 172, 1974.
6. Liotta, R. Fuel, **58**, 724, 1979.
7. Hodek, W.; Kolling, G. Fuel, **52**, 220, 1973.
8. Hessley, R.K. 'Co-Oxidative Depolymerization of Coal,' Final Report for EPRI Project No. 2383-2, June 1985.
9. Mirza, Z.B.; Sarkar, M.K.; Sharma, D.K. Fuel Proc. Tech., **9**, 149, 1984.
10. Sanada, Y.; Honda, H. Fuel, **65**, 295, 1986.
11. Schlosberg, R.H.; Neavel, R.C.; Maa, P.S.; Gorbaty, M.L. Fuel, **59**, 45, 1980.
12. Mochida, I.; Shimohara, T.; Korai, Y.; Fujitsu, H.; Takeshita, K. Fuel, **62**, 659, 1983.
13. Joseph, J.T.; Forrai, T.R. Fuel, **71**, 75, 1992.
14. Vorres, K.S. Energy & Fuels, **4**, 5, 420, 1990.
15. Shin, S.C.; Baldwin, R.M.; Miller, R.L. Energy & Fuels, **3**, 193, 1989.
16. Sharma, D.K.; Sarkar, M.K.; Mirza, Z.B. Fuel, **64**, 449, 1985.
17. Miller, R.N.; Givens, P.H. 'A Geochemical Study of the Inorganic Constituents in Some Low Rank Coals,' Technical Report for DOE Contract No. EX-76-C-01-2494, February 1978.
18. Tyler, R.J.; Schafer, H.N.S. Fuel, **59**, 487, 1980.
19. Franklin, H.D.; Peters, W.A.; Howard, J.B. Prepr. Pap. - Am. Chem. Soc., Div. Fuel Chem., **26**, 121, 1981.

Table I  
Ultimate Analysis of Feed Coals

Wt% Dry Basis	Wyodak	Beulah-Zap	Illinois #6	Pittsburgh #8
Carbon	68.4	65.9	65.7	75.5
Hydrogen	4.9	4.4	4.2	4.8
Nitrogen	1.0	1.0	1.2	1.5
Sulfur	0.6	0.8	4.8	2.2
Oxygen	16.3	18.2	8.6	6.7
Ash	8.8	9.7	15.5	9.3
Coal Rank	Subbit.	Lignite	HVB	HVB
Symbol	WY	BZ	ILL	PIT

Table I (cont.)  
Ultimate Analysis of Feed Coals

Wt% Dry Basis	Blind Canyon	Lewiston-Stockton	Upper Freeport	Pocahontas
Carbon	76.9	66.2	74.2	86.7
Hydrogen	5.5	4.2	4.1	4.2
Nitrogen	1.5	1.3	1.4	1.3
Sulfur	0.6	0.7	2.3	0.7
Oxygen	10.8	7.8	4.8	2.3
Ash	4.7	19.8	13.2	4.8
Coal Rank	HVB	HVB	MVB	LVB
Symbol	BC	LS	UF	POC

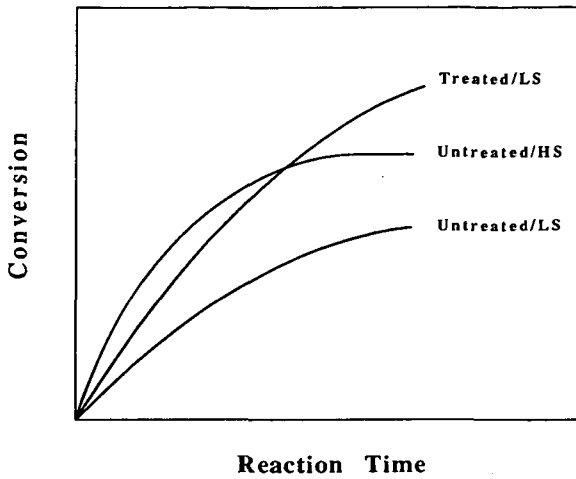


Figure 1 - Schematic Representation of Reactivity Enhancement Using Coal Pretreatment (LS = low reaction severity, HS = high reaction severity)

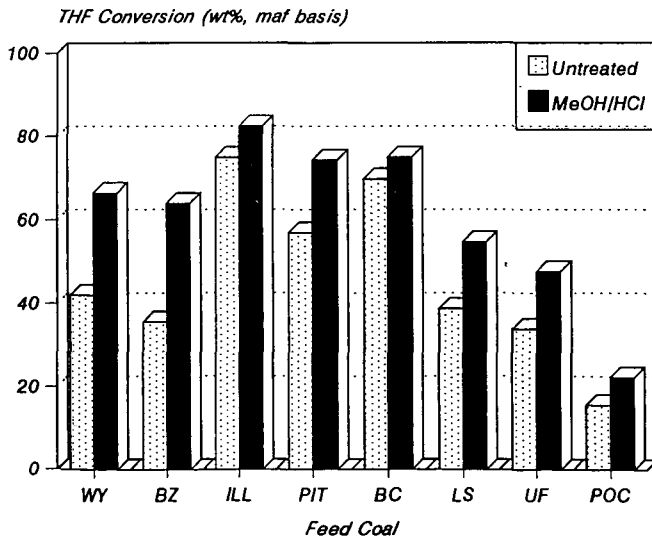


Figure 2 - Effect of Pretreatment with MeOH/HCl on Low Severity Liquefaction Reactivity of Argonne Coals

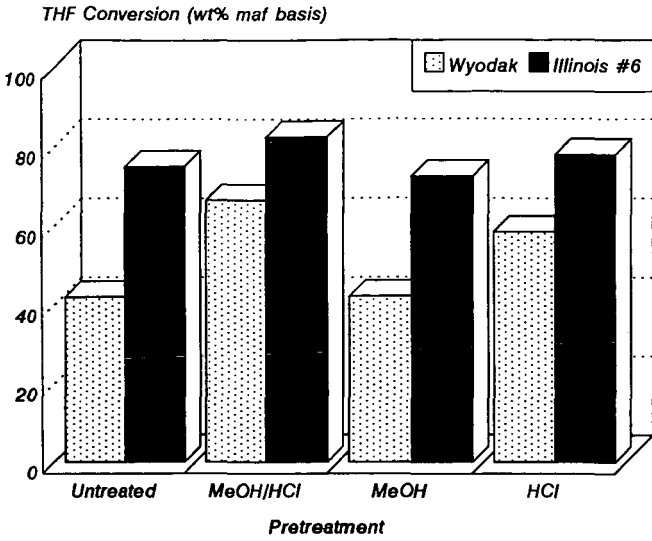


Figure 3 - Effect of Pretreatment with MeOH/HCl, MeOH, or HCl on Low Severity Liquefaction Reactivity of Wyodak and Illinois #6 Coals

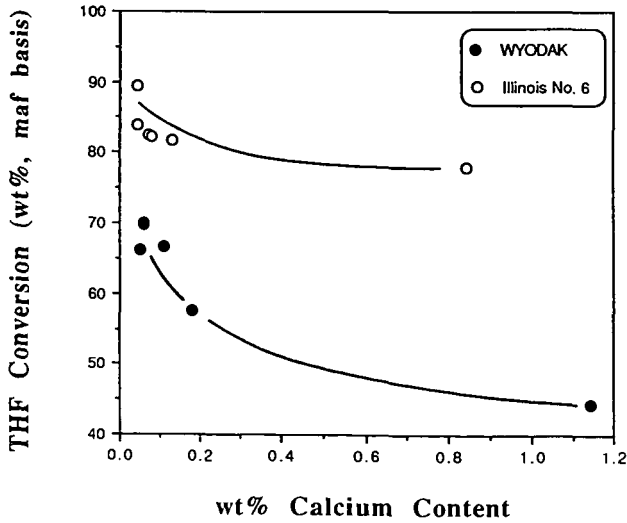


Figure 4 - Effect of Calcium Content on Low Severity Liquefaction Reactivity of Wyodak and Illinois #6 Coals

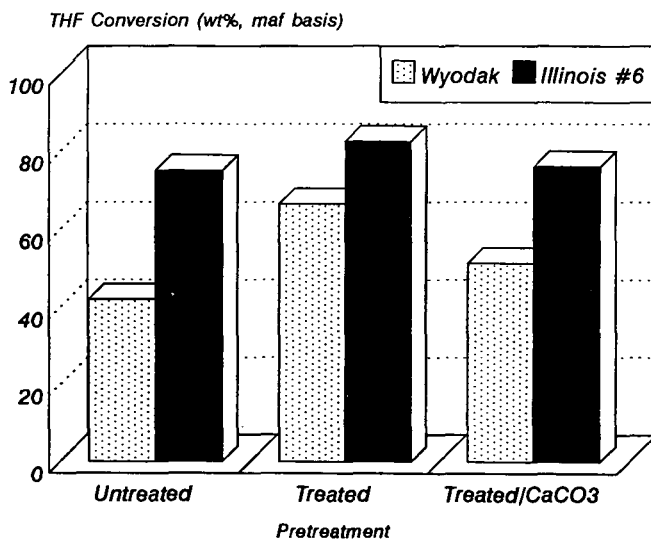


Figure 5 - Effect of Calcium Carbonate Addition on Low Severity Liquefaction Reactivity of Wyodak and Illinois #6 Coals